Quantum Lattice Enumeration in Limited Depth

Nina Bindel[1], Xavier Bonnetain[2], Marcel Tiepelt[3], and Fernando Virdia[4]

[1] SandboxAQ, Palo Alto, CA, USA, nina.bindel@sandboxaq.com
[2] Université de Lorraine, CNRS, Inria, Nancy, France, xavier.bonnetain@inria.fr
[3] KASTEL, Karlsruhe Institute of Technology, Karlsruhe, Germany, marcel.tiepelt@kit.edu
[4] NOVA LINCS, Univerisdade NOVA de Lisboa, Lisbon, Portugal, f.virdia@campus.fct.unl.pt

Abstract In 2018, Aono *et al.* (ASIACRYPT 2018) proposed to use quantum backtracking algorithms (Montanaro, TOC 2018; Ambainis and Kokainis, STOC 2017) to speedup lattice point enumeration. Quantum lattice sieving algorithms had already been proposed (Laarhoven *et al.*, PQCRYPTO 2013), being shown to provide an asymptotic speedup over classical counterparts, but also to lose competitiveness at dimensions relevant to cryptography if practical considerations on quantum computer architecture were taken into account (Albrecht *et al.*, ASIACRYPT 2020). Aono *et al.*'s work argued that quantum walk speedups can be applied to lattice enumeration, achieving at least a quadratic asymptotic speedup *à la* Grover search while not requiring exponential amounts of quantum accessible classical memory, as it is the case for sieving. In this work, we explore how to lower bound the cost of using Aono *et al.*'s techniques on lattice enumeration with extreme cylinder pruning, assuming a limit to the maximum depth that a quantum computation can achieve without decohering, with the objective of better understanding the practical applicability of quantum backtracking in lattice cryptanalysis.

Keywords: Quantum cryptanalysis · Lattice enumeration · Post-quantum cryptography · Quantum circuits

1 Introduction

Cryptographic constructions based on the hardness of computational problems over algebraic lattices have achieved significant popularity in recent years. Part of the reason for this popularity is the conjectured security of protocols built on them against quantum adversaries, due to the apparent resistance of lattice problems against quantum attacks.

The state-of-the-art attacks on lattice problems usually involve the use of lattice reduction techniques, with block reduction algorithms being the most popular choice [75,76,24,14,56,6,33]. The leading cost of block lattice reduction (and therefore, often, of the attacks overall) comes from solving instances of the (approximate [52,4]) shortest vector problem (SVP) in high dimension.

The leading choice for (approximate) SVP solvers are lattice point enumeration [45,30,34,24,13,3] and sieving [2,60,50,17,6] algorithms. Due to the central role these algorithms play in the cryptanalysis of lattice-based constructions [53,9,5] and because multiple post-quantum (PQ) soon-to-be standards are lattice-based [77,54,66], clearly understanding their cost is crucial.

Enumeration and sieving are originally classical algorithms, with asymptotically different *classical* runtime (namely, $2^{O(n \log n)}$ for enumeration and $2^{O(n)}$ for sieving) and memory cost (namely, $O(\text{poly}(n))$ for enumeration and $2^{O(n)}$ for sieving). Several *quantum* speedups on sieving have been proposed [51,46,22,20]. These algorithms improve upon their classical counterparts using a quantum search or a quantum walk to speed up nearest neighbour subroutines. Quantum speedups for enumeration have received significantly less attention. Hypothetical quadratic quantum speedups on enumeration were first suggested in [72]. Aono, Nguyen, and Shen [13] demonstrated them by leveraging quantum backtracking techniques [57,10] on the *enumeration tree* constructed internally as part of enumeration. Bai, van Hoof, Johnson, Lange and Ngu [16] investigated concrete implementations of the arithmetic quantum circuits required.

While applicability of these speedups appears clear in the unbounded-depth logical-qubit model, where quantum computation achieves low error rates for free and does not decohere, our current understanding of quantum computer engineering suggests that this model may be overly optimistic for hypothetical real-world quantum adversaries [65]. For example, Albrecht, Gheorghiu, Postlethwaite and Schanck [7] investigate the impact of error correction on quantum lattice sieving, determining that achieving even small speedups over classical sieving in the cryptanalytic regime requires making several optimistic algorithmic and physical assumptions. We are currently not aware of any similar work on the validity of quantum speedups on enumeration in similarly constrained models.

Our contributions. In this paper, we set to investigate whether quantum speedups on lattice enumeration [13] apply to enumeration with extreme cylinder pruning in the *limited quantum depth* setting. In this setting, we assume the availability of error-corrected logical qubits and quantum-accessible classical memory (QRACM) [36,49,42]. However, we also assume a limit MaxDepth to the depth that a quantum circuit can achieve, as computations with higher depth than MaxDepth are assumed to decohere, returning noise.

This setting has been proposed by the National Institute of Standards and Technology (NIST) in their Call for Proposals for PQ KEMs and digital signatures [62, Sec. 4.A.5]. NIST proposes different values for MaxDepth (namely, of 2^{40}, 2^{64} and 2^{96}), capturing different run-times and quantum computing technology, and proposes costs for key-search attacks against block ciphers and collision-search attacks for hash functions in this setting. As a case-study, we adopt the same MaxDepth limitations, and investigate their effect on quantum enumeration with cylinder pruning against CRYSTALS-Kyber, the key encapsulation mechanism (KEM) selected for standardisation by NIST.

Since our initial results suggest that enumeration trees constructed when attacking Kyber are mostly too large to be directly enumerated quantumly when MaxDepth is considered, we propose a combined classical-quantum enumeration algorithm that allows leveraging any available quantum computation capabilities, regardless of quantum depth budget limits. We provide a detailed yet generous-to-the-adversary analysis of the runtime costs of this combined attack in terms of quantum depth and number of gates under reasonable heuristics that we support with experimental evidence. We identify multiple known unknowns that affect the cost of the combined attack, and provide lower bounds for each one where possible, and otherwise provide experiment-backed heuristics. Finally, we use our analysis to estimate lower bounds on the cost of performing the primal lattice attack on Kyber in various settings, using our combined classical-quantum extreme cylinder pruning enumeration.

Our results suggest that quantum cylinder pruning enumeration techniques are unlikely to affect larger parameters sets for lattice-based schemes when taking into consideration a MaxDepth constraint. While their effect on smaller parameters cannot be fully excluded, successful attacks are contingent on various unknown quantities being favorable to the attacker.

As part of our analysis, we also develop some minor results concerning the structure of lattice enumeration trees, which we report in the full version of this paper [19] together with matching experiments, and that are of independent interest. We have made the source code used to produce our experimental results, tables, and plots publicly available at `https://github.com/mtiepelt/QuantumLatticeEnumeration`.

Related work. The limited quantum depth budget setting has been explored in the case of Grover's algorithm against AES and LowMC by Jaques, Naehrig, Roetteler and Virdia [41]. Follow-up work focused on both optimizing the Grover search oracles [82], and improving the search algorithm [26]. Albrecht, Gheorghiu, Postlethwaite and Schanck [7] investigated the cost of quantum nearest neighbour search for lattice sieving in the non-free error correction setting. In recent independent work, Bai, van Hoof, Johnson, Lange and Ngo [16] investigate circuit designs for the core quantum operator used as part of quantum enumeration, ignoring resource constraints. Most significantly, Ambainis and Kokainis [10] expanded on the work of Montanaro [57] by developing a tree size estimation algorithm and applying it to quantum backtracking to obtain an algorithm that performs as a classical algorithm would in the worst case, resulting in meaningful speedups in case the expected size of the trees being enumerated is much lower than their upper bound. We do not consider this algorithm as in lattice enumeration we experimentally observe the average tree sizes to closely match the analysis we use as upper bound.

Open directions. First, a more careful (and hence less generous) design of quantum circuits used for quantum backtracking could be used to attempt to provide an upper bound on the cost. Another open direction would be the extension of this work to other pruning techniques, such as discrete pruning [13], as well as the theoretical analysis of the multiplicative Jensen's gap (cf. Definition 1) on lattice enumeration trees. In this direction, we outline a possible approach to bounding it in Appendix I.

Roadmap. In Section 2 we cover preliminaries. In Section 3 we describe our lower bounds on the cost of combined classical-quantum enumeration. In Section 4 we estimate the cost of the core circuit used in quantum enumeration. In Section 5 we use our estimates to investigate the cost of quantum enumeration as part of the primal lattice attack on Kyber.

2 Preliminaries

We denote the set of integers by $\mathbb{Z}$ and the set of real numbers by $\mathbb{R}$. We denote logarithms in base 2 by log. We define $[m] := \{1, ..., m\}$. Furthermore, we write the absolute value of $c \in \mathbb{R}$ as $|c|$, the Euclidean norm of $v \in \mathbb{R}^n$ as $||v|| = (v_1^2 + \cdots + v_n^2)^{1/2}$ and the inner product of v, $w \in \mathbb{R}^n$ as $v \cdot w$. Given a finite set S, we denote by $U(S)$ the uniform distribution over S, and write $s \sim U(S)$ for an element being uniformly distributed in S. To describe asymptotic complexities, we write $\mathcal{O}(\cdot)$ for the big-o and $\Omega(\cdot)$ for the big-omega notation.

2.1 Lattices

An n-dimensional lattice Λ is a discrete, additive subgroup of $(\mathbb{R}^n, +)$, generated by a set of linearly independent vectors $B = (b_1, \ldots, b_r) \in \mathbb{R}^{n \times r}$, $b_i \in \mathbb{R}^n$ called a basis. We consider full-rank integer lattices $\Lambda = \{\sum_{i=1}^{r} b_i c_i \mid c_i \in \mathbb{Z}\} \subseteq \mathbb{Z}^n$ with $r = n$ and denote B^* the result of performing Gram-Schmidt orthogonalization on B. We let $\lambda_1(\Lambda) = \min_{v \in \Lambda \setminus \{0\}} ||v||$ denote the first minimum of the lattice. Furthermore, the projection $\pi_{B,i} : \Lambda \to \text{span}(b_1, \cdots, b_{i-1})^\perp$ maps a lattice point onto the span orthogonal to the vector space spanned by $b_1, \ldots, b_{i-1}$. We omit the subscript B and write $\pi_i(\cdot)$ when the basis being used is clear from context. Given a lattice Λ of rank n, the set $\pi_i(\Lambda) = \{\pi_i(v) \mid v \in \Lambda\}$ is itself a lattice in $\mathbb{R}^{n-i+1}$. We sometimes refer to such lattices as *projective sublattices.*

Lattice enumeration. Given an input basis B of Λ and an upper bound $\lambda_1(\Lambda) \leq R$ (e.g., $R = ||b_1^*||$), lattice enumeration finds a vector $v \in \Lambda$ such that $||v|| \leq R$. The procedure performs a depth-first-search on a tree consisting of an "empty node" root on level $k = 0$, and ofa the set of projected lattice points of norm at most R in $\pi_{n-k+1}(\Lambda)$ on level $k > 0$. The leaves of the tree on level $k = n$ are lattice points of norm at most R.

As originally proposed, enumeration algorithms iterated over a tree spanning the complete intersection of the lattice with a ball of radius R around the origin [64,45,31,73]. Modern variants restrict the search space by introducing a branch-and-bound methodology, pruning the tree based on a heuristic bound on the norm $||\pi_i(v)||$ of the target's orthogonal projections [34,55,3]. This slightly reduces the success probability p of the algorithm, since the short vector may be erroneously pruned from the tree, introducing a trade-off between faster traversal speed on the smaller tree versus having to re-run the procedure $\mathcal{O}(p^{-1})$ times on re-randomised versions of the lattice basis. In this work, we focus on the extreme cylinder pruning variant originating from [73, Alg. ENUM] used in [34], with pruning bounds R_k for each level k of the search tree.

Enumeration trees. The key observation behind lattice enumeration algorithms is that orthogonal projections cannot increase the norm of a vector. This means, for a lattice Λ with basis $B = (b_1, \dots, b_n)$, shortest vector v, and sufficiently large R, that $R \geq ||v|| = ||\pi_1(v)|| \geq ||\pi_2(v)|| \geq \cdots \geq ||\pi_n(v)|| \geq 0$, with $\pi_i(v)$ living in an $(n-i+1)$-dimensional subspace of $\mathbb{R}^n$. Thus, to enumerate vectors in Λ of norm at most R, it is sufficient to enumerate vectors in the lower-rank projections $\pi_i(\Lambda)$ for $i \leq n$, discarding guesses for $\pi_i(v)$ if they are too long. Starting from $i = n$, suppose $\pi_n(v) = g_n$ is guessed correctly for some vector $g_n \in \pi_n(\Lambda)$.[1] The enumeration algorithm then attempts to extend this into a guess $g_{n-1} \in \pi_{n-1}(\Lambda)$ for $\pi_{n-1}(v)$ such that $\pi_n(g_{n-1}) = g_n$. If $||g_{n-1}|| \leq R$,[2] one proceeds similarly trying to extend g_{n-1} into a guess for g_{n-2} for $\pi_{n-2}(v)$ and so on; else one attempts to find a different guess $g'_{n-1} \neq g_{n-1}$ for $\pi_{n-1}(v)$ that is short enough, and if no such vector exists one aborts the search in $\pi_{n-1}(\Lambda)$ and attempts to extend a different guess $g'_n \neq g_n$ for $\pi_n(v)$. Every guess g_i for $\pi_i(v)$ of norm at most R becomes a node in the enumeration tree. A node g_i is the *child* of some guess g_{i+1} for $\pi_{i+1}(v)$ such that $\pi_{i+1}(g_i) = g_{i+1}$. Moreover, every node g_i is the *parent* of guesses $\{g_{i-1} \in \pi_{i-1}(\Lambda) \mid \pi_i(g_{i-1}) = g_i\}$ for $\pi_{i-1}(v)$. Careful computation using the Gram-Schmidt vectors $B^* = (b_1^*, \dots, b_n^*)$ and coefficients $\mu_{i,j} = b_i \cdot b_j^* / ||b_j^*||^2$ for $i > j$, shows that given a lattice vector $v = \sum_{i=1}^n c_i b_i$ where $c_i \in \mathbb{Z}$ for all i, its projections are of the form $\pi_j(v) = \sum_{i=j}^n \alpha_i b_i^*$ where $\alpha_j = c_j + \sum_{i>j} \mu_{i,j}\, c_i$. By orthogonality of the $(b_i^*)_i$, we have $||\pi_j(v)||^2 = |\alpha_j|^2 ||b_j^*||^2 + ||\pi_{j+1}(v)||^2$. Hence, for any guess g_{j+1} for $\pi_{j+1}(v)$, a guess g_j for $\pi_j(v)$ with $\pi_{j+1}(g_j) = g_{j+1}$ must satisfy $|\alpha_j|^2 \leq (R^2 - ||\pi_{j+1}(v)||^2)/||b_j^*||^2$, *i.e.*,

$$\Big|c_j + \sum_{i>j} \mu_{i,j}\, c_i\Big| \leq \frac{\sqrt{R^2 - ||\pi_{j+1}(v)||^2}}{||b_j^*||} = \frac{\sqrt{R^2 - \displaystyle\sum_{r=j+1}^{n} \left(c_r + \sum_{i=r+1}^{n} \mu_{i,r} c_i\right)^2 ||b_r^*||^2}}{||b_j^*||}. \quad (1)$$

Remark 1. In the case of pruned enumeration, the main difference in the process is that we are given a *pruning set* $\{R_i \mid i \in [n], 0 < R_1 \leq \cdots \leq R_n = R\}$ rather than a single bound R, with R_{n-j+1} replacing R in Eq. (1).

[1] Since lattices are symmetrical around the origin, in practice implementations consider only half of the possible guesses for $\pi_i(v)$.

[2] To unburden notation, we temporarily consider the non-pruned case with $R_k = R$, $\forall k$.

Expected cost of enumeration. The cost of enumeration is typically estimated to be equal to the number of nodes visited by the algorithm—the "enumeration tree". Let Z_k be the set of nodes on the k^{th} level of the tree (that is, at distance k from the empty root node), H_k be the expected cardinality of Z_k over the distribution of random bases being enumerated,[3] and N be the total number of nodes in the tree. The cardinality of Z_k depends on the pruning strategy and on the geometry of the projective sublattices implied by the lattice bases. The expected number of total nodes is $\mathbb{E}[N] = \frac{1}{2}\sum_{k=1}^{n} \mathbb{E}[|Z_k|] = \frac{1}{2}\sum_{k=1}^{n} H_k$, where the expectation is taken over the distribution from which the lattice is being sampled and the extreme cylinder pruning re-randomization (if any is used), and the $1/2$ factor is due to exploiting lattices' additive symmetry to avoid unnecessarily visiting half of the tree. Cost estimation for the algorithm then reduces to estimating H_k. This is a standard computation that we perform in detail in Appendix A, closely following [34,12].

Solving LWE via lattice reduction. Learning with errors (LWE) [68,69] is a popular hardness assumption for constructing PQ secure primitives, such as Kyber [77]. One of the main approaches to solving LWE is via block lattice reduction algorithms, such as BKZ [75,76]. After building a *lattice embedding* of dimension n of a given LWE challenge, block reduction algorithms will call $O(\text{poly}(n))$ many times an SVP solver, such as lattice enumeration, in dimension $\beta < n$. This process results in a better basis for the LWE lattice embedding that allows the attacker to recover the LWE challenge secret. In our work, we consider modern versions of BKZ using early-termination and approximate-SVP solvers, which have been shown [52,4] to be effective while requiring to find a "short enough" lattice vector, rather than the shortest. In order to go from an LWE challenge to an embedding and a choice of BKZ block size β, we use the `lwe-estimator` [8].

2.2 Quantum Algorithms

We denote quantum registers in the Hilbert space $\mathcal{H}$ as lower case letters $|a\rangle$, and the unitary operator that implements a function f as U_f. We denote by Id the identity operator.

Quantum backtracking. Backtracking search is a depth-first-search algorithm that allows exhaustively finding "marked" leaves on trees. Given a tree $\mathcal{T}$ of height n, we partition the set of nodes into levels $1 \le k \le n$, based on their distance from the root node r. Every node $x \in \mathcal{T}$ corresponds to a partial assignment to a set of variables $x_1, \dots, x_n$ identifying a path to the node, using $*$ to mark yet unassigned values (e.g., the root node r is labelled $(*, \dots, *)$, nodes on level $k = 1$ are labelled $(*, \dots, *, \tilde{x}_n)$ for some values of $\tilde{x}_n$, and so forth). The backtracking algorithm needs to be provided with an oracle for a predicate function $P : \mathcal{T} \to \{\textsc{True}, \textsc{False}, \textsc{Indeterminate}\}$ that given a node returns True if it

[3] In the case of BKZ reduction with extreme cylinder pruning, these are re-randomized instances of a local BKZ block.

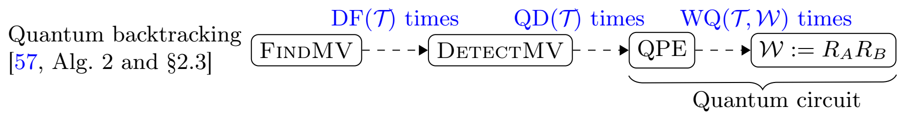

Figure 1: Overview of Montanaro's marked vertex (MV) finding backtracking algorithm [57]. Only part of the algorithm needs to run within MAXDEPTH.

is a marked leaf, FALSE if it can be determined that the node cannot be on the path to a marked leaf, and INDETERMINATE otherwise. Lattice enumeration algorithms are backtracking algorithms with a predicate $P_R(v)$ returning FALSE if $||\pi_i(v)|| > R$, INDETERMINATE if $||\pi_i(v)|| \leq R$ for $i < n$ and no other value $||\pi_j(v)||$ is known with $j < i$, and TRUE if $||\pi_1(v)|| = ||v|| \leq R$.[4]

In [57], Montanaro introduced quantum backtracking algorithms for detecting [57, Alg. 2] and returning [57, § 2.3] marked vertices in a tree, both achieving an asymptotic speedup over classical backtracking. We depict their main subprocedures in Fig. 1. Both of these algorithms are based on a common quantum walk, QPE($\mathcal{W}$), where $\mathcal{W}$ is the operator that corresponds to a single step of the quantum walk using the predicate P_R to decide if a node is marked.

Then the quantum walk can be seen as a quantum phase estimation (QPE) which consecutively applies WQ($\mathcal{T}, \mathcal{W}$) many times $\mathcal{W}$ to a state corresponding to a superposition of the nodes in the backtracking tree $\mathcal{T}$. By the proof of [57, Lem. 2.4], the eigenvectors of $\mathcal{W}$ are the states that admit a path from the root to a marked node. Measuring the root node after a sufficient number of steps allows to identify whether a path to a marked node exists with false positive probability $\leq 1/4$ and false negative probability $\leq 1/2$. The detection algorithm DETECTMV [57, Alg. 2] consists of repeating QD($\mathcal{T}$) $:= \lceil \varepsilon \log(1/\delta_{\mathrm{DMV}}) \rceil$ many times QPE, for some constant $\varepsilon > 0$, to output "marked node exists" or "no marked node exists" with a failure probability of at most δ_{DMV}. We determine bounds on values for ε and δ_{DMV} in Section 3.1 (with a more detailed analysis in [19, App. H]) and refer to the resulting number of calls to the QPE within DETECTMV as QD($\mathcal{T}$).

Theorem 1 ([57, Theorem 1.2], abridged). *Let $\mathcal{T}$ be a backtracking tree of size at most $\#\mathcal{T}^u$ with degree $\mathcal{O}(1)$. Let $P(x)$ be a predicate that returns* TRUE *if and only if x is a marked node. For any $0 < \delta_{\mathrm{DMV}} < 1$,* DETECTMV *outputs "marked node exists" if there exists $x \in \mathcal{T}$ such that $P(x) =$* TRUE *and "marked node does not exist" otherwise, with failure probability at most δ_{DMV}. The algorithm performs $\mathcal{O}\left(\sqrt{\#\mathcal{T}^u n} \log(1/\delta_{\mathrm{DMV}})\right)$ evaluations of P, using poly(n) qubits.*

For the algorithm returning a marked node in $\mathcal{T}$, Montanaro suggests to perform classical depth-first-search on $\mathcal{T}$ by using DETECTMV as a predicate. DETECTMV would be called on the children c_i of the root node, until one on the subtrees rooted at c_i, for some i, returns "marked node exists". It would then

[4] The pruned enumeration case replaces R with R_{n-i+1}, cf. Remark 1.

proceed to search for a child of c_i spawning a subtree with a marked node, and so on, until reaching a marked leaf. For a tree of height n with nodes having at most d children, FindMV will call DetectMV $O(nd)$ times, in the worst case. We will discuss the concrete number of calls (denoted by $\mathrm{DF}(\mathcal{T})$) in Section 3.1. If no upper bound on the number of nodes of $\mathcal{T}$ is known, the search can be repeated with growing values of $\#\mathcal{T}^u = 2^0, 2^1, 2^2, \dots$, resulting in an additional runtime factor of $\mathcal{O}(\log \#\mathcal{T})$. Montanaro also shows that overestimating the tree-size does not affect the quantum walk's success probability.

Quantum backtracking for lattice enumeration. Aono, Nguyen and Shen [13] analyze the asymptotic cost of using quantum backtracking algorithms to perform lattice enumeration in a black-box setting. In [13, Thm. 7(1)], they identify the asymptotic runtime for finding a short non-zero vector using cylinder pruning and $\mathrm{poly}(n)$ many qubits to be $\mathcal{O}\left(\sqrt{\#\mathcal{T}}n^3 \ \mathrm{poly}(\log(1/\delta), \log n)\right)$. In [13, Sec 4.2], they argue that this holds also when performing extreme pruning with M randomized lattice bases $(B_i)_{i\leq M}$, by collecting each enumeration tree into a larger, single tree, resulting in an asymptotic runtime for finding a non-zero vector via quantum extreme pruning of $\mathcal{O}\left(\sqrt{\#\mathcal{T}^M}n^3\lambda \ \mathrm{poly}(\log n, \log(1/\delta), \log(\lambda), \log M)\right)$, where λ is the bit-size of the entries of B_i, for $i \in [M]$ and $\#\mathcal{T}^M$ is the sum of the number of nodes of all M trees.

2.3 Cost Metrics for Quantum Circuits

Circuit depth. Given a circuit instantiating a quantum algorithm using a given set of gates, a common metric to measure its cost is the circuit's *depth*. This can be defined as the longest path from the input state to the output state, if the circuit is considered as a directed graph with quantum gates as nodes. Circuit depth can be seen as an analogous measure to the runtime of a classical computation, by considering that applying a gate must take a non-zero amount of time, and is therefore often used to express the asymptotic cost of quantum algorithms. In this paper, we make two crucial assumptions regarding circuit depth. First, we exclusively measure *T-depth*, that is the circuit depth when only taking into consideration T gates, as preparation of these is expected to be the most time-consuming part of practical quantum computation [44,32]. Second, we investigate the cost of quantum enumeration when imposing a limit MaxDepth to the maximum depth a circuit can achieve while maintaining state coherence. This consideration follows from observing that currently state decoherence seems to be one of the main hurdles to achieving large-scale quantum computation. As part of the call for proposals for its PQ cryptography standardization process, NIST [62] proposed the three possible values of 2^{40}, 2^{64} or 2^{96} for MaxDepth. This limitation means that care should be paid to any circuit parallelization required to stay within MaxDepth circuit depth when measuring the cost of long-running quantum algorithms as these do not always trivially parallelize, such as in the case of Grover's search [81].

Number of gates. Another metric commonly used to express the cost of quantum circuits in the literature is the number of gates, or *G-cost* (which can always be lower-bounded by the depth of the circuit). The use of the G-cost is motivated by the observation that, in practice, quantum gates are not a physical device, but an operation performed on the quantum state. Such operation is likely managed by a classical microcontroller, meaning that the G-cost is a lower bound on the cost of evaluating gates of a quantum circuit. As such cost also consumes classical resources, it can be compared to the cost of classical algorithms [43, Def. 2.4].

As part of their call for proposals, NIST [62] defined security *categories* corresponding to the hardness of breaking AES and SHA. When considering quantum algorithms, they expressed this hardness in terms of G-cost, assuming a MaxDepth limit. We will similarly estimate lower bounds on the G-cost of quantum enumeration, as to simplify comparisons to the rest of the literature.

Memory. Different kinds of memory devices can be used by quantum computers, categorised by their interface [42]. A common metric that we ignore in this work is that of how many qubits are used by the algorithm. The reason is that qubits are currently notoriously difficult to maintain in a coherent state. Another form of useful memory is QRACM. This can be thought of as a classical array $(a_1, \ldots, a_n)$ that can be read by a quantum computer into a state $\sum_{i \leq n} |a_i\rangle$ in $O(n \text{ poly}(\log(n)))$ operations [36,49,42]. All our algorithms use a polynomial amount of qubits, and some of our approaches require an exponential amount of QRACM.

Limits of the NIST metrics. The NIST metrics were designed to give a security goal and allow comparisons between candidates. As all metrics, part of them is arbitrary, and they were not designed to accurately define what could be computable in the long term. In particular, the classical and quantum security levels are incomparable, and a break of a system due to a quantum attack does not imply that the most efficient way to attack it will be, in the long run, quantum. Still, PQ cryptography has to do some optimistic assumptions on the capabilities of quantum computers, as otherwise pre-quantum schemes would suffice.

3 Estimating the Cost of Quantum Enumeration

In this section, we outline the components of our cost estimation of quantum lattice enumeration via backtracking under a MaxDepth restriction. We start by reviewing the gate-cost of Montanaro's FindMV algorithm and the depth of the quantum walk QPE($\mathcal{W}$), since the latter will imply an upper bound to the size of the largest tree that can be searched within a MaxDepth budget for coherent quantum computations. We then proceed to explore the cost of combining quantum enumeration with classical one, to address settings where the trees are too large for the limited quantum depth budget.

3.1 Quantum Backtracking to Find a Marked Vertex

We follow the proof of Theorem 1, aiming to provide concrete lower bounds (rather than asymptotic upper bounds) to the cost of the FindMV algorithm. The quantum backtracking framework laid out in Section 2.2 performs a classical depth-first search on the backtracking tree, where each node is evaluated using multiple, individual quantum walks to decide whether it spawns a subtree containing a marked node. An overview of Montanaro's quantum algorithm is sketched in Fig. 1. Since the depth of a quantum circuit is the principal limitation for our cost model (see Section 2.3) all calls to the quantum circuit $\mathrm{QPE}(\mathcal{W})$ can be viewed independently, meaning their depth does not accumulate towards the MaxDepth limit.

Node degree. While Theorem 1 assumes the tree being enumerated having constant degree, this is not the case for enumeration trees (of depth n) on general lattices where the leaves are lattice vectors of norm at most R. Given a node $(\star, \dots, \star, c_{n-k+1}, \dots, c_n)$ on level k of the tree, an upper bound $\mathcal{C}_k$ on its degree corresponds to an upper bound on the number of possible values $c_{n-k} \in \mathbb{Z}$ such that $(\star, \dots, \star, c_{n-k}, c_{n-k+1}, \dots, c_n)$ is in the backtracking tree. An upper bound on the degree of the tree would then be $\mathcal{C} = \max_k \mathcal{C}_k$. For q-ary lattices as considered in our experiments in Section 5, a bound could be $\mathcal{C}_k = q$ for all k. A better bound is given by Lemma 1 in Appendix C, where we show $\mathcal{C}_k \approx \min(\lfloor 2 \cdot R_{k+1}/||b^*_{n-k}||\rceil, q)$.

Procedures. As outlined in Section 2.2 and Fig. 1, the quantum algorithm that can identify marked vertices in a tree, FindMV, will internally call DetectMV, which detects whether a marked vertex exists in a tree at all. This, in turn, runs quantum phase estimation QPE on the operator $\mathcal{W}$.

Each procedure calls the respective sub-procedure multiple times (with the number of calls depending on the properties of the respective tree $\mathcal{T}$), resulting in total depth and gate cost for FindMV of

$$\text{T-Depth}(\text{FindMV}(\mathcal{T})) = \mathrm{DF}(\mathcal{T}) \cdot \mathrm{QD}(\mathcal{T}) \cdot \mathrm{WQ}(\mathcal{T}, \mathcal{W}) \cdot \text{T-Depth}(\mathcal{W}), \quad (2)$$

$$\text{GCost}(\text{FindMV}(\mathcal{T})) = \mathrm{DF}(\mathcal{T}) \cdot \mathrm{QD}(\mathcal{T}) \cdot \mathrm{WQ}(\mathcal{T}, \mathcal{W}) \cdot \text{GCost}(\mathcal{W}), \quad (3)$$

where $\mathrm{DF}(\cdot)$, $\mathrm{QD}(\cdot)$, and $\mathrm{WQ}(\cdot)$ are the number of calls to the subroutines DetectMV in FindMV, QPE in DetectMV, and $\mathcal{W}$ in QPE, respectively. We will analyze the number of these calls under the assumption that the search tree is of depth n and degree bound by $\mathcal{C}$, prioritizing strict lower bounds.

Number of calls DF$(\cdot)$. Every call to FindMV (cf. Section 2.2) performs a classical search upon input tree $\mathcal{T}$, and outputs a single leaf on level n. Aono, Nguyen and Shen [13] analyze the number of calls to DetectMV made when searching an enumeration tree without an asymptotically constant degree. Their analysis performs an asymptotically convenient implicit transformation of the tree into a binary tree [13, Theorem 5], resulting in $O(n \log \mathcal{C})$ calls in the worst case, where we could take $\mathcal{C} = \max_k\{\min(\lfloor 2 \cdot R_{k+1}/||b^*_{n-k}||\rceil, q)\}$ (cf. Appendix C). This bound is likely tight on average when trees are guaranteed to contain a marked leaf. However, as we will see in Section 3.2, a MaxDepth constraint results in performing quantum walks on (sub-)trees without such a guarantee. Since FindMV requires a single call to DetectMV to identify that a tree has no marked leafs, we instead lower bound $\mathrm{DF}(\cdot) \geq 1$.

The success probability of a call to FindMV depends on that of DetectMV. In the following paragraph we lower bound the cost of DetectMV with success probability 1, so that FindMV also has full success probability.

Number of calls $QD(\cdot)$. An upper bound on the quantum depth required to run DetectMV can be established directly from [57, Alg. 2] and [57, Lemma 2.4].

Corollary 1 (T-Depth of quantum circuit to detect a marked node). *Let $\mathcal{W}$ be a quantum operator of depth* T-Depth($\mathcal{W}$) *that acts on a backtracking tree $\mathcal{T}$ in n (unassigned) variables. Let $QPE(\mathcal{W})$ be the quantum circuit performing phase estimation on $\mathcal{W}$. For any failure probability $\delta_{\mathrm{DMV}} \in (0,1)$, there exists a quantum algorithm* DetectMV *that decides with probability at least $1-\delta_{\mathrm{DMV}}$ if a marked node exists in $\mathcal{T}$ by calling QPE $\lceil \varepsilon \log(1/\delta_{\mathrm{DMV}})\rceil$ times, such that* T-Depth$(QPE) \leq 1/b\sqrt{\#\mathcal{T} \cdot n} \cdot$ T-Depth$(\mathcal{W})$*, for some value $b > 0$ depending on $\mathcal{W}$.*

As mentioned in Section 2.2 and Corollary 1, each call to DetectMV repeats the QPE a total of $\lceil \varepsilon \log(1/\delta_{\mathrm{DMV}})\rceil$ times for some constant $\varepsilon > 0$. The value of ε depends on the failure probability of the quantum phase estimation QPE($\mathcal{W}$), and on the desired failure probability δ_{DMV} of DetectMV. The failure probability of QPE($\mathcal{W}$) in turn depends on the number of applications of the operator $\mathcal{W}$, relative to the tree-size $\#\mathcal{T}$, the dimension n of the lattice and a constant b (cf. Corollary 1). It is important to note that there is a trade-off between the number of repetitions of $\mathcal{W}$ in the QPE, and the number of repetitions of the QPE. We do not consider any optimizations related to this trade-off as they are implementation specific. Instead, since we are determining lower bounds for the number of calls, with $\varepsilon \geq 0$ we lower bound $\mathrm{QD}(\mathcal{T}) \geq 1$.

Number of calls $WQ(\cdot)$. As used inside of DetectMV, QPE needs to be run with precision $b/\sqrt{\#\mathcal{T} \cdot n}$, for some constant $b > 0$, returning after $\approx \sqrt{\#\mathcal{T} \cdot n}/b$ evaluations of $\mathcal{W}$. Or put differently, asymptotically, $\Omega(\sqrt{\#\mathcal{T}n})$ is a lower bound on the query-complexity of detecting a marked node in a tree with $\#\mathcal{T}$ nodes and depth n [1, Theorem 7][58, Sec 4]. Montanaro also notes that Thm. 1.1 and thus Lem. 2.4 of [58] are optimal for $\delta_{\mathrm{DMV}} \in \Omega(1)$. As a consequence, Corollary 1 is an asymptotic lower bound if $b \in \Omega(1)$, where in the black box setting T-Depth$(\mathcal{W}) \in \Omega(1)$.

Finding the hidden constant for the phase estimation is more involved. While explicit constants exist for phase estimation [18], Montanaro's algorithm may not necessarily use the optimal majority voting scheme as part of DetectMV. Let $\overline{MV}$ denote the event that no marked vertex is contained in the tree $\mathcal{T}$. An approximation for the constants in QPE was analyzed by [21, Sec 4.1], who showed that the probability $p_1 \coloneqq \Pr[X_i = 1 \mid \overline{MV}]$ that the QPE outputs *one* even if no marked vertex exists is bounded by $p_1 \leq 2\sqrt{b}(1+o(1))$. In our case, setting p_1 as low as possible leads to $p_1 \leq 1/4$, which implies using at least $b \geq 1/64$. Since we evaluate $\mathcal{W}$ about $\sqrt{\#\mathcal{T} \cdot n}/b$ times and $1/b \leq 64$, it follows

$$\mathrm{WQ}(\mathcal{T}, \mathcal{W}) \approx 64\sqrt{\#\mathcal{T} \cdot n}\,.$$

Notably, there is a trade-off between the number of repetitions of $\mathcal{W}$ in the QPE, and the number of repetitions of the QPE (cf. Appendix H.1). Fewer repetitions of the first (reducing both T-Depth and GCost) results in an increase of the number of repetitions of the QPE (increasing only GCost). We do not consider optimizations related to this trade-off. To ensure generous-to-the-adversary bounds, we settle for the following conjecture for our estimations in Section 5.

Conjecture 1 *The query complexity $WQ(\mathcal{T}, \mathcal{W})$ of quantum phase estimation of $\mathcal{W}$ (QPE($\mathcal{W}$)) is $WQ(\mathcal{T}, \mathcal{W}) \geq \sqrt{\#\mathcal{T} \cdot n}$.*

Beyond lower bounds. The lower bounds on $\mathrm{DF}(\mathcal{T}), \mathrm{QD}(\mathcal{T})$ and $\mathrm{WQ}(\mathcal{T})$ result in a conservative cost estimation at the cost of potentially underestimating the attack cost. In Appendix H, we perform a heuristic analysis of the hidden constants, estimating tighter bounds for these quantities. Indeed, we show that the number of calls to DetectMV is likely $\mathrm{DF}(\mathcal{T}) \in \{1, n \log \mathcal{C}\}$ depending on the subtree being searched. Then a sufficient number of calls to the QPE in DetectMV could be $\mathrm{QD}(\mathcal{T}) = \lceil \varepsilon \cdot \log(n \log(\mathcal{C})) \rceil$ with $\varepsilon = 20$, and a sufficient number of calls to $\mathcal{W}$ during QPE is $\mathrm{WQ}(\mathcal{T}) \approx 64\sqrt{\#\mathcal{T}n}$, adopting a constant $b \geq 1/64$.

While our estimations seem realistic, and support Conjecture 1, for the sake of keeping our analysis as conservative as possible, we will keep using the strict lower bounds above during attack cost estimation in Sections 3.3 and 5. Analogue results to those in Section 5 using the less strict estimates can be found in Appendix H.

Depth of QPE($\mathcal{W}$). With Conjecture 1 in hand, we can attempt to estimate the depth budget required to break practical lattice-based schemes using quantum enumeration as proposed by Aono, Nguyen and Shen [13]. By using the `lwe-estimator` [8] we obtain the block size β required by the BKZ [75,76] algorithm to successfully run key recovery on Kyber [77] using the primal lattice attack. Using $n = \beta$ and $\mathbb{E}[\#\mathcal{T}]$ equal to the returned cost of enumeration when using a custom cost model implementing the lower bound from [12, Eq. 16], and momentarily assuming $\mathbb{E}[\sqrt{\#\mathcal{T}}] \approx \sqrt{\mathbb{E}[\#\mathcal{T}]}$ (cf. Section 3.3), we can see that

$$\log \mathbb{E}[\sqrt{\#\mathcal{T}n}] \approx \frac{\log \mathbb{E}[\#\mathcal{T}] + \log \beta}{2} \approx \begin{cases} 90.3 & \text{for Kyber-512,} \\ 166.2 & \text{for Kyber-768,} \\ 263.7 & \text{for Kyber-1024,} \end{cases}$$

with $\mathcal{T}$ collecting 2^{64} cylinder pruning enumeration trees of dimension β.

While the above numbers are a rule-of-thumb approximation, it can be seen that most likely and regardless of the value of T-DEPTH($\mathcal{W}$), breaking Kyber-768 and Kyber-1024 with a single direct quantum enumeration will not be possible within MAXDEPTH $\leq 2^{96}$. To deal with this issue, we propose combining quantum backtracking with classical enumeration, in a manner similar to classical parallel enumeration.

3.2 Combined Classical-Quantum Enumeration

Generally, parallelization of lattice enumeration [25,40,48] is conceptually simple, as the tree structure directly induces a partitioning to the search problem. This means that when searching for short vectors on a tree n levels deep (where $n = \beta$ is the BKZ block size), one can first serially enumerate all nodes on level $k < n$, and then run in parallel lattice enumeration on the subtrees rooted at level k of depth at most $n - k$.

Following this approach, we will run classical enumeration up to depth k, and proceed to run quantum enumeration on the smaller subtrees of depth $h \leq n - k$, corresponding to sub-lattices of dimension h. We will choose k such that the depth of any call to QPE($\mathcal{W}$) is within the limit of MAXDEPTH, following Corollary 1. We depict the general strategy in Fig. 2.

This combined approach is independent of the implementation of the quantum circuits, particularly of the operator $\mathcal{W}$. This means we would be able to estimate bounds on the cost of the attack given different possible values for T-DEPTH($\mathcal{W}$) and GCOST($\mathcal{W}$), including generous lower bounds (cf. Section 4.1).

The approach is also compatible with pruned enumeration techniques. In the remainder of the paper, we will focus in particular on cylinder pruning [34]. We will start by analyzing the cost of the combined enumeration algorithm on a single (possibly pruned) tree, in Section 3.3, and extend this to the case where M pruned trees are combined to achieve high success probability, in Section 3.4.

3.3 Combined Enumeration of a Single Tree

We start by recalling some notation introduced in Section 2.1 to describe enumeration trees, illustrated in Fig. 2. Given a tree of depth n, its nodes are partitioned into sets $(Z_i)_{i=1}^n$ of expected cardinality $(H_i)_{i=1}^n$ over the distribution of lattices being inspected, where Z_i collects all the nodes "on level i", that is of distance i from the root node r. Any node $g \in Z_k$ generates a subtree $\mathcal{T}(g)$ of depth $h \leq n - k$. The nodes of this subtree are partitioned into sets $(W_{k,i}(g))_{i=1}^h$ of expected cardinality $(S_{k,i})_{i=1}^h$ over random trees and g distributed uniformly in Z_k. The expected number of nodes in the subtree $\mathcal{T}(g)$, including the root g, is $1 + N_{k,h}$, where $N_{k,h} := \sum_{i=1}^h S_{k,i}$, while the expected number of nodes in the entire enumeration tree $\mathcal{T}$, including the root r, equals $1 + \frac{1}{2}\sum_{i=1}^n H_i$. The $\frac{1}{2}$ factor comes from the fact that the tree is symmetric around 0, and hence

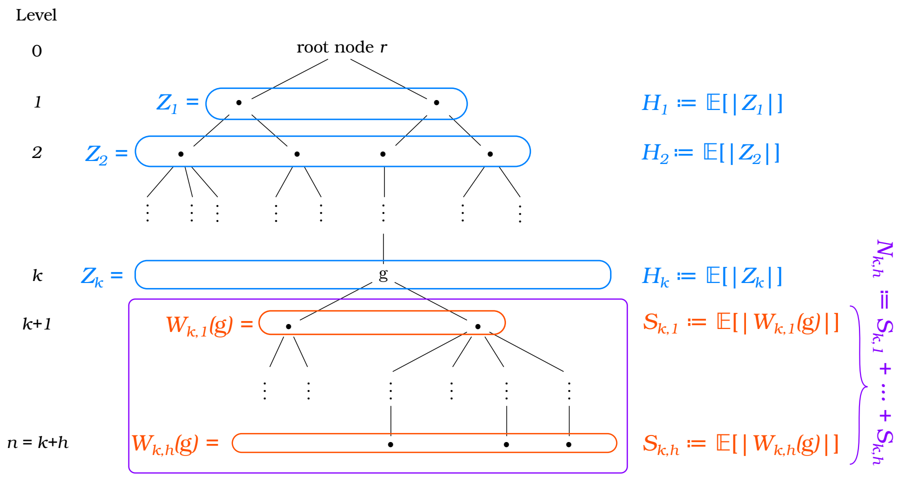
Level
0
1
2
k
k+1
n = k+h
root node r
$Z_1 =$
$Z_2 =$
$Z_k =$
g
$W_{k,1}(g) =$
$W_{k,h}(g) =$
$H_1 := \mathbb{E}[|Z_1|]$
$H_2 := \mathbb{E}[|Z_2|]$
$H_k := \mathbb{E}[|Z_k|]$
$S_{k,1} := \mathbb{E}[|W_{k,1}(g)|]$
$S_{k,h} := \mathbb{E}[|W_{k,h}(g)|]$
$N_{k,h} := S_{k,1} + \dots + S_{k,h}$

Figure 2: Combined classical-quantum enumeration tree. Quantum enumeration will happen on subtrees rooted at level k, here circled in purple.

only half of the tree needs to be searched to identify all the vectors within the enumeration radius, up to sign.

Classically and quantumly enumerated components. We first discuss how we divide the classical and quantum components of the enumeration algorithm.

Classical component. In the setting of combined classical-quantum enumeration, let k be the level up to where classical enumeration is performed. This costs

$$\underset{\substack{\text{random}\\ \text{tree } \mathcal{T}}}{\mathbb{E}}[\text{Classical GCost}] \approx 1 + \frac{1}{2}\sum_{i=1}^{k} H_i, \tag{4}$$

where we equate the cost of classical enumeration to the number of nodes visited by the algorithm, as it is standard in the literature.

Quantum component. After the classical enumeration phase, we have H_k nodes on level k, each admitting a subtree of height $h \leq n - k$, and covering the remaining levels of the full enumeration tree. A natural approach could be to enumerate all H_k subtrees individually (and possibly in parallel). However, it is not known which subtree contains the (likely few) marked nodes, meaning that we would be running $\approx H_k$ calls to quantum enumeration. In both pruned and non-pruned enumeration, the bulk of the nodes contained in the trees being traversed is contained in the "middle" levels Z_i for $i \approx n/2$, with pruning "spreading the bulk" on a larger window of levels around $n/2$ [34, Fig. 1]. For our setting, this would imply three scenarios, depending on k:

$k \approx 1$, in this case most of the tree fits within the quantum enumeration subroutine, and a quadratic speedup is possibly achievable,

$k \approx n/2$, in which case we would be running $\approx H_{n/2}$ quantum enumeration calls, meaning that the GCost of the operation would be proportional to $H_{n/2}$, which is approximately the cost of fully-classical enumeration.

$k \approx n$, which means that we would be running some quantum enumeration, but the bulk of the enumeration would anyway be classical, nullifying any possible speedups from quantum enumeration.

While the case $k \approx 1$ is possible, requiring to tolerate a high enough MaxDepth to traverse most of the enumeration tree within the quantum subroutine is quite restricting; in particular, in light of the rule-of-thumb numbers from Section 3.1.

A possible alternative approach for the quantum phase of the attack is to collect all the subtrees rooted on level k under a single tree, by adding a "virtual" root node as the "parent" to all the nodes in Z_k, and to run quantum enumeration on this tree; we illustrate this in Fig. 3 for multiple virtual nodes. This approach has the advantage of running a single quantum enumeration rather than H_k many, potentially achieving a better speedup than in the previous case. However, this comes at a cost in terms of QRACM [36,49,42], since the $g_i \in Z_k$ would need to be first enumerated and then stored in memory, to be accessible for the quantum algorithm. Except for $k \approx 1$ or $k \approx n$, this approach may require a super-exponential amount H_k of QRACM for any meaningfully small value of k such that a speedup can be achieved (say, for $k \lessapprox n/2$).

Given the issues of the two methods above, we consider an interpolation of both. We assume to have access to enough QRACM to store at a time 2^y nodes on level k. We combine classical and quantum enumeration by using a classical enumeration routine CE to visit up to 2^y nodes $\{g_i\}_i \in Z_k$, and collect them under a *virtual* root node v as to form a tree $\mathcal{T}(v)$. We then run quantum enumeration on $\mathcal{T}(v)$. If we find a short leaf in $\mathcal{T}(v)$, we terminate. Otherwise, we resume CE and repeat the collection and the quantum enumeration processes.

Let $(g_i)_i = g_1, g_2, \dots \in \mathcal{T}$ be the sequence of nodes in the full enumeration tree $\mathcal{T}$ visited in order by CE. Let $g_{k_1}, g_{k_2}, \dots \in Z_k$ be the subsequence of $(g_i)_i$ of nodes *on level* k. Let $S_1 = \{g_{k_1}, \dots, g_{k_{2^y}}\}, S_2 = \{g_{k_{2^y+1}}, \dots, g_{k_{2^y+2^y}}\}, \dots \subset Z_k$ be the subsets of size 2^y that our combined classical-quantum enumeration routine collects under virtual nodes v_i, such that S_i is the set of nodes on the first level of the subtree $\mathcal{T}(v_i)$. To be able to estimate the cost we make the following conjecture.

Conjecture 2 *Consider $V_i :=$ GCost(FindMV($\mathcal{T}(v_i)$)) as random variables under the randomness of the distribution of enumeration trees for random lattices. Then the V_i are identically distributed.*

In Appendix E we present experimental evidence supporting this conjecture in the case of pruned enumeration. Under Conjecture 2, we estimate that the expected quantum gate cost of combined classical-quantum enumeration is approximately

$$\underset{\substack{\text{random}\\ \text{tree } \mathcal{T}}}{\mathbb{E}}[\text{Quantum GCost}] \approx \underset{\substack{\text{random}\\ \text{tree } \mathcal{T}}}{\mathbb{E}}\Big[\sum_{\substack{v,\text{ out of the}\\ (1/2)\cdot H_k/2^y \text{ many}}} \text{GCost}(\text{FindMV}(\mathcal{T}(v)))\Big]$$

$$= \frac{1}{2} \cdot \frac{H_k}{2^y} \cdot \mathbb{E}[\text{GCost}(\text{FindMV}(\mathcal{T}(v)))] \quad (\text{by Wald's identity}), \qquad (5)$$

where the factor of 1/2 is due to the lattice's additive symmetry.

Expected cost of one quantum enumeration. After having illustrated how to divide the classical and quantum components, we move our attention to computing the expected gate-cost of FindMV on subtrees $\mathcal{T}(g)$ rooted at some node g. Here, we repurpose the analysis from Section 3.1, adapting it to the case where the enumerated tree is rooted on level k and has depth $h \leq n - k + 1$.[5]

We start by recalling Eq. (3) for the gate-cost of FindMV for a tree $\mathcal{T}(g)$ of height h and with at most $\mathcal{C}$ children per node, following the analysis in Section 3.1, which is

$$\begin{aligned} \text{GCost}(\text{FindMV}(\mathcal{T}(g))) &= \text{DF}(\mathcal{T}(g)) \cdot \text{QD}(\mathcal{T}(g)) \cdot \text{WQ}(\mathcal{T}(g), \mathcal{W}) \cdot \text{GCost}(\mathcal{W}) \\ &\geq \sqrt{\#\mathcal{T}(g) \cdot h} \cdot \text{GCost}(\mathcal{W}). \end{aligned}$$

The GCost of operator $\mathcal{W}$ and the expected number of repetitions are independent of each other, and thus, the respective cost can be analyzed individually. The cost of the former is explored in Section 4, while we elaborate on the number of repetitions for a single tree next.

To compute $\mathbb{E}\,[\text{GCost}(\text{FindMV}(\mathcal{T}(g)))]$ we first notice that $\text{DF}(\mathcal{T}(g))$ and $\text{QD}(\mathcal{T}(g))$ are constant quantities in our analysis (namely, we set both to 1), although in general they depend on the lattice problem and our setup of the full algorithm (such as in the choice of k, which would be done a priori based on cost estimations), as we describe in Appendix H. Similarly, we set $h = n - k + 1$. Hence, $\text{DF}(\mathcal{T}(g))$, $\text{QD}(\mathcal{T}(g))$, and h do not have a probability distribution, and do not affect the computation of the expectation. Similarly, the design of $\mathcal{W}$ is done *a priori*, and thus, the resulting $\text{GCost}(\mathcal{W})$ is a constant[6] (cf. Section 4).

Remark 2. We must note that if the enumeration bound R is small enough to guarantee only a few marked leaves in the full enumeration tree as in our case, then the subtrees $\mathcal{T}(g)$ will likely often contain no marked leaf, and hence be of height strictly smaller than $n - k + 1$. On the one hand, this means that on most of the $\mathcal{T}(g)$ trees, DetectMV will be called only once at the root, meaning

[5] The "+1" term coming from adding a "virtual" root node.

[6] Before applying the quantum operator $\mathcal{W}$, one has to define the circuit using an upper bound on the depth of the subtrees, since this depth cannot be determined from the root node alone. Since one of them will contained the marked vertex (and hence be of full height), we have to prepare the $\mathcal{W}$ circuit to tolerate traversing a full-height subtree. This is then constant for all calls to $\mathcal{W}$.

$\mathrm{DF}(\mathcal{T}(g)) = 1$ (cf. Section 3.1). On the other hand, as part of $\mathrm{WQ}(\mathcal{T}(g), \mathcal{W})$ we must nonetheless assume "full height" $h = n-k+1$, since the few trees containing marked leaves are of this height. Underestimating the tree height during QPE would mean that the marked leaves would not be found by FindMV. As we are aiming for strict lower bounds, we do not consider the full height of the implicit binary tree from Aono, Nguyen and Shen [13].

This leaves us with having to estimate $\mathbb{E}[\sqrt{\#\mathcal{T}(g)}]$. As pointed out in [13], the probability distribution of the number of nodes in enumeration trees (or subtrees, such as $\mathcal{T}(g)$) is not known. Jensen's inequality gives an upper bound $\sqrt{\mathbb{E}[\#\mathcal{T}(g)]}$ but no clear lower bound. We address this by defining the *multiplicative Jensen's gap*, and evaluate the cost of the attack for different values of it.

Definition 1 (Multiplicative Jensen's gap). *Let X be a random variable. We say X has multiplicative Jensen's gap 2^z if $\sqrt{\mathbb{E}[X]} = 2^z\,\mathbb{E}[\sqrt{X}]$.*

This leaves us to having to estimate $\mathbb{E}[\#\mathcal{T}(g)]$. Given a "virtual" node g collecting 2^y subtrees rooted at nodes $\{g_1, \dots, g_{2^y}\} \subset Z_k$, by linearity of expectations

$$\mathop{\mathbb{E}}_{\mathcal{T},\{g_i\}_i}[\#\mathcal{T}(g)] = 1 + \sum_{i=1}^{2^y} \mathop{\mathbb{E}}_{\mathcal{T},\{g_i\}_i}[\#\mathcal{T}(g_i)] = 1 + 2^y\,(1 + N_{k,h}) = 1 + 2^y + 2^y \sum_{j=1}^{h} S_{k,j},$$

where the expectation is taken over the distribution of random trees $\mathcal{T}$, and $\{g_1, \dots, g_{2^y}\}$ is assumed to be as a set of random elements of Z_k. While this may not be exactly true, as it may be easier to find "related" elements in Z_k, where their coefficient vectors are similar, we believe this gives a good approximation of the cost.

To lower bound $S_{k,j}$, we start by observing that the $W_{k,j}(g)$ partition the set Z_{k+j}, since every element in the latter descends from a unique element $g \in Z_k$. By the definition of expectation,

$$S_{k,j} = \mathop{\mathbb{E}}_{\substack{g\sim U(Z_k)\\ \text{rand. } \mathcal{T}}}[|W_{k,j}(g)|] = \mathop{\mathbb{E}}_{\substack{\text{random}\\ \text{tree } \mathcal{T}}}\left[\sum_{g\in Z_k} \frac{|W_{k,j}(g)|}{|Z_k|}\right] = \mathop{\mathbb{E}}_{\substack{\text{random}\\ \text{tree } \mathcal{T}}}\left[\frac{|Z_{k+j}|}{|Z_k|}\right].$$

We then make a further conjecture to bound the expectation.

Conjecture 3 *Given a random enumeration tree generated as part of BKZ-β reduction for β large enough such that the Gaussian heuristic applies,*[7] *a level $k \geq 1$, and a node $g \in Z_k$, the expected number of nodes in level $k+j$ descending from g is $\mathbb{E}\left[\frac{|Z_{k+j}|}{|Z_k|}\right] \geq \frac{1}{2} \cdot \frac{\mathbb{E}[|Z_{k+j}|]}{\mathbb{E}[|Z_k|]} = \frac{1}{2} \cdot \frac{H_{k+j}}{H_k}$, where the expectation is taken over the distribution of random trees $\mathcal{T}$, and g is uniformly distributed in Z_k.*

In Appendix B, we provide experimental evidence supporting Conjecture 3. In Appendix C we further observe that in practice often the stronger approximation $S_{k,j} \approx H_{k+j}/H_k$ holds.

[7] Experimentally, $\beta > 45$ appears to be sufficient.

Combining all the steps above gives us a heuristic estimation of

$$\begin{aligned}\underset{\substack{\text{random}\\ \text{tree } \mathcal{T}}}{\mathbb{E}}[\text{Quantum GCost}] &\approx \frac{1}{2}\cdot\frac{H_k}{2^y}\cdot\mathbb{E}\left[\text{GCost}(\text{FindMV}(\mathcal{T}(g)))\right]\\ &\geq \frac{1}{2}\cdot\frac{H_k}{2^y}\left(\frac{1}{2^z}\sqrt{\left(1+2^y+2^{y-1}\sum_{j=1}^{n-k+1}\frac{H_{k+j}}{H_k}\right)(n-k+1)}\right)\text{GCost}(\mathcal{W}),\end{aligned} \quad (6)$$

reducing the estimation of a lower bound on the expected cost to the estimation of H_i and $\text{GCost}(\mathcal{W})$. The estimation of H_i can be done using standard lattice cryptanalysis techniques; we provide a detailed derivation in the case of no pruning and of extreme cylinder pruning in Appendix A. Estimations for $\text{GCost}(\mathcal{W})$ are discussed in Section 4.1.

The same approach can be used to determine the depth of quantum phase estimation of $\mathcal{W}$, which is the limiting factor in a runtime analysis with limited depth budget, resulting in

$$\begin{aligned}&\text{T-Depth}(\text{QPE}(\mathcal{W}))\\ &\quad\geq \frac{1}{2^z}\sqrt{\left(1+2^y+2^{y-1}\sum_{j=1}^{n-k+1}\frac{H_{k+j}}{H_k}\right)(n-k+1)}\cdot\text{T-Depth}(\mathcal{W}).\end{aligned} \quad (7)$$

3.4 Combined Enumeration of a Set of Trees

In the context of enumeration with extreme pruning [34] one considers a trade-off between the success probability of finding a short vector and the number of nodes pruned. Let p be the probability that the enumeration tree contains a node corresponding to a sufficiently short lattice point, that is $p = 1$ if the full tree is enumerated and $p < 1$ if branches are pruned. In the case of extreme pruning, $p \ll 1$, meaning that enumeration of the tree is much cheaper, but likely to fail. To boost the success probability, the original lattice basis is re-randomized M times, for some large value of M. Under assumptions of independence between the resulting re-randomized pruned trees, the probability of finding a short vector in at least one of the M pruned trees is $1-(1-p)^M = 1-(1-Mp+\mathcal{O}(p^2))$, which is high if $M \approx 1/p$ as $M \gg 1$. It should be noticed that in practice re-randomization usually lowers the quality of the bases, essentially "undoing" some of the lattice reduction [3, §2.5]. However, we will ignore this effect for the sake of finding a simple lower bound and assume that the quality of re-randomized bases for the same lattice is the same as the one for the original basis. Moreover, we assume that pruned trees corresponding to these re-randomized bases are independent of each other.

For our purposes, we will collect the M trees corresponding to M bases into a single tree $\mathcal{T}^M$, by adding a top "super-tree" connecting their roots to an overall root. Let r be the root node of this new tree and let $r_1, r_2, ..., r_M$ be the root nodes

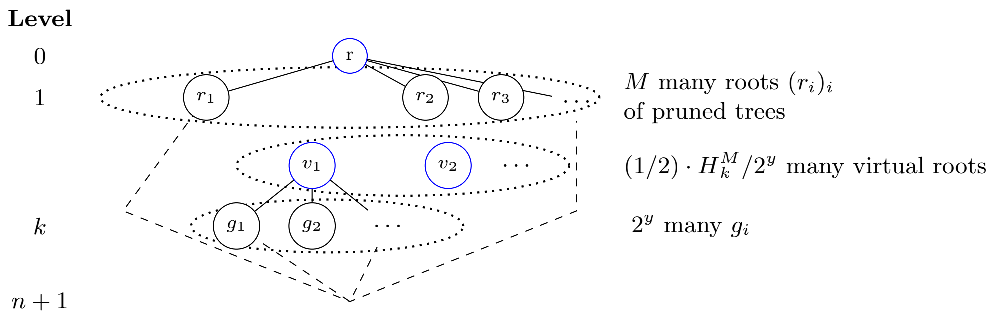
Level
0
1
k
$n+1$
r
r_1
r_2
r_3
v_1
v_2
g_1
g_2
M many roots $(r_i)_i$ of pruned trees
$(1/2) \cdot H_k^M / 2^y$ many virtual roots
2^y many g_i

Figure 3: Full enumeration tree $\mathcal{T}^M$ for combined classical-quantum enumeration. Nodes and links in blue correspond to "virtual" nodes.

of the enumeration trees with the re-randomized bases $(B_i)_{i=1}^M$. We arrange r as parent node of the r_i; a sketch of the full tree is illustrated in Fig. 3. The backtracking predicate (cf. Section 2.2) that decides on branching on input of a node r_i will always return INDETERMINATE on the levels 0 and 1, since all enumeration subtrees rooted at the respective r_i are independent of each other due to basis re-randomisation. We define a quantity H_k^M counting the expected number of nodes on level k of $\mathcal{T}^M$, in terms of $H_k^{(i)} := \mathbb{E}[\#\{\text{nodes on level } k \text{ of } \mathcal{T}(r_i)\}]$ (that is "H_k from tree $\mathcal{T}(r_i)$"), where $\mathcal{T}(r_i)$ is the pruned enumeration tree rooted at r_i. It follows that $H_0^M = 1$, $H_1^M = M$, and $H_k^M = \sum_{i \in [M]} H_{k-1}^{(i)} = M \cdot H_{k-1}$ if $k > 1$. From H_k^M we can then redefine $S_{k,j}^M$ similarly to $S_{k,j}$, reducing it to H_{k-1}. This means that we can "port" our cost formulae from Section 3.3 by replacing H_k with H_k^M. We estimate H_k^M in the cases of no pruning and of extreme cylinder pruning in Appendix A, since this is a standard computation taken from [34,12], and continue with the cost estimation GCOST($\mathcal{W}$) in the next subsection.

4 Instantiations for the Quantum Operator $\mathcal{W}$

In this section, we focus on exploring lower bound costs for the quantum operator $\mathcal{W}$. At its core, quantum enumeration consists of multiple repetitions of QPE on the operator $\mathcal{W}$ (see Fig. 1). In estimating whether quantum enumeration could be leveraged under a MAXDEPTH constraint, $\mathcal{W}$ plays two roles. First, its depth T-DEPTH($\mathcal{W}$) plays a part in determining how much classical *versus* quantum enumeration is used, by constraining the admissible values for k, y and z (cf. Eq. (7)) based on the requirement that T-DEPTH(QPE($\mathcal{W}$)) $\leq$ MAXDEPTH, since by Corollary 1 the gate depth of QPE is partly determined by T-DEPTH($\mathcal{W}$). Second, its gate-cost GCOST($\mathcal{W}$) is a factor in estimating the total cost of the attack.

Table 1: Used T-gate count and depth asymptotics for quantum arithmetic circuits on x-bit numbers.

Operation	T-Depth	GCost	Reference
Addition and Comparison	$\mathcal{O}(\log x)$	$\mathcal{O}(x)$	[28] or [37, Table 2]
Multiplication and Squaring	$\mathcal{O}(\log^2 x)$	$\mathcal{O}(x \log(x) \log(\log(x)))$	[61]

4.1 Query-Based Model

The query-based model assumes access to a black-box oracle that computes on-demand the operator $\mathcal{W}$ on any input. Therefore, we account any query to the operator as having "unit cost", meaning $\text{T-Depth}(\mathcal{W}) = \text{GCost}(\mathcal{W}) = 1$. This setting implies a conservative lower bound on the cost of quantum enumeration. It also represents the setting where classical-quantum enumeration can make the most of any hypothetical quantum speedups.

4.2 Circuit-Based Model

Here, we aim to estimate the size of a *minimal* or *smallest known* quantum operator $\mathcal{W}$ in the circuit-model. The objective is to provide a more realistic lowest-known bound on the gate cost (*i.e.*, number of T gates) of $\mathcal{W}$ than the very conservative query-based model. Our focus is on finding an approximate smallest T-count and T-depth for arithmetic operations used inside of $\mathcal{W}$. We claim that, at a minimum, the operator $\mathcal{W}$ has to implement a predicate P deciding whether a projected lattice point has norm larger than the pruning bound R_i. We assume that each coefficient of the state vector $|c_i\rangle$ consists of $\lambda = \lceil \log q \rceil$ qubits. Whenever we require floating point arithmetic, we follow [40] assuming double precision is used, meaning $\xi = 53$ bits of precision are required. To estimate a lower bound to the cost of the minimal circuit for $\mathcal{W}$, we ignore the cost for all operations except for the bare minimum arithmetic that is required to compute the single, most expensive lattice point projection.

Size of quantum arithmetic circuits. The quantum arithmetic literature contains many design proposals for integer and floating point adders and multipliers. We report the smallest (to our knowledge) in Table 1. During our computations, we will be ignoring constants and lower order terms hidden by the $\mathcal{O}$. We refer the reader to Appendix F for a more detailed literature review.

Depth and cost estimation of $\mathcal{W}$. In our setting, quantum enumeration is being performed on a tree $\mathcal{T}(g \in Z_k)$ corresponding to a lattice coset of dimension $h = n-k$, where n is the dimension of the full lattice $\Lambda = \Lambda(b_1, \dots, b_n)$ being enumerated. This process would require performing arithmetic using the projected lattice basis vectors $(\pi_{n-\ell+1}(b_{n-\ell+1}), \dots, \pi_{n-\ell+1}(b_{n-k}))$ of Λ for all levels $k < \ell \leq n$. An operator $U_P^{\min}$ is designed as to evaluate the predicate P which identifies projected vectors $v \in \pi_{n-\ell+1}(\Lambda)$ such that $||v|| \leq R_\ell$ and $\pi_{n-k+1}(v) = g$.

Table 2: Assumed cost of arithmetic operations to implement predicate. Each operation has input numbers of bit length x_i and outputs numbers of size x_{i+1}.

Operation	Input bit lengths	T-DEPTH	GCOST
1, parallel multiplication	$x_0 = \min(\lambda, \xi)$	$\log^2(x_0)$	$h^2 \cdot x_0 \log(x_0) \log(\log(x_0))$
2, binary tree addition	$x_1 = \lambda + \xi$	$\log h \cdot \log(x_1)$	$h^2 \cdot x_1$
3, squaring	$x_2 = x_1 + \log h$	$\log^2(x_2)$	$h \cdot x_2 \log(x_2) \log(\log(x_2))$
4, binary tree addition	$x_3 = 2\, x_2$	$\log h \cdot \log(x_3)$	$h \cdot x_3$
5, comparison	$x_4 = x_3 + \log h$	$\log(x_4)$	x_4

In order to lower-bound the cost of operation, we only consider the case of evaluating this inequality at $\ell = n$, where $(\pi_{n-\ell+1}(b_{n-\ell+1}), \ldots, \pi_{n-\ell+1}(b_{n-k})) = (b_1, \ldots, b_h)$. Evaluating predicate P becomes checking whether $|| \sum_{i \leq h} c_i b_i||^2 \leq R^2 - ||g||^2$ for some integer coefficients $(c_i)_i$. Since $(b_1, \ldots, b_h)$ span an h-dimensional vector space, we consider them to be h-dimensional by assuming an appropriate change of basis was applied.[8] Our estimate for the cost of $U_P^{\min}$ is derived as in Table 2 applying the following sequence of operations:

1. Parallel multiplication of h^2 pairs $(c_i, (b_i)_j) \mapsto c_i(b_i)_j$, of λ- and ξ-bit length, outputting numbers of bit length $\lambda + \xi$.
2. Addition of coefficients $(c_1(b_1)_j, \ldots, c_h(b_h)_j) \mapsto \sum_i c_i(b_i)_j$ for $j \in [h]$. These additions can be run in parallel over j. For a fixed j, the corresponding sum is run by adding terms in pairs, forming a binary tree of sums. Each $\sum_i c_i(b_i)_j$ output is $\lambda + \xi + \log h$ bits long.
3. Squaring $\sum_i c_i(b_i)_j$ sums in parallel (output bit length $2(\lambda + \xi + \log h)$).
4. Adding the squared sums in a binary-tree fashion to obtain $|| \sum_{i \leq h} c_i b_i||^2 = \sum_j (\sum_i c_i(b_i)_j)^2$ of bit length $2(\lambda + \xi + \log h) + \log h$.
5. Comparison with the (adjusted) pruning bound $R^2 - ||g||^2$.

In this setting, for the purpose of estimating a minimum cost of the attack we consider the depth and gate-cost of $\mathcal{W}$ to correspond to the sum of depths and costs of the five operations above, resulting in Corollaries 2 and 3.

Corollary 2. *The* GCOST *in the "Circuit-Based Model" is*

$$\begin{aligned}\mathrm{GCost}(\mathcal{W}) \geq\ & h^2 \cdot \min(\lambda, \xi) \log(\min(\lambda, \xi)) \log(\log(\min(\lambda, \xi))) \\ & + h^2 \cdot (\lambda + \xi) \\ & + h \cdot ((\lambda + \xi) + \log h) \log(((\lambda + \xi) + \log h)) \log(\log(((\lambda + \xi) + \log h))) \\ & + h \cdot 2\,((\lambda + \xi) + \log h) + \ 2\,((\lambda + \xi) + \log h) + \log h.\end{aligned} \quad (8)$$

[8] In classical implementations, this computation benefits from caching of Gram-Schmidt orthogonalisation operations and results [78]. Asymptotically, the number of individual arithmetic operations is the same as computing directly from $(b_1, \ldots, b_h)$.

Table 3: Kyber parameters [77, Sec 4.3] with respective BKZ block-sizes required for the primal attack; column $\log \#\mathcal{T}^M$ reports our estimated lower bound on the number of nodes of the enumeration tree of dimension β using extreme cylinder pruning with $M = 2^{64}$ and success probability ≈ 1, following [12, Eq. (16)].

Scheme	LWE dim. n	Modulus q	Block-size β	$\log \#\mathcal{T}^M$	targeted AES security
Kyber-512	512	3329	406	172.5	AES-128
Kyber-768	768	3329	623	323.2	AES-192
Kyber-1024	1024	3329	873	517.7	AES-256

Corollary 3. *The* T-Depth *in the "Circuit-Based Model" is*

$$\begin{aligned}\text{T-Depth}(\mathcal{W}) \geq &\log^2(\min(\lambda, \xi)) + \log h \cdot \log((\lambda + \xi)) \\ &+ \log^2(((\lambda + \xi) + \log h)) \\ &+ \log h \cdot \log(2\,((\lambda + \xi) + \log h)) \\ &+ \log(2\,((\lambda + \xi) + \log h) + \log h).\end{aligned} \tag{9}$$

5 Estimating Quantum Enumeration Attacks on Kyber

In Sections 3 and 4, we have described methods to explore the enumeration tree under a MaxDepth limitation (cf. Sections 3.3 and 3.4), and introduced two different instantiations of the quantum backtracking operator $\mathcal{W}$. In this section, we leverage these results to present cost estimations for primal lattice reduction attacks using quantum enumeration against *Kyber* [77], the PQ KEM selected by NIST for standardisation in 2022. To that end, we compute lower bounds on the cost of combined classical-quantum cylinder pruning in the gate-cost metric against the three different parametrisations of Kyber (cf. Table 3). For each of them, we consider attacks within MaxDepth $= 2^{40}, 2^{64}, 2^{96}$, as suggested by NIST [62], each assuming the two different instantiations of the operator $\mathcal{W}$ outlined in Section 4.

5.1 Attack Setting

Our aim in this section is to estimate a lower bound on the possible cost of classical-quantum enumeration in the setting of lattice-based cryptography. As a case-study, we look at the *primal attack* on Kyber, where a block lattice reduction algorithm is used to recover the secret key of the cryptosystem by reducing an embedding lattice [15] constructed using the public key.

We follow the convention of using BKZ as the lattice reduction algorithm, and assume that its SVP oracle is instantiated using our classical-quantum enumeration approach. The common approach to primal attack estimates is to choose a *cost model* for BKZ that accounts for the cost of running the SVP oracle and for the number of calls made [5]. Normally, cost models will use a closed formula for the cost of enumeration in dimension β to account for the cost of the SVP oracle, either fitted or derived from theory or experiments. This is then used with some estimation script such as the `lwe-estimator` [8], which will simulate the effect of lattice reduction and find the cheapest parametrisation of the attack leading to high success probability.

Since our setting involves an implicit relation between the gate-cost of the SVP oracle and the MaxDepth constraint, we do not attempt to fit our results on a curve as a function of β. Instead, we opt for calling an estimator script assuming the optimistic cost of classical enumeration obtained as part of our analysis (cf. Appendix A), which assumes that input bases achieve a linear lattice profile (as predicted by the Geometric Series Assumption, using the root-Hermite factor $((\pi\beta)^{1/\beta}\beta/(2\pi e))^{1/(2(\beta-1))}$ from [23]) resulting in a generous lower bound of the cost of solving SVP via enumeration, $2^{\beta \log \beta/8+O(\beta)}$, and assuming specifically the lower bound costs for extreme cylinder pruning proven in [12]. From this cost estimation we obtain three different block sizes β for the three parameter sets of Kyber, reported in Table 3. We then proceed to estimate the gate-cost of classical-quantum enumeration in dimension β under different MaxDepth values, and compare these with the corresponding approximate gate-cost of Grover search on AES for the corresponding category (e.g., Kyber-512 with AES-128).

It is important to highlight an issue towards claiming lower bounds on the cost of classical-quantum enumeration, and how we address it. As pointed out in [13] and mentioned in Section 3, the expected speedup of quantum enumeration over equivalent classical enumeration may be more than quadratic, depending on the probability distribution of the size of the trees being enumerated, due to Jensen's inequality implying $\mathbb{E}[\sqrt{\#\mathcal{T}}] \leq \sqrt{\mathbb{E}[\#\mathcal{T}]}$. Since we would like to provide lower bounds to the expected attack cost, we define $z \geq 0$ such that $\mathbb{E}[\sqrt{\#\mathcal{T}}] = 2^{-z}\sqrt{\mathbb{E}[\#\mathcal{T}]}$, and estimate the attack cost for $z = 0, \ldots, 64$. While we do not know what the value of z may be for lattices encountered in cryptanalysis,[9] this allows us to delegate the estimation of the concrete cost to future analysis on the distribution of $\#\mathcal{T}$, while clearly identifying *threshold values* z_0, such that $z \geq z_0$ may imply possible effective attacks, while $z < z_0$ would indicate that classical-quantum enumeration would not threaten Kyber's security.

We note that an alternative approach could be deriving a lower bound to the Jensen's gap, depending on some other parameter of the problem. We attempt this approach in Appendix I, where we derive bounds depending on the variance of $\#\mathcal{T}$. This, however, presents the same issue as above, namely that we are not aware of the exact distribution of $\#\mathcal{T}$. This means that while it provides a different formulation of the problem, it currently does not represent a better alternative to testing many values of z and looking for threshold values. We do, however, note that preliminary results in Appendix E suggest that the distribution may be relatively narrowly distributed about its mean.

[9] Albeit not at cryptographically relevant sizes, in Appendix D we present the results of small-dimension measurements of the Jensen's gap against q-ary lattices. For pruned enumeration in dimension $\beta \approx 60$, the gap appears to be around $z \approx 1$.

Table 4: Attack parameters for experimental evaluation.

$\text{MaxDepth} \in \{2^{40}, 2^{64}, 2^{96}\}$,	$y \in \{0, \dots, 64\}$,	$z \in \{0, \dots, 64\}$,	$M = 2^{64}$,
$n \in \{406, 623, 873\}$,	$k \in [n]$, $h = n-k+1$,	$\text{DF}(\cdot) = \text{QD}(\cdot) = 1$,	$\text{WQ}(\mathcal{T}) = \sqrt{\#\mathcal{T} \cdot h}$

Overall, our estimation code for the cost of enumeration on a β-dimensional lattice bases is given on input a multiplicative Jensen's gap 2^z, a MaxDepth constraint, a number of bases M used during extreme pruning (here, $M = 2^{64}$), a maximum number Y of tree nodes that can be stored in QRACM (here, $Y = 2^{64}$), an estimate on the size of the quantum backtracking operator $\mathcal{W}$ and on the values for DF, QD, and WQ, and pruning parameters for estimating upper bounds on H_k, and optimizes the level k which separates classical and quantum enumeration as well as the maximal number 2^y of nodes on this level to be combined under a virtual root, looking for the cheapest possible attack. We estimate the cost assuming extreme pruning attacks targeting success probability ≈ 1.

An overview over all parameters used in the estimation process is given in Table 4, while the costing loop is presented in Figure 4. We have made the source code used to produce our experimental results, tables, and plots publicly available at https://github.com/mtiepelt/QuantumLatticeEnumeration.

5.2 Cost Estimation of the Attack

Cost metrics and success conditions. As mentioned in Section 2.3, the cost of a quantum algorithm can be measured using various metrics. In this paper, we prefer to focus on the number of classical and quantum gates required by the attack in total, since, plausibly, applying one quantum gate requires running one classical computation on some microcontroller [43], meaning that to some extent these two quantities can be compared and combined. As such, one could say a classical-quantum enumeration attack was successful if the total number of gates required[10] was lower than some threshold capturing some security notion.

The success of an attack can be defined in multiple ways. One can note that submissions to the NIST standardization process, such as Kyber, were required to propose parameters for cryptographic primitives as hard to break as AES or SHA (depending on the targeted security category). This would imply a notion where a quantum attack against Kyber may be considered successful only if its cost is lower than the number of gates required to run Grover search against AES, which we estimate using Tables 10 and 12 of [41].[11] It should be noticed

[10] We lower bound this as the number of nodes visited in the classical phase plus the number of quantum gates applied during the quantum phase of the attack.

[11] Under no MaxDepth constraint, [41, Table 10] suggests that the GCost of key recovery against AES-128 (resp. AES-192, AES-256) with success probability ≈ 1 is $\approx 2^{83}$ (resp. 2^{115}, 2^{148}). Under a depth constraint, [41, Table 12] suggests the GCost $\approx 2^{157}/\text{MaxDepth}$ (resp. $2^{221}/\text{MaxDepth}$, $2^{285}/\text{MaxDepth}$). We note that further improvements in the design of the Grover oracles against AES have achieved minor speedups in terms of overall gate cost.

that the reason for such a separation between classical and quantum attacks is due to the assumed and yet-unknown hidden costs of quantum computation.

While the comparison with the cost of Grover on AES is our primary success metric for the attack, in Appendix G.1 we investigate the cost of the attack with respect to possible alternative success metrics. In the following paragraphs we proceed to explore whether combined classical-quantum enumeration could *plausibly* be cheaper than Grover search on AES, where plausibility depends on the value of the multiplicative Jensen's gap required (cf. Definition 1). To be conservative, we compare the cost of Grover search to a simple sum of classical and quantum gate costs for enumeration, which is likely an extremely generous approach towards quantum computation cost estimation.

Dependence on pruning parameters. Since enumeration is being performed on pruned enumeration trees, pruning parameters play an important role in determining the cost of the attacks. Lower bounds for the pruning radii and for the values of H_k in the extreme cylinder pruning setting can be found in [12], while upper bounds can be found via optimization techniques, thanks to the seminal work of Gama, Nguyen and Regev [34]. We discuss in more detail how we obtain both bounds in Appendix A.2. Yet, we want to briefly speculate about three different ways these can be combined to produce different attack cost estimates that we reproduce in Table 5.

Subtree-size estimation is performed leveraging Conjecture 3 where the ratios H_{k+j}/H_k are used to lower bound $\mathbb{E}[|Z_{k+j}|/|Z_k|]$. A first cautious approach, that we label "**LB/UB**", is to strictly lower bound H_{k+j}/H_k by taking the lower bound of H_{k+j} and dividing it by the upper bound of H_k. A more speculative approach could be that of assuming that the pruning parameters obtained via optimisation, and used to determine the upper bound, cannot be significantly improved. In this scenario, that we label "**UB/UB**", the upper bounds are assumed to be exact values, and the previous numerator can be replaced with an upper bound for H_{k+j}. Finally, one could instead speculate that the optimal pruning parameters found are only a local optimum, and pruning radii closer to the lower bounds can potentially be found. In this scenario, that we label "**LB/LB**", one could imagine that the radii for H_k, when $k < n$, could be improved, leading to $\mathbb{E}[|Z_{k+j}|/|Z_k|]$ being closer to the ratio of lower bounds from [12]. This latter scenario could counter-intuitively reduce the overall cost of classical enumeration, but increase the average size of subtrees rooted on level k. In the remainder of the article, we report gate-cost estimates in these three scenarios.

Cost estimation without MaxDepth restrictions. We start by estimating the cost of enumeration without MaxDepth restrictions—the most favorable setting to the adversary. In this setting, a quadratic speedup in terms of quantum depth can be achieved as the full enumeration tree can be enumerated directly within a call to FindMV, meaning no classical phase is required. This means, the attack consists of calling FindMV($\mathcal{T}^M$) once. No QRACM is needed, and the classical cost is null. We do notice that this is not necessarily optimal but we

```
CostingLoop($n$, MaxDepth, $Y = 2^{64}$, $Z = 2^{64}$)
1 :  for $z \in \{0, 1, 2, ..., \log(Z)\}$
2 :    $k \leftarrow n + 1$
3 :    while $LB$(T-Depth(QPE($\mathcal{W}$))) $\leq$ MaxDepth and $k \geq 0$
4 :        $y \leftarrow$ Largest $y \in \{0, 1, 2, ..., \log(Y)\}$
5 :              s.t. $LB$(T-Depth(QPE($\mathcal{W}$))) $\leq$ MaxDepth
6 :        // store classical cost and quantum cost
7 :        CC $\leftarrow \mathbb{E}_{\text{random tree } \mathcal{T}}$[Classical GCost]
8 :        QC $\leftarrow LB(\mathbb{E}_{\text{random tree } \mathcal{T}}$[Quantum GCost])
9 :        GCost[$z$][$y, k$] $\leftarrow$ CC + QC
10 :       $k \leftarrow k - 1$
11 : return $\left(\min_{y,k}(\text{GCost}[z])\right)_{z \in \{0,1,2,...,\log(Z)\}}$
```

Figure 4: Pseudocode for cost estimation under MaxDepth constraint, following Eq. (7). GCost$[z][y, k]$ is the total cost associated with the quantum enumeration (*i.e.*, the sum of Eq. (6) and Eq. (4)) with $M = 2^{64}$. Operator $\mathcal{W}$ is instantiated according to Section 4.1 and Section 4.2, respectively. $LB(\cdot)$ stands for "lower bound of".

consider it as it is a good reference for the cost of other attacks. We report the cost of this attack under MD $= \infty_{k=0}$ in Table 5. This is also the state of the art prior to the introduction of combined classical-quantum enumeration. The dependency between the cost of the attack and the Jensen's gap 2^z is straightforward in this setting, with the quantum cost exponentially reducing as z increases. It appears from our estimates that quantum enumeration on Kyber-768 and -1024 may be more expensive than key-search on AES in this setting. Only Kyber-512 appears to be plausibly approachable, $z \geq 7$ sufficing, yet this is still only considering the query model for $\mathcal{W}$. A significantly larger Jensen's gap of $z \geq 32$ is already required in the circuit-based model of $\mathcal{W}$ in Section 4.2. We remark that in this setting Grover search on AES can be very competitive, achieving a full quadratic speedup.

We also consider the cost of running our combined classical-quantum enumeration attack in unlimited depth. Differently from the attack mentioned above, we decide not to fit the entire tree within one quantum enumeration, and rather first perform an optimal amount of classical precomputation. We report the results of this cost estimation in Table 5, under the "MD $= \infty$" rows. This is the minimal cost we find when unlimited quantum depth is available. The results are quite similar to those of fully-quantum enumeration, with only Kyber-512 and -768 appearing possibly easier to attack in the case where Conjecture 3 is instantiated using "**LB**/**UB**" numbers. Yet, even the most aggressive setting ($\mathcal{W}$ as in Section 4.1, using **LB**/**UB**), the query complexity of quantum enumeration on Kyber-512 essentially matches the query complexity of Grover search on

Table 5: Summary of the values for the Jensen's gap 2^z at crossover points of our combined classical-quantum enumeration attacks against Kyber and the cost of Grover's search against AES (cf. [41, Tables 10 and 12]). We remark that exact crossovers happen at fractional values of z. In this table we round down threshold values of z. MaxDepth is abbreviated to MD. X/Y refers to how $\mathbb{E}[|Z_{k+j}|/|Z_k|]$ is estimated for displayed level k (c.f. Section 5.2), Cost is as in Table 6.

less likely to be feasible — more likely to be feasible

		Crossover points when comparing Cost of Grover on AES against the total GCost (cf. Table 6) with …					
		…$\mathcal{W}$ as in Section 4.1			…$\mathcal{W}$ as in Section 4.2		
MD	Kyber	LB/UB	UB/UB	LB/LB	LB/UB	UB/UB	LB/LB
2^{40}	-512	$z \geq 0, k \leq 25$ Cost $\geq 2^{63}$	$z \geq 20, k \leq 11$ Cost $\geq 2^{116}$	$z \geq 12, k \leq 83$ Cost $\geq 2^{115}$	$z \geq 0, k \leq 27$ Cost $\geq 2^{94}$	$z \geq 36, k \leq 22$ Cost $\geq 2^{115}$	$z \geq 28, k \leq 79$ Cost $\geq 2^{115}$
	-768	$z \geq 2, k \leq 84$ Cost $\geq 2^{179}$	$z \geq 61, k \leq 33$ Cost $\geq 2^{180}$	$z \geq 56, k \leq 106$ Cost $\geq 2^{179}$	$z \geq 17, k \leq 73$ Cost $\geq 2^{180}$	$z > 64$	$z > 64$
	-1024	$z \geq 50, k \leq 105$ Cost $\geq 2^{242}$	$z > 64$	$z > 64$	$z > 64$	$z > 64$	$z > 64$
2^{64}	-512	$z \geq 0, k \leq 26$ Cost $\geq 2^{63}$	$z \geq 20, k \leq 9$ Cost $\geq 2^{92}$	$z \geq 12, k \leq 64$ Cost $\geq 2^{91}$	$z \geq 0, k \leq 26$ Cost $\geq 2^{75}$	$z \geq 36, k \leq 5$ Cost $\geq 2^{92}$	$z \geq 28, k \leq 54$ Cost $\geq 2^{91}$
	-768	$z \geq 1, k \leq 64$ Cost $\geq 2^{155}$	$z \geq 61, k \leq 26$ Cost $\geq 2^{156}$	$z \geq 56, k \leq 77$ Cost $\geq 2^{155}$	$z \geq 17, k \leq 67$ Cost $\geq 2^{156}$	$z > 64$	$z > 64$
	-1024	$z \geq 49, k \leq 100$ Cost $\geq 2^{220}$	$z > 64$	$z > 64$	$z > 64$	$z > 64$	$z > 64$
2^{96}	-512	$z \geq 0, k \leq 26$ Cost $\geq 2^{63}$	$z \geq 15, k \leq 1$ Cost $\geq 2^{82}$	$z \geq 7, k \leq 40$ Cost $\geq 2^{82}$	$z \geq 0, k \leq 26$ Cost $\geq 2^{75}$	$z \geq 40, k \leq 1$ Cost $\geq 2^{82}$	$z \geq 31, k \leq 40$ Cost $\geq 2^{82}$
	-768	$z \geq 1, k \leq 53$ Cost $\geq 2^{124}$	$z \geq 61, k \leq 8$ Cost $\geq 2^{124}$	$z \geq 56, k \leq 44$ Cost $\geq 2^{123}$	$z \geq 19, k \leq 43$ Cost $\geq 2^{124}$	$z > 64$	$z > 64$
	-1024	$z \geq 51, k \leq 79$ Cost $\geq 2^{187}$	$z > 64$	$z > 64$	$z > 64$	$z > 64$	$z > 64$
∞	-512	$z \geq 0, k \leq 26$ Cost $\geq 2^{63}$	$z \geq 15, k \leq 1$ Cost $\geq 2^{82}$	$z \geq 7, k \leq 40$ Cost $\geq 2^{82}$	$z \geq 0, k \leq 26$ Cost $\geq 2^{75}$	$z \geq 40, k \leq 1$ Cost $\geq 2^{82}$	$z \geq 31, k \leq 40$ Cost $\geq 2^{82}$
	-768	$z \geq 0, k \leq 37$ Cost $\geq 2^{113}$	$z \geq 59, k \leq 3$ Cost $\geq 2^{114}$	$z \geq 51, k \leq 31$ Cost $\geq 2^{114}$	$z \geq 24, k \leq 37$ Cost $\geq 2^{114}$	$z > 64$	$z > 64$
	-1024	$z \geq 59, k \leq 33$ Cost $\geq 2^{147}$	$z > 64$	$z > 64$	$z > 64$	$z > 64$	$z > 64$
$\infty_{k=0}$	-512	$z \geq 7, k = 0$ Cost $\geq 2^{82}$	$z \geq 15, k = 0$ Cost $\geq 2^{82}$	$z \geq 7, k = 0$ Cost $\geq 2^{82}$	$z \geq 32, k = 0$ Cost $\geq 2^{82}$	$z \geq 40, k = 0$ Cost $\geq 2^{82}$	$z \geq 32, k = 0$ Cost $\geq 2^{82}$
	-768	$z \geq 51, k = 0$ Cost $\geq 2^{114}$	$z \geq 56, k = 0$ Cost $\geq 2^{114}$	$z \geq 51, k = 0$ Cost $\geq 2^{114}$	$z > 64$	$z > 64$	$z > 64$
	-1024	$z > 64$	$z > 64$	$z > 64$	$z > 64$	$z > 64$	$z > 64$

AES-128 in the same unbounded depth setting, with the query-complexity of enumeration on Kyber-768 is greater than that of Grover search on AES-192.

Cost estimation with MaxDepth restrictions. We now consider the effect of depth restrictions on the cost of the attack. Depth restrictions mean that we will need to use a combined classical-quantum attack as described in Sections 3.2 and 3.3, where classical enumeration is run up to level k, as to create subsets $\{g_1, \ldots, g_{2^y}\} \subset Z_k$. A "virtual" root node v is added as "parent" of these, and quantum enumeration is run on the resulting tree $\mathcal{T}(v)$. This process requires about 2^y QRACM to store the $\{g_i\}_{i \leq 2^y}$, and is run on the extreme cylinder pruning enumeration tree $\mathcal{T}^M$ from Section 3.4.

To compute Eq. (6) given a Jensen's gap 2^z, we minimize the total cost of the combined classical-quantum enumeration with extreme cylinder pruning using $M = 2^{64}$ re-randomized bases and overall success probability ≈ 1 over $2^y \leq 2^{64}$ and $k \leq n$. For each set of parameters, we only consider those where the depth of QPE($\mathcal{W}$) (cf. Eq. (7)) is no larger than MaxDepth. For every $z \in \{0, ..., 64\}$, we output (y, k) minimizing the total cost. We report our results in Table 5, under the "MD $= 2^{40}, 2^{64}, 2^{96}$" rows.

First, we observe that attacks on Kyber-1024 appear unlikely to beat key-search on AES-256 in all settings. The value of z required to reach an attack costs on Kyber-512 and -768 smaller than those of Grover on AES is relatively low when assuming the strict "LB/UB + query-based model for $\mathcal{W}$" setting (cf. Section 4.1). However, assuming the circuit-based model for $\mathcal{W}$, immediately raises the requirements for a successful attack on Kyber-768 up to $z \geq 17$, suggesting a successful attack may not be too likely. This is likely a fairer comparison, since in the "$\mathcal{W}$ as in Section 4.1" columns we are anyway comparing query-complexity of enumeration versus gate-complexity of Grover on AES. As for Kyber-512, while we cannot fully exclude attacks due to the very conservative analysis made, we note that the estimated gate cost of the attack significantly increases assuming the need for non-trivial circuits for $\mathcal{W}$ ($2^{63} \to 2^{75}$–2^{94}), or that the pruning radii found via optimisation cannot be improved (2^{82}–2^{116}, c.f. the "UB/UB" columns). We note that the cost of Kyber-512 is the same in the MaxDepth $= 2^{96}$ and MaxDepth $= \infty$ cases, since in either case the quantum depth budget is large enough to fit the attack achieving the overall optimal classical-quantum enumeration tradeoff.

We remark that for all attacks identified within $z \leq 64$, we have $k \leq n/2$. This matches our analysis in Section 3.3 since as $k \to n/2$, the cost of the classical phase of combined classical-quantum enumeration would approach the cost of fully classical enumeration, while introducing a further quantum overhead.

An important difference between the bounded- and unbounded-depth settings for combined classical-quantum enumeration is the dependency of the total cost on the Jensen's gap 2^z. Indeed, while in the unbounded setting the cost of the attack is simply proportional to 2^{-z}, in the bounded setting different values of MaxDepth and z imply different amounts of classical precomputation.

Since we do not have a clear prediction of the exact value of z for different enumeration tree distributions, we investigate how sensitive the total cost of the attack is to small changes in z by plotting the predicted classical and quantum gate costs and QRACM requirements as a function of z. In Fig. 5 we show the resulting plots for Kyber-1024 at MaxDepth $= 2^{40}$ and 2^{96} in the query-based model as a representative example. Plots for MaxDepth $= 2^{64}$, Kyber-512 and -768, and for the circuit-based model can be found in Appendix G. Overall, costs appear to decrease smoothly as z increases without major sudden changes. A peculiar phenomenon can be observed, namely the optimal attack is not achieved when the two phases of the attack are balanced. We will elaborate on this next.

Unbalanced classical and quantum cost. In Fig. 5 as well as in Appendix G, the figures show a gap between the costs of the classical and quantum phases, rather

Table 6: Legend for plots and tables reporting attack costs under MaxDepth constraint.

Exp. cost of Grover on AES	Expected GCost for AES key recovery [41, Tab. 12] with prob. ≈ 1
Quantum GCost	Expected combined cost of all quantum circuits enumerating levels below k, cf. Eq. (6)
Exp. cost of class. enum.	Lower bounds on the cost of enumeration with extreme cylinder pruning [12]
Classical GCost	Expected # nodes (cf. Eq. (4)) enumerated classically up to level k
2^{128}, 2^{192}, 2^{256}	Canonical bit security
Total GCost	Classical cost + quantum cost
Quasi-Sqrt (class. cost)	Asymptotic runtime of quantum enumeration, $\approx (2^y \cdot N^M_{k,n-k} \cdot (n-k))^{1/2}$
QRACM	Max. amount of quantum accessible classical memory, constraint on 2^y
2^z	Multiplicative Jensen's Gap, cf. Definition 1
Cost	Value of total GCost at this point
k	Level up to which tree is enumerated classically
MaxDepth	Constraint on T-Depth(QPE($\mathcal{W}$)), cf. Eq. (7)
2^y	# subtrees rooted at level k combined under a single FindMV call, cf. Section 3.3

than having these be balanced. The only parameter determining the classical cost is k. Since in our observed case the classical cost is always smaller than the quantum one, the only option for balancing the two would be by increasing k. Increasing $k \mapsto k+1$ means that the classical cost increases by an additive term $H_{k+1}/2$, while the quantum cost and the quantum depth approximately change by a factor $\sqrt{\frac{n-k-1}{n-k}\frac{H_{k+1}}{H_k}}$ and $\sqrt{\frac{n-k-1}{n-k}\frac{H_k}{H_{k+1}}}$, respectively. How this affects the quantum cost overall will depend on whether H_{k+1}/H_k is larger or smaller than 1 as well as whether a different value of y is chosen as to keep using exactly MaxDepth quantum depth during the attack. From Table 5, it appears that the optimal attacks we find are in the $k < n/2$ regime where $H_{k+1}/H_k > 1$ [34], meaning that increasing k may increase both classical and quantum costs, which is undesirable. Due to the complexity of an analytic analysis, we believe the safer approach is looking for the optimal attack computationally. It would then appear that the lowest *classical plus quantum* cost is achieved with unbalanced quantum and classical costs within the constraints we consider.

Cost estimation beyond lower bounds for $QD(\mathcal{W})$ and $WQ(\mathcal{T}, \mathcal{W})$. In Appendix H, we explore more likely values for $QD(\mathcal{W})$ and $WQ(\mathcal{T}, \mathcal{W})$, and re-estimate the costs presented in this section. Overall, comparing those results (Table 11 in Appendix H) with Table 5 it would appear that the impact of using the results from Appendix H.1 over the query-model numbers in Table 5 is smaller than the impact of moving from a query-based to a circuit-based model for $\mathcal{W}$.

Conclusions. In this paper, we introduced a new quantum algorithm that combines classical and quantum enumeration to circumvent likely restrictions to serial quantum computation, developed a heuristic analysis of its cost in terms of classical and quantum gates and quantum depth, provided lower bounds for the cost, and studied its hypothetical impact on the cryptanalysis of Kyber in various settings as a case-study. On the way, we produced various experimental results on the distribution of subtrees of enumeration trees, and on the hidden constants of quantum enumeration algorithms. From our estimates on Kyber, we see that the asymptotic square-root speedup suggested by previous analysis of quantum enumeration with extreme cylinder pruning are not necessarily guaranteed under a MaxDepth constraint. Rather, achieving asymptotic speedups and "breaks" depends on a vast array of hypothetical developments, such as cheap quantum computation and QRACM, better pruning radii and small quantum circuits for floating point arithmetic, and on known unknowns such as the Jensen's gap for the distribution of enumeration subtree sizes.

While we can say with some confidence that quantum enumeration does not seem to threat parameters in the Kyber-1024 regime, the picture is less clear for smaller schemes. Yet, we stress again the very conservative nature of our analysis. Requiring non-trivial circuits for $\mathcal{W}$ such as those in [16] would likely imply security with respect to AES for Kyber-768 and large absolute gate-costs for attacks against Kyber-512.

We believe that the take-home message of this case-study is that, as analogously noticed in the key-search setting [41], imposing MaxDepth limitations to quantum backtracking appears to present a significant obstacle towards leveraging this technique for lattice cryptanalysis.

Acknowledgements. We would like to thank Sam Jaques for multiple fruitful conversations, Joe Rowell and Shi Bai for help understanding the source code of `fplll`, and Martin R. Albrecht for offering computing power for running our experiments.

This work was supported by the IQC. IQC is supported in part by the Government of Canada and the Province of Ontario. This work was partially funded by the topic Methods for Engineering Secure Systems (No. 46.23.01) of the Helmholtz Association (HGF) and by KASTEL Security Research Labs. This work has been partially supported by the French Agence Nationale de la Recherche through the France 2030 program under grant agreement No. ANR-22-PETQ-0007 EPiQ and ANR-22-PETQ-0008 PQ-TLS. This work was partly supported by the Zurich Information Security and Privacy Center. This work is supported by NOVA LINCS ref. UIDB/04516/2020 (https://doi.org/10.54499/UIDB/04516/2020) and ref. UIDP/04516/2020 (https://doi.org/10.54499/UIDP/04516/2020) with the financial support of FCT.IP.

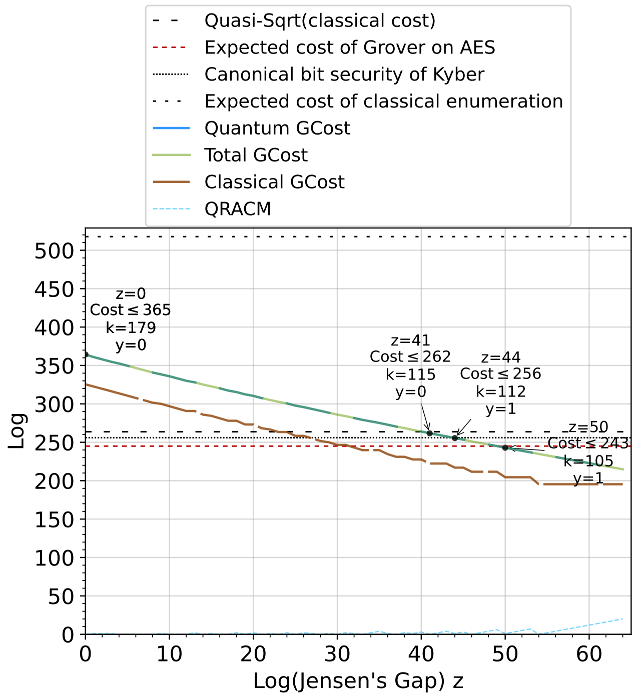

(a) Kyber-1024, MaxDepth $= 2^{40}$.

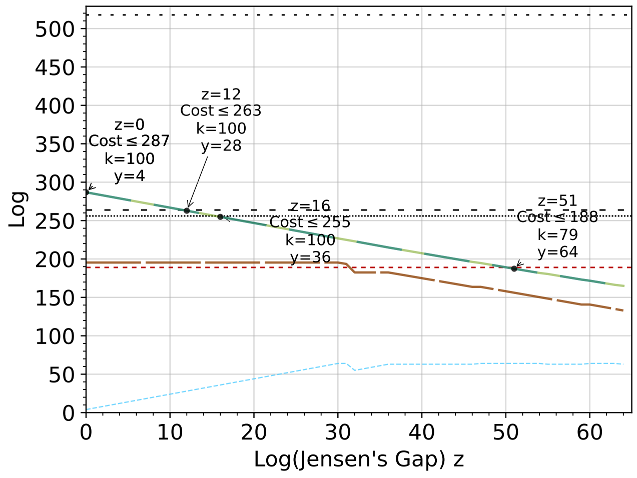

(b) Kyber-1024, MaxDepth $= 2^{96}$.

Figure 5: Cost estimation for Kyber-1024 under MaxDepth restrictions with the instantiation for operator $\mathcal{W}$ as in Section 4.1 corresponding to the lower bound (LB/UB) for Conjecture 3, cf. Table 6 for an expanded legend.

References

1. Aaronson, S., Ambainis, A.: Quantum search of spatial regions. pp. 200–209 (2003). https://doi.org/10.1109/SFCS.2003.1238194
2. Ajtai, M., Kumar, R., Sivakumar, D.: A sieve algorithm for the shortest lattice vector problem. pp. 601–610 (2001). https://doi.org/10.1145/380752.380857
3. Albrecht, M.R., Bai, S., Fouque, P.A., Kirchner, P., Stehlé, D., Wen, W.: Faster enumeration-based lattice reduction: Root hermite factor $k^{1/(2k)}$ time $k^{k/8+o(k)}$. pp. 186–212 (2020). https://doi.org/10.1007/978-3-030-56880-1_7
4. Albrecht, M.R., Bai, S., Li, J., Rowell, J.: Lattice reduction with approximate enumeration oracles - practical algorithms and concrete performance. pp. 732–759 (2021). https://doi.org/10.1007/978-3-030-84245-1_25
5. Albrecht, M.R., Curtis, B.R., Deo, A., Davidson, A., Player, R., Postlethwaite, E.W., Virdia, F., Wunderer, T.: Estimate all the LWE, NTRU schemes! pp. 351–367 (2018). https://doi.org/10.1007/978-3-319-98113-0_19
6. Albrecht, M.R., Ducas, L., Herold, G., Kirshanova, E., Postlethwaite, E.W., Stevens, M.: The general sieve kernel and new records in lattice reduction. pp. 717–746 (2019). https://doi.org/10.1007/978-3-030-17656-3_25
7. Albrecht, M.R., Gheorghiu, V., Postlethwaite, E.W., Schanck, J.M.: Estimating quantum speedups for lattice sieves. pp. 583–613 (2020). https://doi.org/10.1007/978-3-030-64834-3_20
8. Albrecht, M.R., Player, R., Scott, S.: On the concrete hardness of learning with errors. Journal of Mathematical Cryptology **9**(3), 169–203 (2015). https://doi.org/doi:10.1515/jmc-2015-0016, https://doi.org/10.1515/jmc-2015-0016
9. Alkim, E., Ducas, L., Pöppelmann, T., Schwabe, P.: Post-quantum key exchange - A new hope. pp. 327–343 (2016)
10. Ambainis, A., Kokainis, M.: Quantum algorithm for tree size estimation, with applications to backtracking and 2-player games. In: Hatami, H., McKenzie, P., King, V. (eds.) Proceedings of the 49th Annual ACM SIGACT Symposium on Theory of Computing, STOC 2017, Montreal, QC, Canada, June 19-23, 2017. pp. 989–1002. ACM (2017). https://doi.org/10.1145/3055399.3055444, https://doi.org/10.1145/3055399.3055444
11. Aono, Y., Espitau, T., Nguyen, P.Q.: Random lattices: Theory and practice, preprint, available at https://espitau.github.io/bin/random_lattice.pdf
12. Aono, Y., Nguyen, P.Q., Seito, T., Shikata, J.: Lower bounds on lattice enumeration with extreme pruning. pp. 608–637 (2018). https://doi.org/10.1007/978-3-319-96881-0_21
13. Aono, Y., Nguyen, P.Q., Shen, Y.: Quantum lattice enumeration and tweaking discrete pruning. pp. 405–434 (2018). https://doi.org/10.1007/978-3-030-03326-2_14
14. Aono, Y., Wang, Y., Hayashi, T., Takagi, T.: Improved progressive BKZ algorithms and their precise cost estimation by sharp simulator. pp. 789–819 (2016). https://doi.org/10.1007/978-3-662-49890-3_30
15. Bai, S., Galbraith, S.D.: Lattice decoding attacks on binary lwe. In: Information Security and Privacy: 19th Australasian Conference, ACISP 2014, Wollongong, NSW, Australia, July 7-9, 2014. Proceedings 19. pp. 322–337. Springer (2014)
16. Bai, S., van Hoof, M.I., Johnson, F.B., Lange, T., Ngo, T.: Concrete analysis of qantum lattice enumeration. In: Guo, J., Steinfeld, R. (eds.) Advances in Cryptology – ASIACRYPT 2023. pp. 131–166. Springer Nature Singapore, Singapore (2023)

17. Becker, A., Ducas, L., Gama, N., Laarhoven, T.: New directions in nearest neighbor searching with applications to lattice sieving. In: Krauthgamer, R. (ed.) Proceedings of the Twenty-Seventh Annual ACM-SIAM Symposium on Discrete Algorithms, SODA 2016, Arlington, VA, USA, January 10-12, 2016. pp. 10–24. SIAM (2016). https://doi.org/10.1137/1.9781611974331.ch2, https://doi.org/10.1137/1.9781611974331.ch2
18. Bessen, A.J.: Lower bound for quantum phase estimation. Physical Review A **71**(4), 042313 (2005)
19. Bindel, N., Bonnetain, X., Tiepelt, M., Virdia, F.: Quantum lattice enumeration in limited depth. Cryptology ePrint Archive, Paper 2023/1423 (2023), https://eprint.iacr.org/2023/1423, https://eprint.iacr.org/2023/1423
20. Bonnetain, X., Chailloux, A., Schrottenloher, A., Shen, Y.: Finding many collisions via reusable quantum walks - application to lattice sieving. In: Hazay, C., Stam, M. (eds.) Advances in Cryptology - EUROCRYPT 2023 - 42nd Annual International Conference on the Theory and Applications of Cryptographic Techniques, Lyon, France, April 23-27, 2023, Proceedings, Part V. Lecture Notes in Computer Science, vol. 14008, pp. 221–251. Springer (2023). https://doi.org/10.1007/978-3-031-30589-4_8, https://doi.org/10.1007/978-3-031-30589-4_8
21. Campbell, E., Khurana, A., Montanaro, A.: Applying quantum algorithms to constraint satisfaction problems. Quantum **3**, 167 (jul 2019). https://doi.org/10.22331/q-2019-07-18-167, https://doi.org/10.22331%2Fq-2019-07-18-167
22. Chailloux, A., Loyer, J.: Lattice sieving via quantum random walks (2021)
23. Chen, Y.: Réduction de réseau et sécurité concrète du chiffrement complètement homomorphe. Ph.D. thesis, Paris 7 (2013), https://archive.org/details/PhDChen13, available at https://archive.org/details/PhDChen13
24. Chen, Y., Nguyen, P.Q.: BKZ 2.0: Better lattice security estimates. pp. 1–20 (2011). https://doi.org/10.1007/978-3-642-25385-0_1
25. Dagdelen, Ö., Schneider, M.: Parallel enumeration of shortest lattice vectors. Cryptology ePrint Archive, Report 2010/097 (2010), https://eprint.iacr.org/2010/097
26. Davenport, J.H., Pring, B.: Improvements to quantum search techniques for block-ciphers, with applications to AES. pp. 360–384 (2020). https://doi.org/10.1007/978-3-030-81652-0_14
27. Detrey, J., Hanrot, G., Pujol, X., Stehlé, D.: Accelerating lattice reduction with FPGAs. pp. 124–143 (2010)
28. Draper, T.G., Kutin, S.A., Rains, E.M., Svore, K.M.: A logarithmic-depth quantum carry-lookahead adder. Quantum Info. Comput. **6**(4), 351–369 (jul 2006)
29. Elandt-Johnson, R.C., Johnson, N.L.: Survival models and data analysis. Wiley Series in Probability and Statistics, John Wiley & Sons, Nashville, TN (Sep 1980)
30. Fincke, U., Pohst, M.: Improved methods for calculating vectors of short length in a lattice, including a complexity analysis. Mathematics of computation **44**(170), 463–471 (1985)
31. Fincke, U., Pohst, M.E.: Improved methods for calculating vectors of short length in a lattice. Mathematics of Computation (1985)
32. Fowler, A.G., Mariantoni, M., Martinis, J.M., Cleland, A.N.: Surface codes: Towards practical large-scale quantum computation. Physical Review A **86**(3) (sep 2012). https://doi.org/10.1103/physreva.86.032324, https://doi.org/10.1103%2Fphysreva.86.032324
33. Gama, N., Nguyen, P.Q.: Finding short lattice vectors within Mordell's inequality. pp. 207–216 (2008). https://doi.org/10.1145/1374376.1374408
34. Gama, N., Nguyen, P.Q., Regev, O.: Lattice enumeration using extreme pruning. pp. 257–278 (2010). https://doi.org/10.1007/978-3-642-13190-5_13

35. Gao, X., Sitharam, M., Roitberg, A.E.: Bounds on the jensen gap, and implications for mean-concentrated distributions. Australian Journal of Mathematical Analysis and Applications **16**(2), 1–16 (2019), https://ajmaa.org/cgi-bin/paper.pl?string=v16n2/V16I2P14.tex
36. Giovannetti, V., Lloyd, S., Maccone, L.: Quantum random access memory. Phys. Rev. Lett. **100**, 160501 (Apr 2008). https://doi.org/10.1103/PhysRevLett.100.160501, https://link.aps.org/doi/10.1103/PhysRevLett.100.160501
37. Häner, T., Jaques, S., Naehrig, M., Roetteler, M., Soeken, M.: Improved quantum circuits for elliptic curve discrete logarithms. In: Ding, J., Tillich, J.P. (eds.) Post-Quantum Cryptography. pp. 425–444. Springer International Publishing, Cham (2020)
38. Häner, T., Roetteler, M., Svore, K.M.: Factoring using 2n + 2 qubits with toffoli based modular multiplication. Quantum Info. Comput. **17**(7–8), 673–684 (jun 2017)
39. Hanrot, G., Pujol, X., Stehlé, D.: Analyzing blockwise lattice algorithms using dynamical systems. pp. 447–464 (2011). https://doi.org/10.1007/978-3-642-22792-9_25
40. Hermans, J., Schneider, M., Buchmann, J., Vercauteren, F., Preneel, B.: Parallel shortest lattice vector enumeration on graphics cards. pp. 52–68 (2010)
41. Jaques, S., Naehrig, M., Roetteler, M., Virdia, F.: Implementing grover oracles for quantum key search on AES and LowMC. pp. 280–310 (2020). https://doi.org/10.1007/978-3-030-45724-2_10
42. Jaques, S., Rattew, A.G.: Qram: A survey and critique (2023)
43. Jaques, S., Schanck, J.M.: Quantum cryptanalysis in the RAM model: Claw-finding attacks on SIKE. pp. 32–61 (2019). https://doi.org/10.1007/978-3-030-26948-7_2
44. Jones, N., Van Meter, R., Fowler, A., McMahon, P., Kim, J., Ladd, T., Yamamoto, Y.: Layered architecture for quantum computing. Physical Review X **2** (10 2010). https://doi.org/10.1103/PhysRevX.2.031007
45. Kannan, R.: Improved algorithms for integer programming and related lattice problems. pp. 193–206 (1983). https://doi.org/10.1145/800061.808749
46. Kirshanova, E., Mårtensson, E., Postlethwaite, E.W., Moulik, S.R.: Quantum algorithms for the approximate k-list problem and their application to lattice sieving. pp. 521–551 (2019). https://doi.org/10.1007/978-3-030-34578-5_19
47. Koch, D., Samodurov, M., Projansky, A., Alsing, P.M.: Gate-based circuit designs for quantum adder-inspired quantum random walks on superconducting qubits. International Journal of Quantum Information **20**(03), 2150043 (2022)
48. Kuo, P.C., Schneider, M., Dagdelen, Ö., Reichelt, J., Buchmann, J., Cheng, C.M., Yang, B.Y.: Extreme enumeration on GPU and in clouds - - how many dollars you need to break SVP challenges -. pp. 176–191 (2011). https://doi.org/10.1007/978-3-642-23951-9_12
49. Kuperberg, G.: Another subexponential-time quantum algorithm for the dihedral hidden subgroup problem (2011), arXiv preprint arXiv:1112.3333
50. Laarhoven, T.: Sieving for shortest vectors in lattices using angular locality-sensitive hashing. pp. 3–22 (2015). https://doi.org/10.1007/978-3-662-47989-6_1
51. Laarhoven, T., Mosca, M., van de Pol, J.: Solving the shortest vector problem in lattices faster using quantum search. pp. 83–101 (2013). https://doi.org/10.1007/978-3-642-38616-9_6
52. Li, J., Nguyen, P.Q.: A complete analysis of the BKZ lattice reduction algorithm. Cryptology ePrint Archive, Report 2020/1237 (2020), https://eprint.iacr.org/2020/1237

53. Lindner, R., Peikert, C.: Better key sizes (and attacks) for LWE-based encryption. pp. 319–339 (2011). https://doi.org/10.1007/978-3-642-19074-2_21
54. Lyubashevsky, V., Ducas, L., Kiltz, E., Lepoint, T., Schwabe, P., Seiler, G., Stehlé, D., Bai, S.: CRYSTALS-DILITHIUM. Tech. rep., National Institute of Standards and Technology (2022), available at https://csrc.nist.gov/Projects/post-quantum-cryptography/selected-algorithms-2022
55. Micciancio, D., Walter, M.: Fast lattice point enumeration with minimal overhead. pp. 276–294 (2015). https://doi.org/10.1137/1.9781611973730.21
56. Micciancio, D., Walter, M.: Practical, predictable lattice basis reduction. pp. 820–849 (2016). https://doi.org/10.1007/978-3-662-49890-3_31
57. Montanaro, A.: Quantum-walk speedup of backtracking algorithms. Theory Comput. **14**(1), 1–24 (2018). https://doi.org/10.4086/toc.2018.v014a015, https://doi.org/10.4086/toc.2018.v014a015
58. Montanaro, A.: Quantum-walk speedup of backtracking algorithms. Theory of Computing **14**(15), 1–24 (2018). https://doi.org/10.4086/toc.2018.v014a015, https://theoryofcomputing.org/articles/v014a015
59. Muñoz-Coreas, E., Thapliyal, H.: Quantum circuit design of a t-count optimized integer multiplier. IEEE Transactions on Computers **68**(5), 729–739 (2019). https://doi.org/10.1109/TC.2018.2882774
60. Nguyen, P.Q., Vidick, T.: Sieve algorithms for the shortest vector problem are practical. J. Math. Cryptol. **2**(2), 181–207 (2008). https://doi.org/10.1515/JMC.2008.009, https://doi.org/10.1515/JMC.2008.009
61. Nie, J., Zhu, Q., Li, M., Sun, X.: Quantum circuit design for integer multiplication based on schönhage-strassen algorithm. IEEE Transactions on Computer-Aided Design of Integrated Circuits and Systems pp. 1–1 (2023). https://doi.org/10.1109/TCAD.2023.3279300
62. NIST: Submission requirements and evaluation criteria for the post-quantum cryptography standardization process (2016), https://csrc.nist.gov/CSRC/media/Projects/Post-Quantum-Cryptography/documents/call-for-proposals-final-dec-2016.pdf
63. Pham, P., Svore, K.M.: A 2d nearest-neighbor quantum architecture for factoring in polylogarithmic depth. Quantum Inf. Comput. **13**(11-12), 937–962 (2013)
64. Pohst, M.: On the computation of lattice vectors of minimal length, successive minima and reduced bases with applications. SIGSAM Bull. **15**(1), 37–44 (feb 1981). https://doi.org/10.1145/1089242.1089247, https://doi.org/10.1145/1089242.1089247
65. Preskill, J.: Quantum Computing in the NISQ era and beyond. Quantum **2**, 79 (Aug 2018). https://doi.org/10.22331/q-2018-08-06-79, https://doi.org/10.22331/q-2018-08-06-79
66. Prest, T., Fouque, P.A., Hoffstein, J., Kirchner, P., Lyubashevsky, V., Pornin, T., Ricosset, T., Seiler, G., Whyte, W., Zhang, Z.: FALCON. Tech. rep., National Institute of Standards and Technology (2022), available at https://csrc.nist.gov/Projects/post-quantum-cryptography/selected-algorithms-2022
67. Pujol, X., Stehlé, D.: Rigorous and efficient short lattice vectors enumeration. pp. 390–405 (2008). https://doi.org/10.1007/978-3-540-89255-7_24
68. Regev, O.: On lattices, learning with errors, random linear codes, and cryptography. In: Gabow, H.N., Fagin, R. (eds.) Proceedings of the 37th Annual ACM Symposium on Theory of Computing, Baltimore, MD, USA, May 22-24, 2005. pp. 84–93. ACM (2005). https://doi.org/10.1145/1060590.1060603, https://doi.org/10.1145/1060590.1060603

69. Regev, O.: On lattices, learning with errors, random linear codes, and cryptography. J. ACM **56**(6), 34:1–34:40 (2009). https://doi.org/10.1145/1568318.1568324, https://doi.org/10.1145/1568318.1568324
70. Rubinstein, R.Y., Kroese, D.P.: The cross-entropy method: a unified approach to combinatorial optimization, Monte-Carlo simulation, and machine learning, vol. 133. Springer (2004)
71. Ruiz-Perez, L., Garcia-Escartin, J.C.: Quantum arithmetic with the quantum fourier transform. Quantum Information Processing **16**, 1–14 (2017)
72. Schanck, J.M., Hulsing, A., Rijneveld, J., Schwabe, P.: NTRU-HRSS-KEM. Tech. rep., National Institute of Standards and Technology (2017), available at https://csrc.nist.gov/projects/post-quantum-cryptography/post-quantum-cryptography-standardization/round-1-submissions
73. Schnorr, C., Euchner, M.: Lattice basis reduction: Improved practical algorithms and solving subset sum problems. Mathematical Programming **66**, 181–199 (08 1994). https://doi.org/10.1007/BF01581144
74. Schnorr, C.: Lattice reduction by random sampling and birthday methods. In: Alt, H., Habib, M. (eds.) STACS 2003, 20th Annual Symposium on Theoretical Aspects of Computer Science, Berlin, Germany, February 27 - March 1, 2003, Proceedings. Lecture Notes in Computer Science, vol. 2607, pp. 145–156. Springer (2003). https://doi.org/10.1007/3-540-36494-3_14, http://dx.doi.org/10.1007/3-540-36494-3_14
75. Schnorr, C.P., Euchner, M.: Lattice basis reduction: Improved practical algorithms and solving subset sum problems. In: FCT (1991)
76. Schnorr, C.P., Euchner, M.: Lattice basis reduction: Improved practical algorithms and solving subset sum problems. Mathematical Programming (1994)
77. Schwabe, P., Avanzi, R., Bos, J., Ducas, L., Kiltz, E., Lepoint, T., Lyubashevsky, V., Schanck, J.M., Seiler, G., Stehlé, D., Ding, J.: CRYSTALS-KYBER. Tech. rep., National Institute of Standards and Technology (2022), available at https://csrc.nist.gov/Projects/post-quantum-cryptography/selected-algorithms-2022
78. development team, T.F.: fplll, a lattice reduction library, Version: 5.4.2 (2023), https://github.com/fplll/fplll, available at https://github.com/fplll/fplll
79. development team, T.P.: Progressive bkz library (2022), https://www2.nict.go.jp/security/pbkzcode/, available at https://www2.nict.go.jp/security/pbkzcode/
80. The Sage Developers: SageMath, the Sage Mathematics Software System (Version 9.3) (2021), `https://www.sagemath.org`
81. Zalka, C.: Grover's quantum searching algorithm is optimal. Physical Review A **60**(4), 2746 (1999)
82. Zou, J., Wei, Z., Sun, S., Liu, X., Wu, W.: Quantum circuit implementations of AES with fewer qubits. pp. 697–726 (2020). https://doi.org/10.1007/978-3-030-64834-3_24

A Estimating the Size of Lattice Enumeration Trees

In this appendix we perform some standard computations on the size of enumeration trees. We use these to compute the value of H_k in Sections 3 and 5. This analysis closely follows [34].

Size of the enumeration tree. The cost of lattice enumeration is typically estimated to be equal to the number of nodes visited by the algorithm. These nodes form the "enumeration tree". If we let Z_k be the set of nodes on the k^{th} level of the tree (that is, at distance k from the root node), H_k be the expected cardinality of Z_k for the enumeration tree of a random lattice basis and N the expected total number of nodes in the tree visited by the algorithm, we have

$$N := \mathop{\mathbb{E}}_{\substack{\text{random}\\ \text{tree } \mathcal{T}}}[\#\mathcal{T}] = \frac{1}{2}\sum_{k=1}^{n} \mathop{\mathbb{E}}_{\substack{\text{random}\\ \text{tree } \mathcal{T}}}[|Z_k|] = \frac{1}{2}\sum_{k=1}^{n} H_k,$$

where the 1/2 factor is due to exploiting lattices' additive symmetry to avoid visiting half of the tree. The cardinality of Z_k depends on the pruning strategy and on the geometry of the projective sublattices implied by the lattice bases, and can be estimated using the Gaussian heuristic. For example, we have

$$Z_k = \begin{cases} \mathrm{Ball}_k(\vec{0}, R) \cap \pi_{n-k+1}(\Lambda), & \text{using no pruning,} \\ C_{R_1,\dots,R_k} \cap \pi_{n-k+1}(\Lambda), & \text{using cylinder pruning,} \end{cases}$$

where $C_{R_1,\dots\, R_k} := \{(x_1,\dots,x_k) \in \mathbb{R}^k \mid \sum_{i\leq j} x_i^2 \leq R_j^2 \text{ for all } j \leq k\}$ is the intersection of cylinders of increasing dimension and non-decreasing radius, and where the covolume of the projected sublattices $\pi_{n-k+1}(\Lambda)$ depends on the quality of the input lattice basis $B = (b_1,\dots,b_n)$, with $\mathrm{covol}(\pi_{n-k+1}(\Lambda)) = \prod_{i=n-k+1}^{n} ||b_i^*|| = \mathrm{covol}(\Lambda)/\prod_{i=1}^{n-k} ||b_i^*||$, where $B^* = (b_1^*,\dots,b_n^*)$ is the Gram-Schmidt orthogonalisation of B.

Cost estimation for the algorithm then reduces to estimating H_k, as done in [34,12], noting that $\log N \leq \log(n \cdot \max_k H_k/2) \in O(\log \max_k H_k)$. We proceed to illustrate how to estimate H_k in the case of non-pruned enumeration. We will use these results, together with the analysis of [12], to numerically estimate lower bounds for H_k in the case of cylinder pruning.

A.1 Computing H_k when no Pruning is Used

We start analysing the simpler case of non-pruned enumeration. We start by recalling the following common heuristics used in lattice cryptanalysis.

Heuristic 1 (Gaussian heuristic) *Given a lattice $\Lambda \subset \mathbb{R}^n$ of rank n and a* nice enough *set $S \subset \mathbb{R}^n$, the Gaussian heuristic states that*

$$|\Lambda \cap S| \approx \frac{vol(S)}{covol(\Lambda)}.$$

For cryptanalytic purposes, often S is set to be an n-ball of radius $R \geq 1$. Choosing S to be the n-ball of unit radius, gives an approximation for the first minimum of Λ:

$$\lambda_1(\Lambda) \approx \frac{\Gamma(1+n/2)^{1/n}}{\sqrt{\pi}} covol(\Lambda)^{1/n}. \tag{10}$$

Heuristic 2 (Geometric Series Assumption (GSA) for BKZ [74]) *Let $B = (b_1, \dots, b_n)$ be a BKZ-β-reduced basis for a rank-n lattice λ, and let $B^* = (b_1^*, \dots, b_n^*)$ be the corresponding Gram-Schmidt vectors. Let $||b_1^*||, \dots, ||b_n^*||$ be the* basis profile. *Then the basis profile follows a geometric series*

$$||b_i^*|| \approx \alpha_\beta^{i-1} ||b_1^*||, \text{ where } \alpha_\beta \approx \left((\pi\beta)^{1/\beta} \frac{\beta}{2\pi e} \right)^{-1/(\beta-1)}.$$

Furthermore, by an elementary computation using $covol(\Lambda) = \prod_{i=1}^n ||b_i^*||$, we have

$$||b_1|| \approx (\alpha_\beta^{-1/2})^{n-1} covol(\Lambda)^{1/n}.$$

Heuristic 3 (BKZ-n-reduced inputs) *Whenever we enumerate a lattice Λ of rank n, we assume the input basis satisfies Heuristic 2, that is that the norms of the Gram-Schmidt vectors follow a geometric series with constant α_n.*

We briefly justify making these assumptions in our setting. To simplify our analysis, we will assume that quantum enumeration is being performed as a subroutine to the BKZ lattice reduction algorithm [75,76]. Heuristic 1 is commonly assumed, and considered to be accurate already in relatively small dimensions [24], and asymptotically tight [11]. Regarding Heuristic 2, while it is known that the output of BKZ does not exactly match the output of the GSA due to fluctuations in the head of the basis profile and a concavity due to the tail being HKZ-reduced, the GSA practically "holds" for most of the basis profile. Regarding Heuristic 3, in practice it is known [24,39,52] that the quality of a lattice basis tends to converge to the GSA within the first few tours. Since the runtime of enumeration improves as the basis quality does, we will conservatively assume that in the first few tours the GSA for BKZ-β is achieved, and that from then on all enumeration calls on blocks of rank β satisfy Heuristic 3.[12] As we will see, this will imply an asymptotic cost of $2^{\frac{\beta \log \beta}{8} + O(\beta)}$ for enumeration. We note that in practice the $\beta \log \beta / 8$ exponent can indeed be achieved with appropriate local block preprocessing when running enumeration within block lattice reduction [3].

Armed with Heuristics 2 and 3, we can now estimate the asymptotic cost of non-pruned enumeration as an SVP solver in rank n. We start considering

[12] This is an overly optimistic assumption, both because it ignores the HKZ-shape of the basis that in practice causes a significant slowdown [3], and because we will rely on this analysis for the case of cylinder pruning, where the basis is re-randomised, causing a loss in reduction quality.

an arbitrary enumeration radius R. Let $\mathrm{Ball}_k(\vec{0}, R)$ be the k-ball of radius R centered at the origin. Using the Gaussian heuristic,

$$\begin{aligned}
H_k &= \mathop{\mathbb{E}}_{\substack{\text{random}\\ \text{tree } \mathcal{T}}}\left[\left|\mathrm{Ball}_k(\vec{0}, R) \cap \pi_{n-k+1}(\Lambda)\right|\right] \approx \frac{\mathrm{vol}(\mathrm{Ball}_k(\vec{0}, R))}{\mathrm{covol}(\pi_{n-k+1}(\Lambda))} \\
&= \mathrm{vol}(\mathrm{Ball}_k(\vec{0}, R)) \cdot \frac{\prod_{i=1}^{n-k} ||b_i^*||}{\mathrm{covol}(\Lambda)} = \mathrm{vol}(\mathrm{Ball}_k(\vec{0}, R)) \cdot \frac{||b_1^*||^{n-k} \alpha_n^{\frac{(n-k-1)(n-k)}{2}}}{\mathrm{covol}(\Lambda)} \\
&= \frac{R^k \pi^{k/2}}{\Gamma(\frac{k}{2}+1)} \cdot \frac{||b_1^*||^{n-k} \alpha_n^{\frac{(n-k-1)(n-k)}{2}}}{\mathrm{covol}(\Lambda)}. \qquad (11)
\end{aligned}$$

By letting R be the Gaussian heuristic for the first minimum of the lattice (cf. Eq. (10)), we have

$$\begin{aligned}
H_k &\approx \frac{R^k \pi^{k/2}}{\Gamma(\frac{k}{2}+1)} \frac{||b_1^*||^{n-k} \alpha_n^{\frac{(n-k-1)(n-k)}{2}}}{\mathrm{covol}(\Lambda)} \\
&= \frac{\Gamma(\frac{n}{2}+1)^{k/n}}{\pi^{k/2}} \mathrm{covol}(\Lambda)^{k/n} \frac{\pi^{k/2}}{\Gamma(\frac{k}{2}+1)} \frac{||b_1^*||^{n-k} \alpha_n^{\frac{(n-k-1)(n-k)}{2}}}{\mathrm{covol}(\Lambda)} \\
&= \frac{\Gamma(\frac{n}{2}+1)^{k/n}}{\Gamma(\frac{k}{2}+1)} ||b_1^*||^{n-k} \alpha_n^{\frac{(n-k-1)(n-k)}{2}} \mathrm{covol}(\Lambda)^{k/n-1} \\
&= \frac{\Gamma(\frac{n}{2}+1)^{k/n}}{\Gamma(\frac{k}{2}+1)} ||b_1^*||^{n-k} \alpha_n^{\frac{(n-k-1)(n-k)}{2}} \left(\prod_{i=1}^{n} \alpha_n^{i-1} ||b_1^*||\right)^{k/n-1} \\
&= \frac{\Gamma(\frac{n}{2}+1)^{k/n}}{\Gamma(\frac{k}{2}+1)} ||b_1^*||^{n-k} \alpha_n^{\frac{(n-k-1)(n-k)}{2}} ||b_1^*||^{k-n} \alpha_n^{\frac{(n-1)n}{2}\frac{k-n}{n}} \\
&= \frac{\Gamma(\frac{n}{2}+1)^{k/n}}{\Gamma(\frac{k}{2}+1)} \alpha_n^{\frac{k(k-n)}{2}}.
\end{aligned}$$

Using Stirling's approximation for the Γ function on $\mathbb{R}^+$,

$$\Gamma(x+1) = \sqrt{2\pi x}\left(\frac{x}{e}\right)^x \left(1 + \frac{1}{12x} + O\left(\frac{1}{x^2}\right)\right),$$

we can further simplify the result as

$$H_k \approx \frac{(\pi n)^{\frac{k}{2n}} \left(\frac{n}{2e}\right)^{\frac{k}{2}}}{\sqrt{\pi k}\left(\frac{k}{2e}\right)^{\frac{k}{2}}} \alpha_n^{\frac{k(k-n)}{2}} \approx (\pi n)^{\frac{1}{2}\left(\frac{k}{n}-1\right)} \left(\frac{n}{k}\right)^{\frac{k}{2}} \alpha_n^{\frac{k(k-n)}{2}} \qquad (12)$$

In [34], it is observed that most of the nodes are located around level $k \approx n/2$. There, the approximation becomes $N \approx H_{n/2} \approx (\pi n)^{-\frac{1}{4}} 2^{\frac{n}{4}} \cdot \alpha_n^{-\frac{n^2}{8}}$. Using the "rule of thumb" approximation $\alpha_n^{-\frac{1}{2}} \approx n^{\frac{1}{2n}}$, the leading term in $H_{n/2}$ becomes

$n^{\frac{1}{2n}\frac{n^2}{4}} = 2^{\frac{n}{8}\log n}$. Using Sagemath's [80] `find_fit` function over the approximation derived from Eq. (12) for $N = \frac{1}{2}\sum_{k=1}^{n} H_k$ (with α_n as in Heuristic 2) evaluated it on $\{100, 200, \ldots, 1000\}$, we find $\log N \approx 0.12463\, n \log n - 0.25483\, n + 0.35621\, \log n - 0.26238$.

A.2 Estimating H_k when Cylinder Pruning is Used

Cylinder pruning indicates a potentially vast family of pruning strategies, depending on how the pruning radii $0 < R_1 \leq \cdots \leq R_n = R$ are chosen, *i.e.* on the *pruning strategy*. Gama *et al.* [34] analyse the runtime of four pruning strategies: linear pruning, where $R_i^2 = (i/n) \cdot R^2$, for $i = 1, \ldots, n$; step pruning functions, where the $R_i = \alpha \cdot R$ for some $\alpha \in (0, 1)$, whenever $i \leq n/2$, and $R_i = R$ otherwise; piece-wise linear pruning, a combination of the above; and numerically optimised pruning.

Upper bounds. For linear, step and piece-wise linear pruning, Gama *et al.* [34] obtain asymptotic results on the value of H_k. While these suggest closed formulae, in the extreme pruning setting using numerically optimised pruning radii appears to be the strategy returning the smallest enumeration costs.

In their analysis, Gama *et al.* suggest an approach to deriving a closed formula for the size of H_k whenever the pruning radii are pairwise equal, meaning $R_1 = R_2 \leq R_3 = R_4 \leq \cdots \leq R_{n-1} = R_n$, and n is even. A similar analysis allows them to determine the success probability of finding the shortest vector using such a pruning profile. They suggest using interpolation techniques to heuristically extend this analysis to arbitrary pruning radii and to odd dimensions. While their exposition is left somewhat implicit, Chen [23, Sec. 3.3] provides fully specified algorithms to reproducing and extending their analysis.

In practice, finding upper bounds to the values of H_k reduces to finding optimised pruning radii R_i that achieve a required minimum success probability, and estimating the volume of the cylinder intersections $C_{R_1,\ldots,R_k}$, following the cited analysis [34,23].

The search for optimised radii requires some form of automated monotonic optimisation technique applied to the cost of pruned enumeration for a given set of radii. Public implementations include gradient descent and Nelder-Mead optimisation methods, available in `fplll` [78], and methods based on cross-entropy techniques [70] introduced by Chen [23] and Aono *et al.* [12], available in the `202205` version of the Progressive BKZ library [79,14].

For our cost estimates, our starting point is the `fplll` pruning code. We apply some minor modifications to adapt it to our setting (cf. Section 5.1):

- We disable some minor undocumented tweaks that the `fplll` team applied to the volume computations by Chen;
- We change the overall cost function being minimised to assume a single full-dimension enumeration, rather than multiple enumerations with basis preprocessing;

– We let the code assume an input basis profile following Heuristic 3.

The resulting code is used to generate optimal pruning radii for the Kyber attack parameters targeting success probability 2^{-64}. We attempted this using four different pruning strategies in `fplll` ("greedy", "gradient descent", "Nelder-Mead" and "zealous", ie. gradient descent followed by Nelder-Mead), and chose the sets attaining the smallest cost (in all cases, these are the "zealous" parameters).

We have then attempted to use these parameters as a starting point for the cross-entropy optimisation code in the Progressive BKZ library, but unfortunately this did not terminate within a reasonable amount of time, meaning that we kept the "zealous" sets from `fplll`.

Lower bounds. In [12], Aono *et al.* propose a technique for computing lower bounds to the complexity of cylinder pruning in general, for which they are able to give a closed formula [12, Eq. 16], in terms of the inverse regularized incomplete beta function and of the values for H_k in the case of no pruning. Aono *et al.* concluded that their results should be reasonably tight. Given the ease of computing the lower bounds in [12] and their relative tightness, we use them to estimate a lower bound to H_k numerically as part of our cost estimations.

B Conjecture 3

In this section we report experiments on the quality of $\mathbb{E}[X]/\mathbb{E}[Y]$ as an "approximate lower bound" for $\mathbb{E}[X/Y]$, *i.e.*, we provide experimental evidence supporting Conjecture 3.

Experimental setup. We run this experiment using either no pruning ($n = 46, 48, 50, 52$) or using linear pruning ($n = 40, 42, \dots, 66$). For each n, we generate 30 random lattices and proceed to perform enumeration using `fplll` [78], with pruning radius $R = 1.05 \cdot \lambda_1(\Lambda)$. For each lattice enumerated, we measure $|Z_k|$ for $k = 1, \dots, n$ and estimate for all $k \geq 1$ and $k + j \geq k$ the relative size of $\frac{\mathbb{E}[|Z_{k+j}|]}{\mathbb{E}[|Z_k|]}$ compared to $\mathbb{E}\left[\frac{|Z_{k+j}|}{|Z_k|}\right]$. To do this, we collect the measured values of $|Z_i|$ for every level i of every generated lattice, and estimate

- H_i as the mean value of $|Z_i|$ across generated lattices,
- $\mathbb{E}[1/|Z_i|]$ as the mean value of $1/|Z_i|$ across lattices,
- $\mathrm{Cov}\left(|Z_{k+j}|, \frac{1}{|Z_k|}\right)$ as the sample covariance between those quantities across lattices.

We then derive an estimate for $\mathbb{E}\left[\frac{|Z_{k+j}|}{|Z_k|}\right]$ by observing that $\mathrm{Cov}(X, Y) = \mathbb{E}[XY] - \mathbb{E}[X]\mathbb{E}[Y]$, and replacing $X = |Z_{k+j}|$ and $Y = 1/|Z_k|$.

Random lattice generation. We generate random lattices as done in [24], and use to model lattice blocks found during the BKZ reduction. These lattices have been used to produce predictions for the quality of lattice reduction in [24], resulting in a popular "BKZ simulator", and we therefore deem them a viable tool to model projected sublattices found during block reduction.

Results. In Figs. 6 and 7, we present a representative selection of the resulting measurements of $\frac{\mathbb{E}[|Z_{k+j}|]/\mathbb{E}[|Z_k|]}{\mathbb{E}[|Z_{k+j}|/|Z_k|]}$ for every $1 \leq k < k+j \leq n$, for the largest attained values of n. All plots are available in the code release. Throughout our experiments, we observe $\mathbb{E}\left[\frac{|Z_{k+j}|}{|Z_k|}\right] \geq \frac{1}{1.5}\frac{\mathbb{E}[|Z_{k+j}|]}{\mathbb{E}[|Z_k|]}$, even as dimension increases. Some instances ($n = 50$ without pruning, $n = 58$ with linear pruning) appear to peak more than the others. Interestingly, this happens both with and without pruning, and does not appear to be a function of dimension.

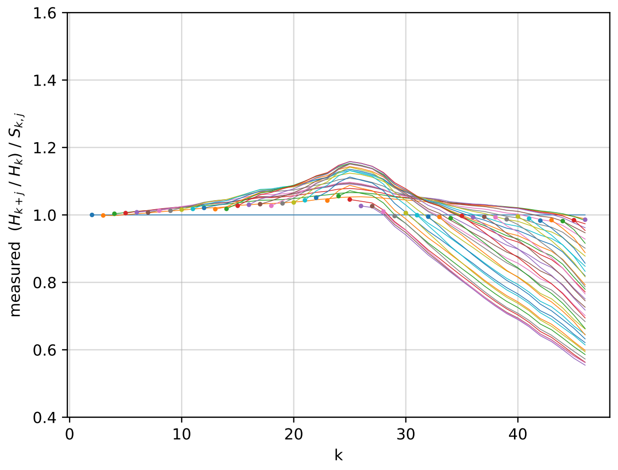

(a) $n = 46$

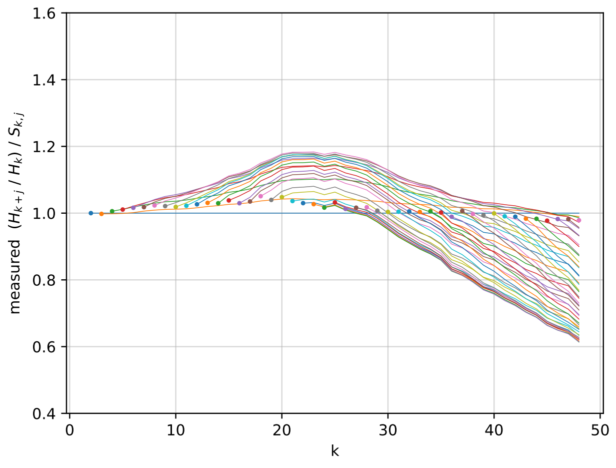

(b) $n = 48$

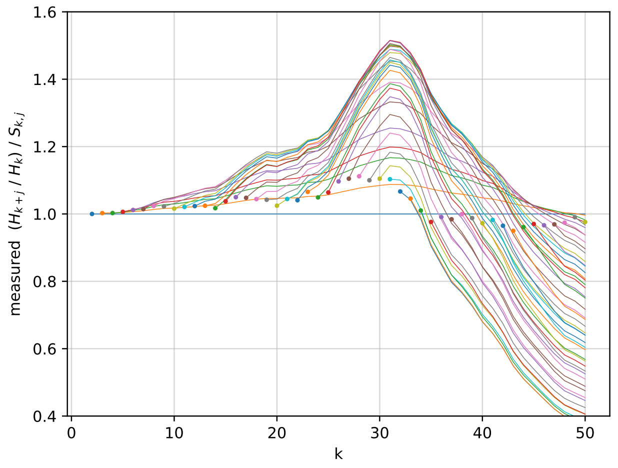

(c) $n = 50$

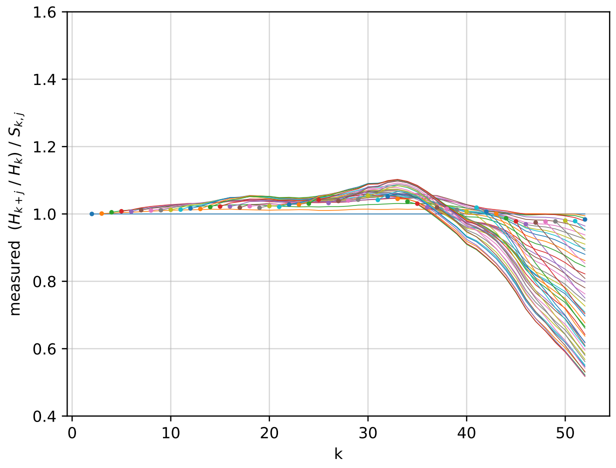

(d) $n = 52$

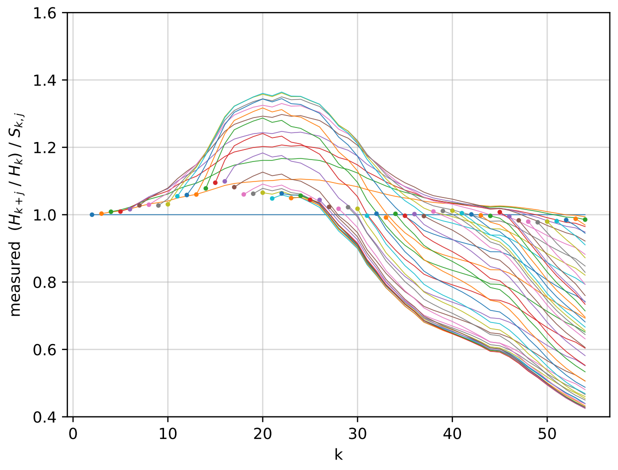

(e) $n = 54$

Figure 6: Measured values for $\frac{\mathbb{E}[|Z_{k+j}|]/\mathbb{E}[|Z_k|]}{\mathbb{E}[|Z_k+j|/|Z_k|]} = \frac{H_{k+j}/H_k}{S_{k,j}}$ for every $1 \leq k < k+j \leq n$, in experiments where no pruning is used. Every line represents $\frac{H_{k+j}/H_k}{S_{k,j}}$ for a fixed root level k. The initial larger dot is the value evaluated at $j = 1$. We observe throughout that Conjecture 3 holds.

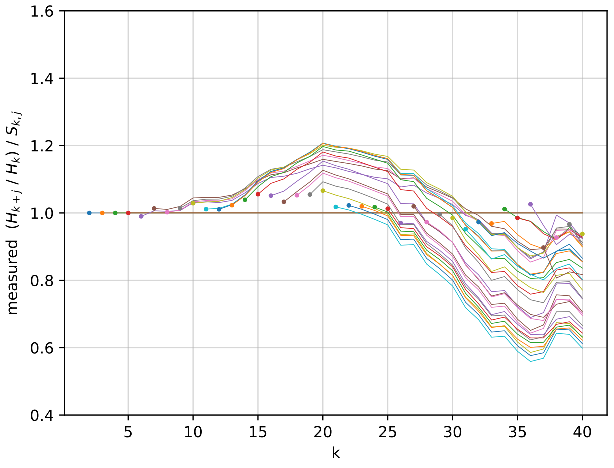

(a) $n = 40$

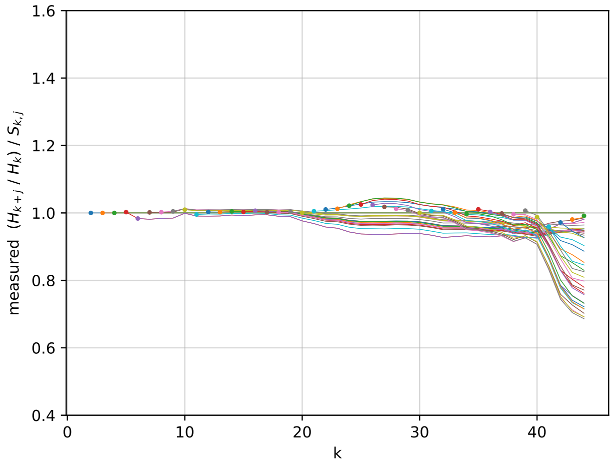

(b) $n = 44$

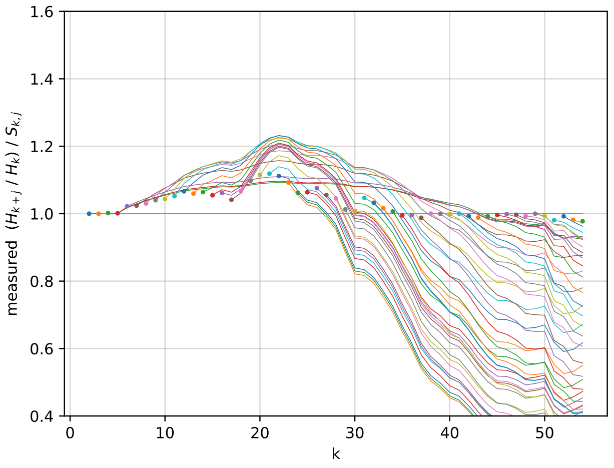

(c) $n = 54$

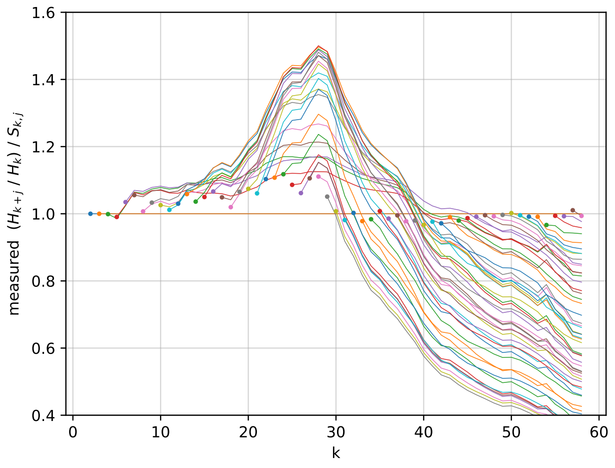

(d) $n = 58$

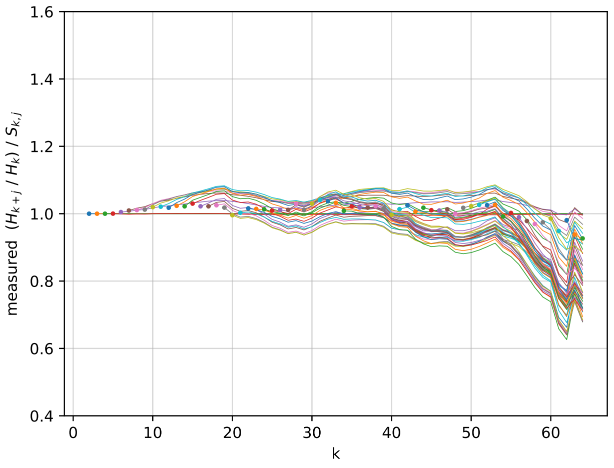

(e) $n = 64$

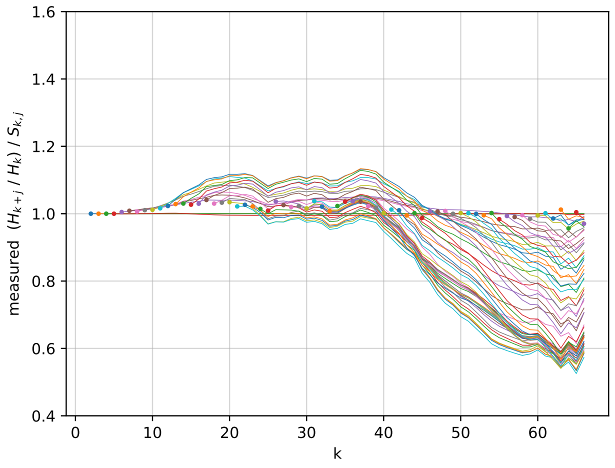

(f) $n = 66$

Figure 7: Measured values for $\frac{\mathbb{E}[|Z_{k+j}|]/\mathbb{E}[|Z_k|]}{\mathbb{E}[|Z_k+j|/|Z_k|]} = \frac{H_{k+j}/H_k}{S_{k,j}}$ for every $1 \leq k < k + j \leq n$, in experiments where linear pruning is used. Every line represents $\frac{H_{k+j}/H_k}{S_{k,j}}$ for a fixed root level k. The initial larger dot is the value evaluated at $j = 1$. We observe throughout that Conjecture 3 holds.

C Estimating the Size of Lattice Enumeration Subtrees

In this section we elaborate on the number of descendants $|W_{k,j}(g)|$ of a node g, in general for $j \geq 1$ and in particular for the number of children $C(g) = |W_{k,1}(g)|$.

C.1 Theoretical Analysis

First, we obtain an upper bound to the number of children of a node.

Lemma 1 (Upper bound of $C(g)$). *Let $R_1 \leq \cdots \leq R_n$ be the enumeration radii in pruned enumeration. Let B be a basis of the lattice Λ of rank n. Let g_{j+1} be a guess for $\pi_{j+1}(v)$ on level $k = n-(j+1)+1$ of the enumeration tree . The number of children of g_{j+1} on the tree is at most approximately $\lfloor x \cdot R_{k+1}/||b_j^*||\rceil = \lfloor x \cdot R_{k+1}/||b_{n-k}^*||\rceil$, were $x = 1$ if $k = 0$ and 2 otherwise.*

Proof. Recall Eq. (1),

$$\left|c_j + \sum_{i>j} \mu_{i,j}\, c_i\right| \leq \frac{1}{||b_j^*||}\sqrt{R_{k+1}^2 - ||\pi_{j+1}(v)||^2}$$

$$= \frac{1}{||b_j^*||}\sqrt{R_{k+1}^2 - \sum_{r=j+1}^{n}\left(c_r + \sum_{i=r+1}^{n}\mu_{i,r}c_i\right)^2 ||b_r^*||^2}.$$

Guessing a value g_j for $\pi_j(v)$ consists of picking $c_j \in \mathbb{Z}$ satisfying Eq. (1) given fixed values for c_i for $i > j$ and for Gram-Schmidt vectors and coefficients. Letting RHS be the right-hand side of Eq. (1), $c_j \in [-\mathrm{RHS} - \sum_{i>j}\mu_{i,j}\, c_i, \mathrm{RHS} - \sum_{i>j}\mu_{i,j}\, c_i] \cap S$ where $S = \mathbb{Z}$ if $k > 0$ and $S = \mathbb{Z}_{\geq 0}$ if $k = 0$. The size of such intersection, and hence the number of valid guesses for c_j, is approximately $\lfloor x \cdot \mathrm{RHS}\rceil$ for $x = 2$ if $k > 0$ and $x = 1$ otherwise. Finally, we note that $\mathrm{RHS} \leq R_{k+1}/||b_j^*||$, proving the result. □

Expected value of $\mathbb{E}[|W_{k,j}(g)|]$. As part of experiments reported in Appendix C.2 on non-pruned enumeration for verifying Conjecture 3, we observed a stronger approximation result, *i.e.* that Conjecture 3 appears tight for $j \approx 1$. We present an attempt at a proof of this heuristic, pointing out the argument that we are missing for completing it.

Conjecture 4 *The lower bound of Conjecture 3 is tight for $j \approx 1$, i.e.,*

$$\mathop{\mathbb{E}}_{g \sim U(Z_k)}[|W_{k,j}(g)|] = \mathop{\mathbb{E}}_{\substack{random\\ tree\ \mathcal{T}}}\left[\frac{|Z_{k+j}|}{|Z_k|}\right] \approx \frac{H_{k+j}}{H_k} \quad \text{for } j \approx 1.$$

The approximation follows from taking the expectation of the Taylor series of $\frac{x}{y}$ evaluated at $(x, y) = (\mathbb{E}[|Z_{k+j}|], \mathbb{E}[|Z_k|])$ [Eq. 3.87-88][29].

The error term in the approximation is quadratic in $(|Z_{k+j}| - \mathbb{E}[|Z_{k+j}|])$ and $(|Z_k| - \mathbb{E}[|Z_k|])$. An argument that these estimates are tight would complete the proof, however they would also imply tightness for general j, and not just for $j \approx 1$. While we do not provide a proof, we give experimental support next.

Table 7: LWE parameters used in lattice reduction experiments.

Secret dimension n	Modulo q	Standard deviation σ	#Samples m
72	97	1.0	87

C.2 Experimental Evidence

In the following, we provide experimental evidence for the accuracy of Conjecture 4, as well as for the validity of Conjecture 3 and Lemma 1, in the setting of lattice enumeration *without pruning*. To verify our conjectures, we modified a copy of `fplll` version 5.4.2 [78] to record the average number of descendants $S_{k,j} = \mathbb{E}[|W_{k,j}(g)|]$ of nodes $g \in Z_k$, where the descendants are located j levels below g. This includes measuring the average number of children $S_{k,1} = \mathbb{E}[C(g)] = \mathbb{E}[|W_{k,1}(g)|]$. We run experiments on lattices built using the primal attack embedding by Bai and Galbraith [15][13] on LWE instances (with standard deviation σ used for instantiating discrete Gaussian samplers for error and secret vector coefficients) estimated to be solved using BKZ with block size $\beta = 60$. Given the first minimum λ_1 of the blocks being enumerated, the enumeration radius is set to $R = 1.1 \cdot \lambda_1$. We list the parameters in Table 7.

Since Conjecture 3 requires computing H_k, we run our experiments on trees generated by enumeration without pruning, to avoid the issue of having to compute the volumes of the cylinder intersections used in pruned enumeration as part of the Gaussian heuristic. While this means that our predictions for the lower bound are easier to compute, it also means that we run experiments only up to block size $\beta = 40$.

Remark 3. Our theoretical treatment of lattices happens in a generous model where lattice bases achieve the GSA corresponding to BKZ-β reduced-ness at all basis indices. Experimentally, this is not easily achievable. To account for this we take a few precautions:

- We inspect experiment results starting at 10 completed tours of BKZ-β, in order to give some time for the basis profile to approach the GSA.
- We inspect experiments happening on blocks located approximately half-way through the basis, in order to protect them from GSA deviations:
  - Towards the initial bases vectors due to the presence of several q-vectors;
  - Towards the final β bases vectors due to these being HKZ reduced, causing a clear deviation from the GSA.
- We select the highest possible block sizes `fplll` would successfully execute within a reasonable time, to enter the Gaussian heuristic "regime" as much as possible; unfortunately due to checking heuristics for enumeration without pruning this means attempting relatively small block sizes.
- As an extra caution we over-impose a plot showing the basis profile on the block being enumerated for every experiment, and the [24] simulation of the corresponding block.

[13] Positioning the q-vectors at the beginning of the basis.

Results on $C(g) = |W_{k,1}(g)|$. We observe close agreement between our heuristics and the measurements at block size $\beta = 40$. In Fig. 8, we provide two example plots of a characteristic measurement.

Results on $|W_{k,j}(g)|$, when $j > 1$. In Figs. 9 to 11, we provide example plots of characteristic measurements. In order to imitate the combined classical-quantum methodology from Section 3, we pick subtrees reaching towards the lowest level on the tree. This means fixing a height $h \in \{20, 30\}$, and picking $k = \beta - h$ when measuring statistics.

We compute $\mathbb{E}[|Z_{k+j}|]/\mathbb{E}[|Z_k|]$ for $1 \leq j \leq h$ three times per experiment: using the measured basis profile, using a simulated basis profile following [24], and using the geometric series assumption, in order to observe how much the predictions can differ. We observe that our experiments deviate from the expected results more than in the case of $C(g)$.

Given the caveats listed in Remark 3, we believe that the measured data should be compared to the prediction for the lower bound obtained using the measured basis profile. Out of the cases presented, those where $k = 10, h = 30$ satisfy the stronger inequality $\mathbb{E}[|Z_{k+j}|/|Z_k|] \geq \mathbb{E}[|Z_{k+j}|]/\mathbb{E}[|Z_k|]$ when using the measured profile. This is not always the case for the $k = h = 20$ case, where $\mathbb{E}[|Z_{k+j}|]/\mathbb{E}[|Z_k|]$ can be slightly above $\mathbb{E}[|Z_{k+j}|/|Z_k|]$, in accordance with the experiments in Appendix B and with Conjecture 3, although the general shape seems to be captured by the predictions.

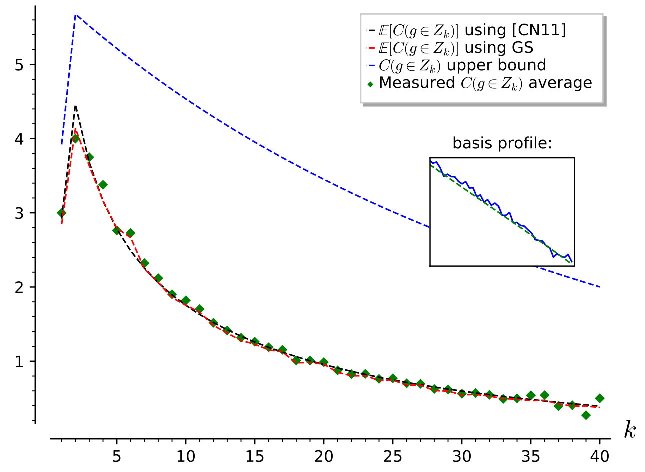

(a) $n = 72$, block size $\beta = 40$, 10th tour, block $\pi_{80}(\text{span}_{\mathbb{Z}}(b_{80}, \ldots, b_{80+\beta-1}))$.

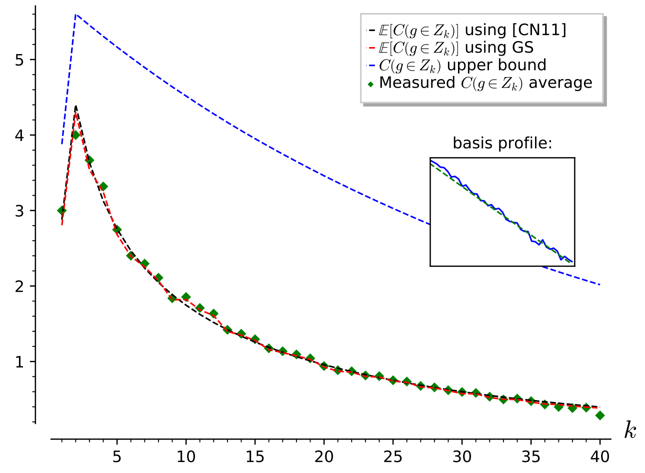

(b) $n = 72$, block size $\beta = 40$, 15th tour, block $\pi_{70}(\text{span}_{\mathbb{Z}}(b_{70}, \ldots, b_{70+\beta-1}))$.

Figure 8: Plots displaying our predictions and measurements for the number of children $C(g)$ of a node $g \in Z_k$ as a function of k. The green dots are the averages we measure during the call to enumeration. The blue dashed line is our upper bound for $C(g)$ given by Lemma 1. Red and black dashed lines are $\mathbb{E}[C(g)]$ based on Conjecture 4 using the measured $||b_k^*||$ ("GS") and a prediction based on the [24] simulator ("[CN11]"), respectively. In the sub-plot, the green dashed line is the BKZ simulator's [24] prediction for the basis profile $\log ||b_k^*||$, the blue line is our measurement.

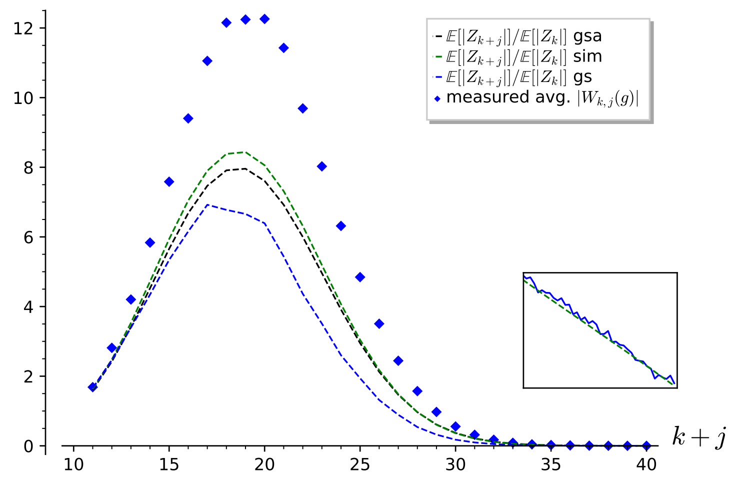

(a) $n = 72$, block size $\beta = 40$, 10th tour, block $\pi_{80}(\mathrm{span}_{\mathbb{Z}}(b_{80}, \ldots, b_{80+\beta-1}))$, $k = 10$.

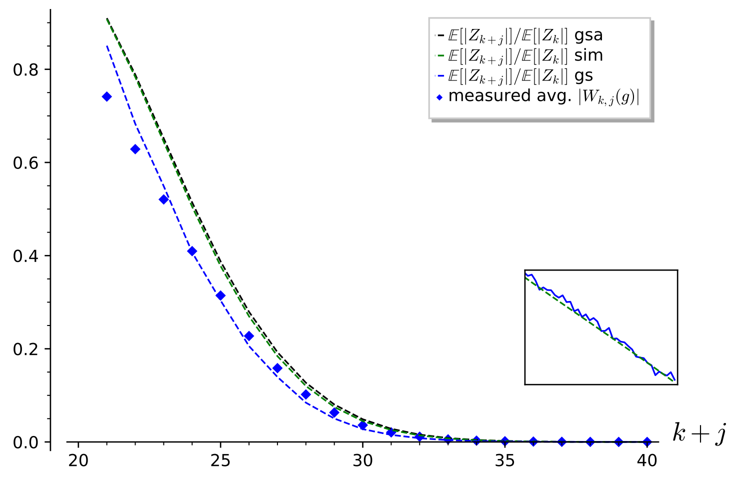

(b) $n = 72$, block size $\beta = 40$, 10th tour, block $\pi_{80}(\mathrm{span}_{\mathbb{Z}}(b_{80}, \ldots, b_{80+\beta-1}))$, $k = 20$.

Figure 9: Plots displaying our predictions and measurements for the number of descendants $|W_{k,j}(g)|$ on level $k + j$ of a node $g \in Z_k$ as a function of $k + j$. The blue dots are the averages we measure during the call to enumeration. The blue dashed line is our lower bound for $|W_{k,j}(g)|$ given by Conjecture 4, computed using the measured $||b_k^*||$ ("gs") to evaluate $\mathbb{E}[|Z_k|]$ and $\mathbb{E}[|Z_{k+j}|]$ using the Gaussian heuristic. Green and black dashed lines are the same lower bound computed using the BKZ simulator's [24] predictions ("sim") and the geometric series assumption ("gsa"), respectively. In the sub-plot, the green dashed line is the BKZ simulator's [24] prediction for the basis profile $\log ||b_k^*||$, the blue line is our measurement.

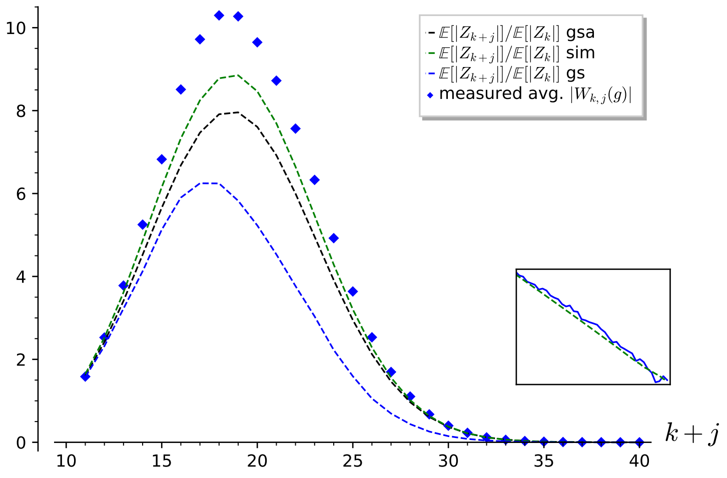

(a) $n = 72$, block size $\beta = 40$, 10^{th} tour, block $\pi_{90}(\text{span}_{\mathbb{Z}}(b_{90}, \ldots, b_{90+\beta-1}))$, $k = 10$.

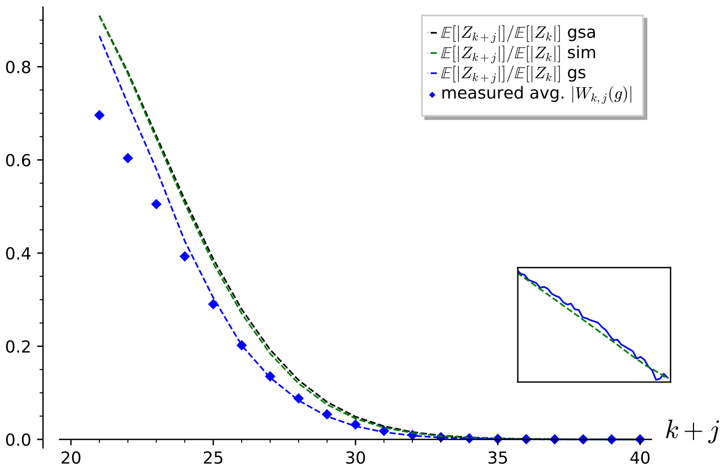

(b) $n = 72$, block size $\beta = 40$, 10^{th} tour, block $\pi_{90}(\text{span}_{\mathbb{Z}}(b_{90}, \ldots, b_{90+\beta-1}))$, $k = 20$.

Figure 10: Continuation of Fig. 9.

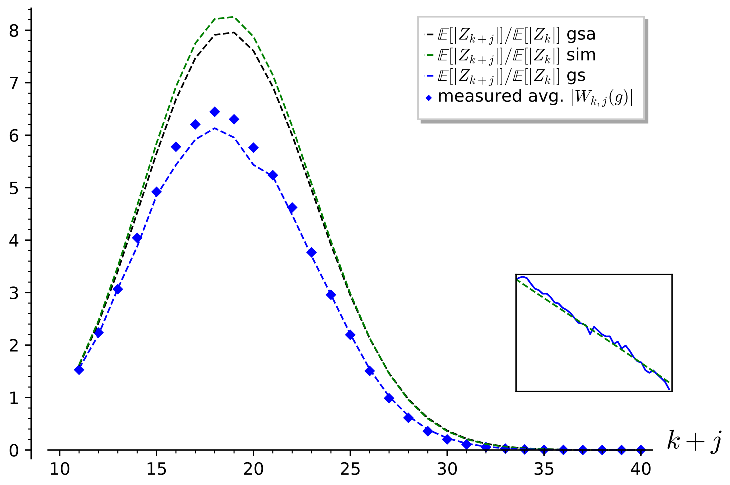

(a) $n = 72$, block size $\beta = 40$, 15th tour, block $\pi_{80}(\mathrm{span}_{\mathbb{Z}}(b_{80}, \ldots, b_{80+\beta-1}))$, $k = 10$.

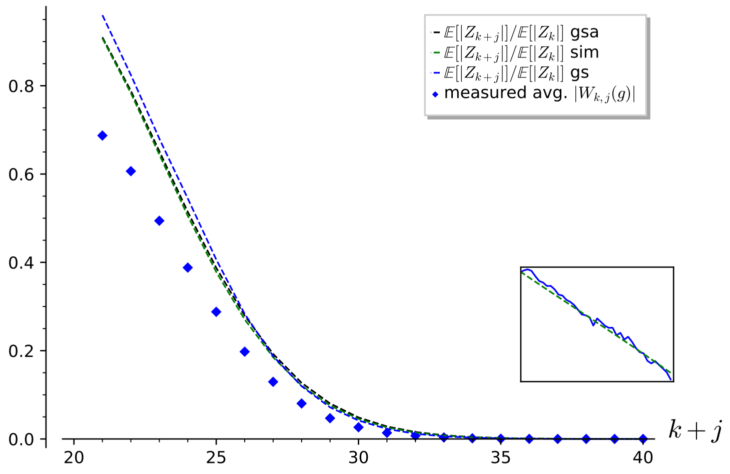

(b) $n = 72$, block size $\beta = 40$, 15th tour, block $\pi_{80}(\mathrm{span}_{\mathbb{Z}}(b_{80}, \ldots, b_{80+\beta-1}))$, $k = 20$.

Figure 11: Continuation of Fig. 9.

D Experiments on the Multiplicative Jensen's Gap

In Section 5, we presented approximate lower bounds on the cost of combined classical-quantum enumeration, identifying values of the multiplicative Jensen's gap for which the attacks would achieve certain threshold costs. We displayed these in Table 5 and Tables 9 to 13 in Appendix H.

In this appendix, we present some experiments run on pruned enumeration trees using `fplll` version 5.4.2 [78], on the same lattices as used in Appendix C. We measured the multiplicative Jensen's gap for subtrees rooted at level k of height $h = \beta - k$, for every enumeration tree explored during BKZ reduction during enumeration of the block spanned by the basis $\pi_i(\mathrm{span}_{\mathbb{Z}}(b_i, \ldots, b_{i+\beta-1}))$, indexed by i. Unlike in Appendix C, in this case we do not need to predict $\mathbb{E}[|Z_k|]$, meaning that we can use pruned enumeration as set by default in `fplll`. This means that we can run experiments for block sizes $\beta > 40$.

We present our measurements in Figs. 12 and 13. We observe that the Jensen gap in the experiments we have attempted seems to be around $2^z \leq 2$. While our experiments are in low dimension and therefore cannot be extrapolated into cryptanalytic claims, they also suggest that the possibility of enumeration tree subtrees achieving small multiplicative Jensen's gaps cannot be immediately disregarded.

Remark 4. As the block size increases, more re-randomization is performed by `fplll`'s default pruning strategy, consequently resulting in a denser dataset for $\beta = 70$ than for $\beta = 50$.

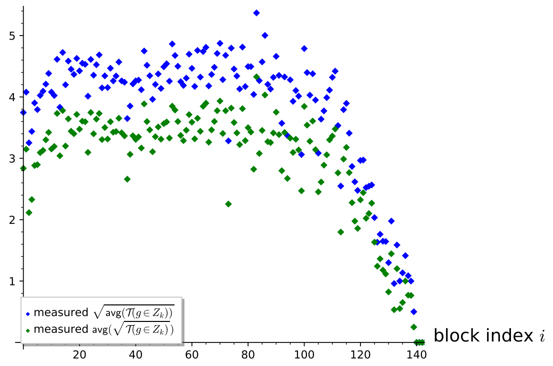

(a) $n = 72$ (cf. Table 7), block size $\beta = 50$, 10th tour, $k = 20$.

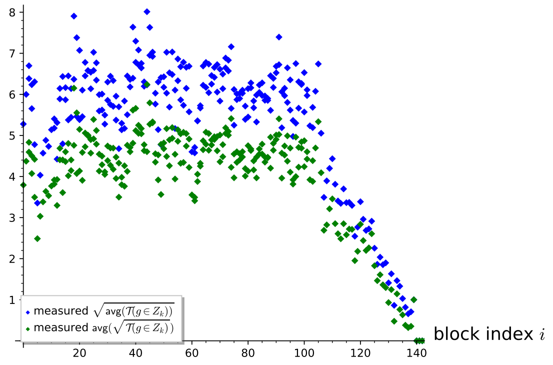

(b) $n = 72$ (cf. Table 7), block size $\beta = 60$, 10th tour, $k = 20$.

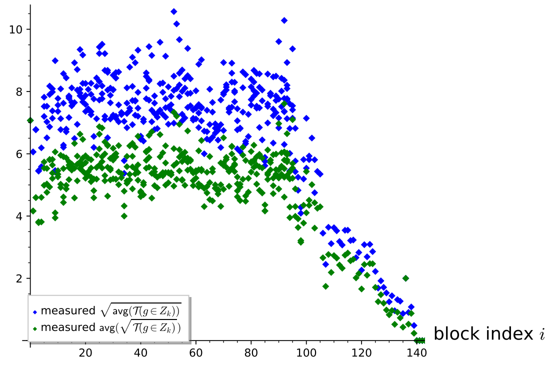

(c) $n = 72$ (cf. Table 7), block size $\beta = 70$, 10th tour, $k = 20$.

Figure 12: Measurement on the Jensen's gap of subtrees of height $h = \beta - k$ rooted on level k in pruned enumeration experiments. The height h is reduced in the last few blocks of the basis of dimension smaller than β. As the block index i increases, we plot the measurements done during enumeration of the projective sublattice $\pi_i(\text{span}_{\mathbb{Z}}(b_i, \ldots, b_{i+\beta}))$. Blue dots are the squared root of the average, green dots are the average of the squared root.

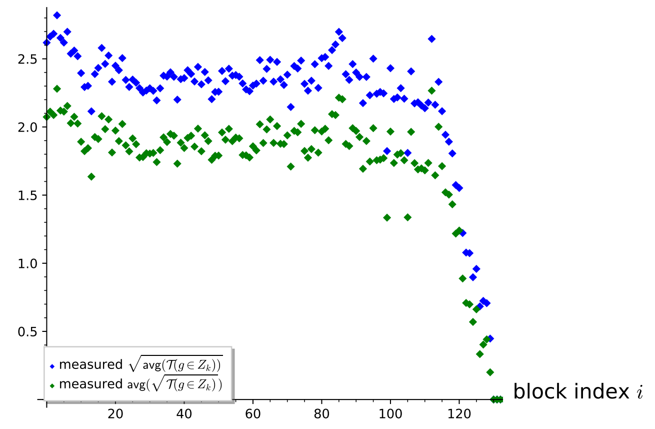

(a) $n = 72$ (cf. Table 7), block size $\beta = 50$, 10th tour, $k = 30$.

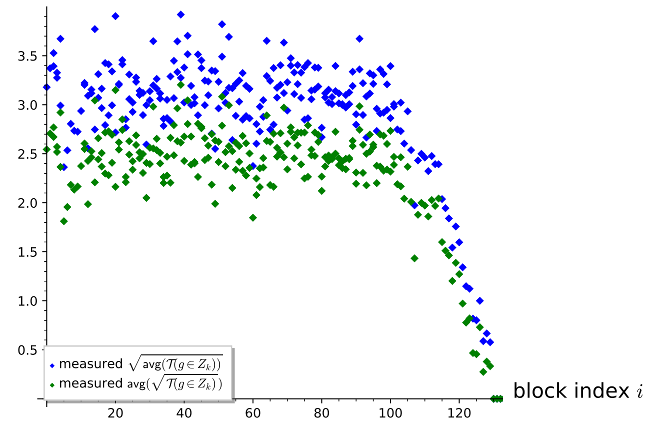

(b) $n = 72$ (cf. Table 7), block size $\beta = 60$, 10th tour, $k = 30$.

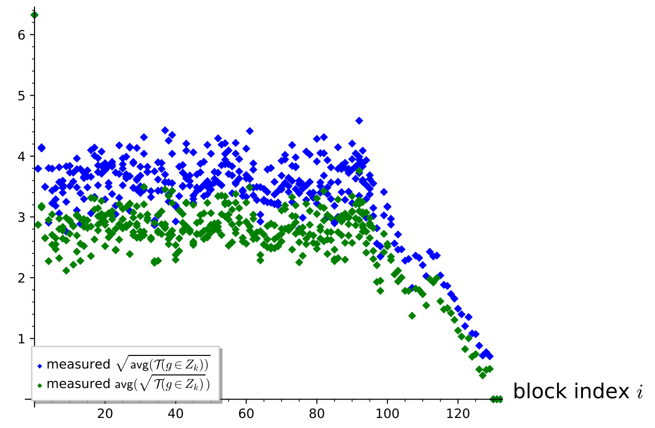

(c) $n = 72$ (cf. Table 7), block size $\beta = 70$, 10th tour, $k = 30$.

Figure 13: Continuation of Fig. 12.

E Conjecture 2

In this section we report experimental evidence supporting Conjecture 2, that is the observation that the number of nodes in subtrees of the enumeration tree rooted at the same level k is approximately constant, independently of the number of subtrees previously visited.

We reuse the same experimental setup and lattices used in Appendix D, and record the size of each subtree $\mathcal{T}(g)$ rooted on some node $g \in Z_k$. We refer the reader to Appendix D for details on the lattices being reduced.

We report results for $(n, k) = (40, 20), (50, 30)$. While we ran experiments on larger dimensions, the number of subtrees grows fast enough that storage of intermediate results becomes a bottleneck.

In Figs. 14 and 15, we plot the size of each subtree rooted on level k that we encounter, in the order we encounter them. We also plot the mean size we measure, as well as the measured value of $\sum_{j\geq1} |Z_{k+j}|/|Z_k|$, which which should exactly match the mean (and does), as $\sum_{j\geq1} |Z_{k+j}|$ includes all nodes in all subtrees rooted at level k. We observe that the sizes of the visited subtrees appear to be similar regardless of when a subtree is encountered, except for a handful of initial subtrees which correspond to the initial moments of enumeration, where the coefficient vectors being tried are very sparse, and hence the subtrees are plausably full of relatively short vectors.

To test whether this similarity of subtree size would translate to collections of trees, in Figs. 16 and 17 we collect sequential nodes in sets S_i of size 2^y, for $y = 4$, akin to the trees that would be collected under "virtual nodes" in combined classical-quantum enumeration. We exclude form this collection the very first subtree, which as we mentioned appears uncharacterisitcally larger than the others. We also plot the average size of these sets S_i, as well as $2^y \cdot \sum_{j\geq1} |Z_{k+j}|/|Z_k|$ (which in this case may slightly deviate from the average due to the last virtual tree not necessarily collecting exactly 2^y subtrees and due to the exclusion of the first large subtree). While a mildly decreasing trend appears in the $n = 40$ plots, this is not apparent in the $n = 50$ plots.

A natural question that arises regards what exactly is the distribution of the number of nodes in a subtree. In Figs. 18 and 19 we present histograms corresponding to the encountered sizes of subtrees rooted on level k. For legibility purposes, we exclude from the plot the first and larger subtree, which causes the histograms to be significantly compressed due to the plotting software trying to fit the outlier bin with a single item inside. We can see that the distribution appears bimodal, with a first mode around very small subtrees, followed by a second, wider mode with a local peak around the average size of subtrees. We observe that successfully modeling this distribution would possibly allow for a theoretical estimation of the multiplicative Jensen's gap, either directly or via one of the lower bounds in Appendix I, and hence would allow to clearly determine for which parameter sets a quantum enumeration attack would not work.

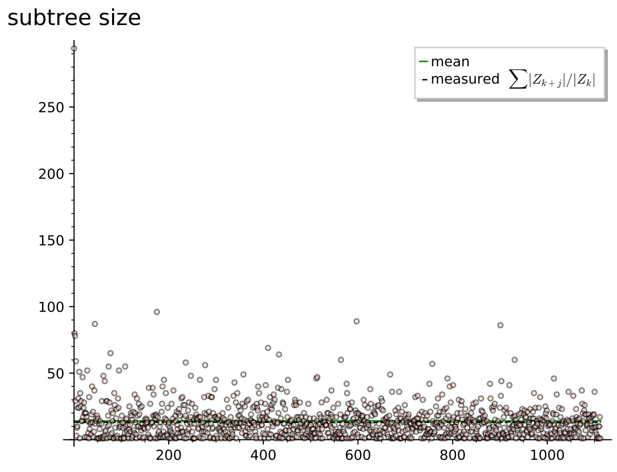

(a) $n = 40, k = 20, \text{tour} = 5$, BKZ block starting at b^*_{51}.

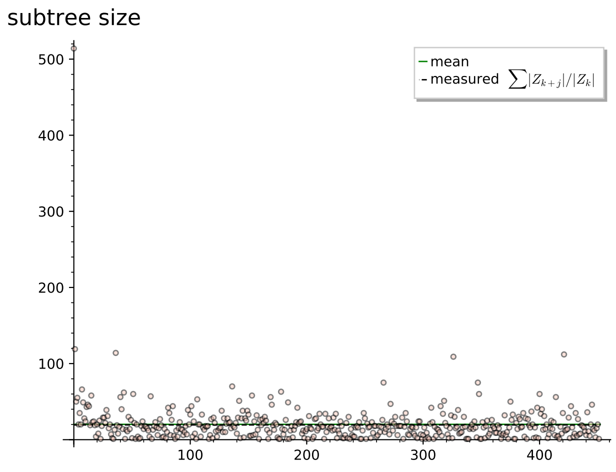

(b) $n = 40, k = 20, \text{tour} = 5$, BKZ block starting at b^*_{101}.

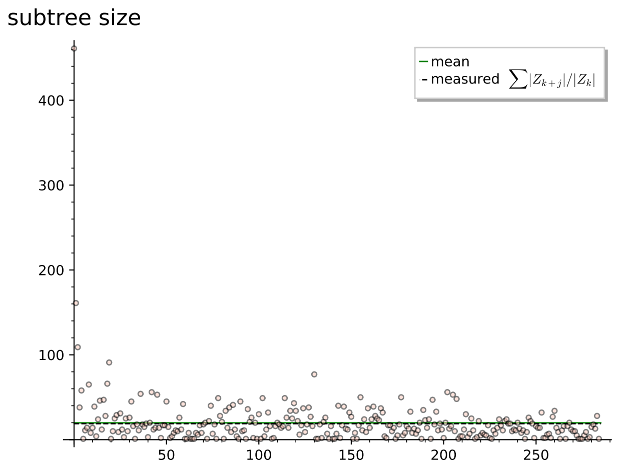

(c) $n = 40, k = 20, \text{tour} = 10$, BKZ block starting at b^*_{51}.

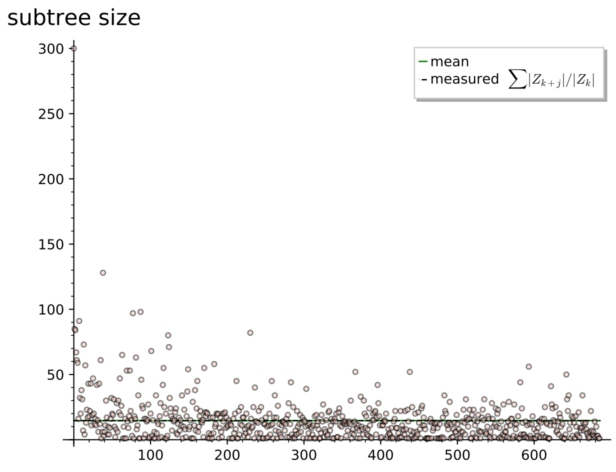

(d) $n = 40, k = 20, \text{tour} = 10$, BKZ block starting at b^*_{101}.

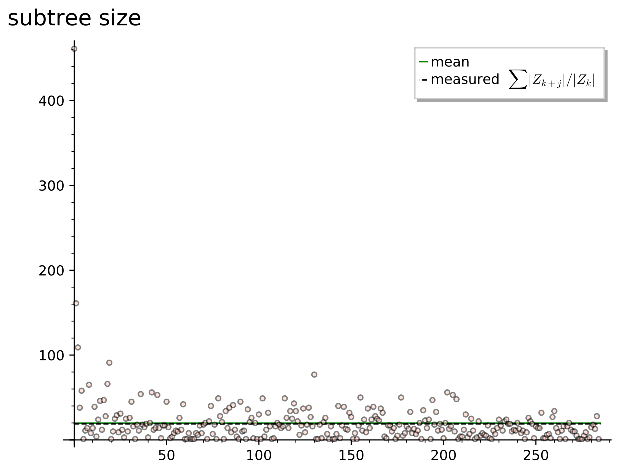

(e) $n = 40, k = 20, \text{tour} = 15$, BKZ block starting at b^*_{51}.

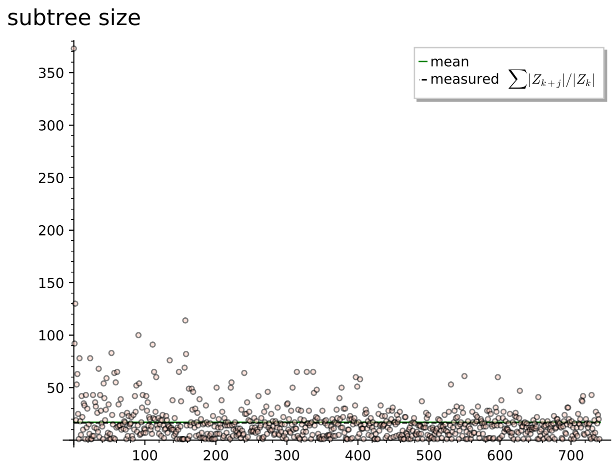

(f) $n = 40, k = 20, \text{tour} = 15$, BKZ block starting at b^*_{101}.

Figure 14: Size of subtrees routed at level k for various lattices encountered during BKZ reduction. The further along the x-axis, the later the subtree was encountered.

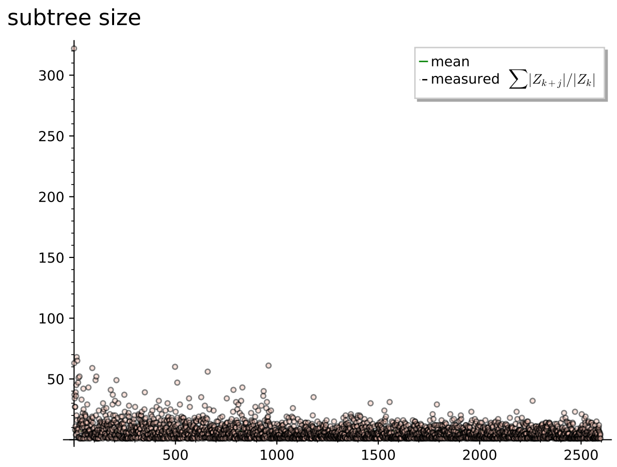

(a) $n = 50, k = 30, \mathrm{tour} = 5$, BKZ block starting at b_{51}^*.

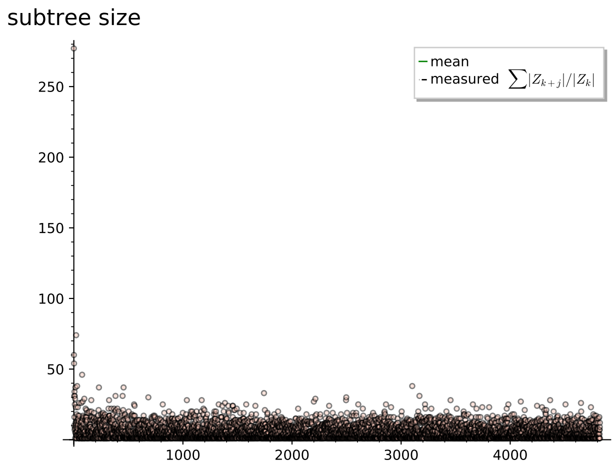

(b) $n = 50, k = 30, \mathrm{tour} = 5$, BKZ block starting at b_{101}^*.

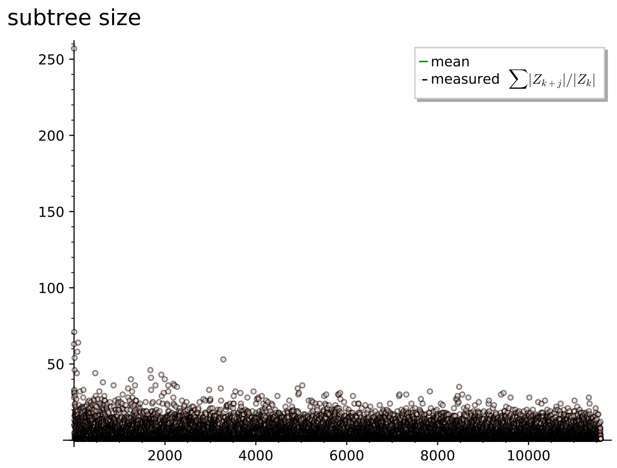

(c) $n = 50, k = 30, \mathrm{tour} = 10$, BKZ block starting at b_{51}^*.

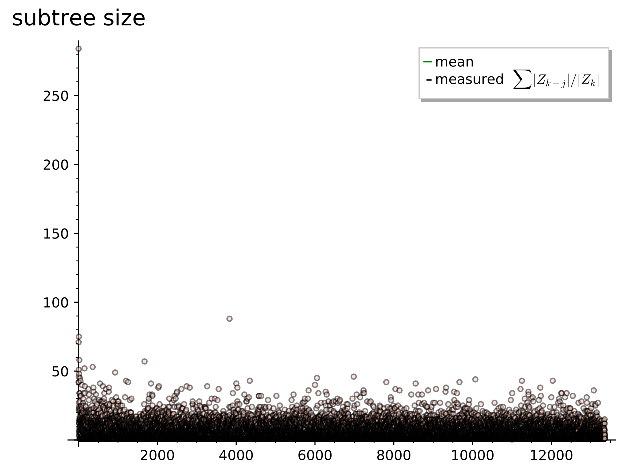

(d) $n = 50, k = 30, \mathrm{tour} = 10$, BKZ block starting at b_{101}^*.

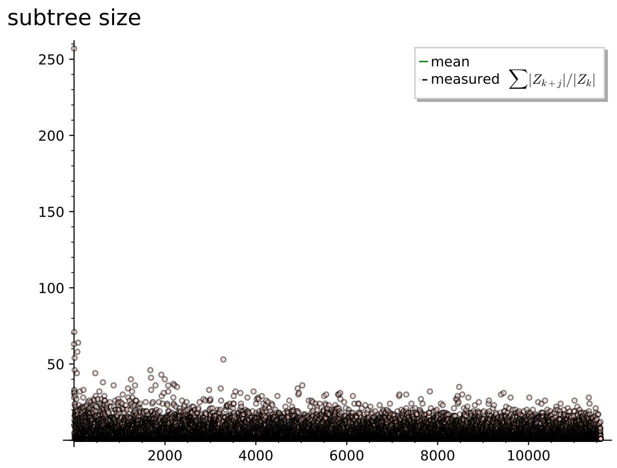

(e) $n = 50, k = 30, \mathrm{tour} = 15$, BKZ block starting at b_{51}^*.

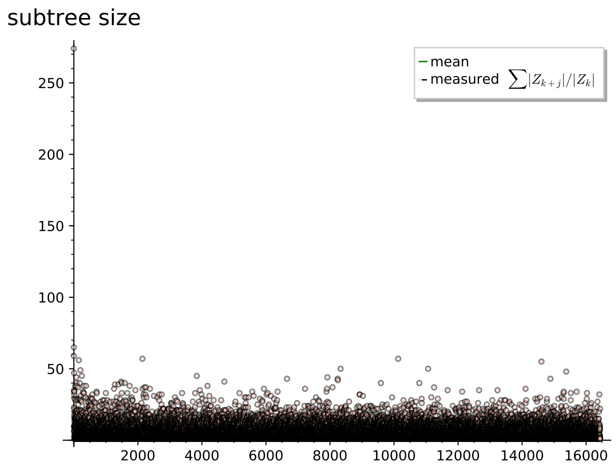

(f) $n = 50, k = 30, \mathrm{tour} = 15$, BKZ block starting at b_{101}^*.

Figure 15: Size of subtrees routed at level k for various lattices encountered during BKZ reduction. The further along the x-axis, the later the subtree was encountered.

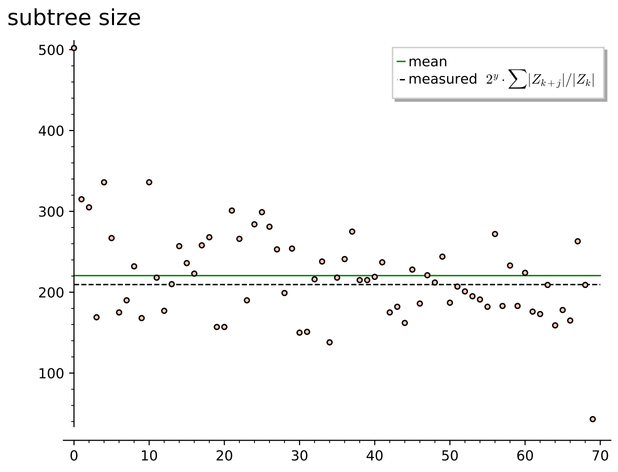

(a) $n = 40, k = 20, \text{tour} = 5$, BKZ block starting at b_{51}^*.

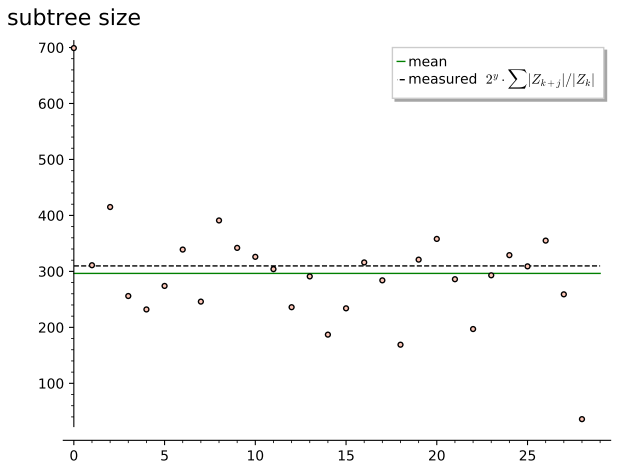

(b) $n = 40, k = 20, \text{tour} = 5$, BKZ block starting at b_{101}^*.

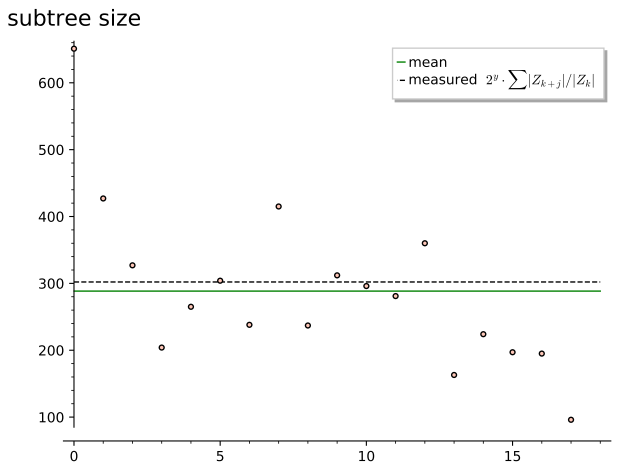

(c) $n = 40, k = 20, \text{tour} = 10$, BKZ block starting at b_{51}^*.

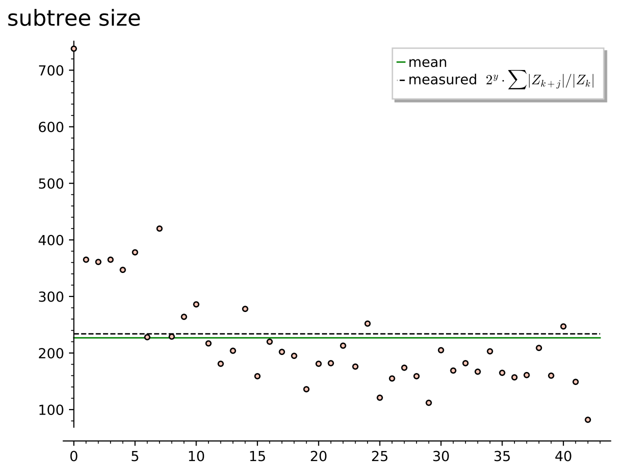

(d) $n = 40, k = 20, \text{tour} = 10$, BKZ block starting at b_{101}^*.

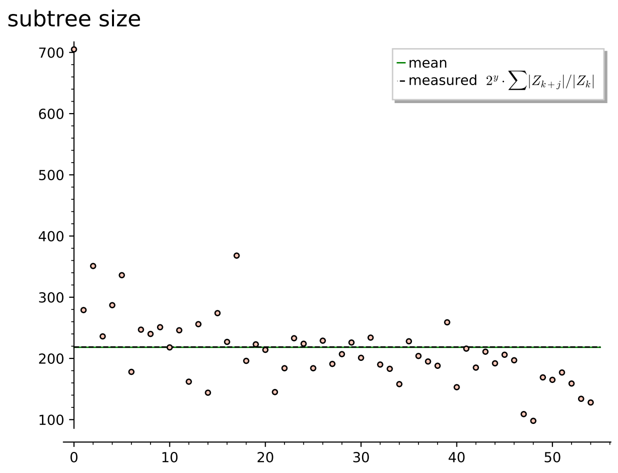

(e) $n = 40, k = 20, \text{tour} = 15$, BKZ block starting at b_{51}^*.

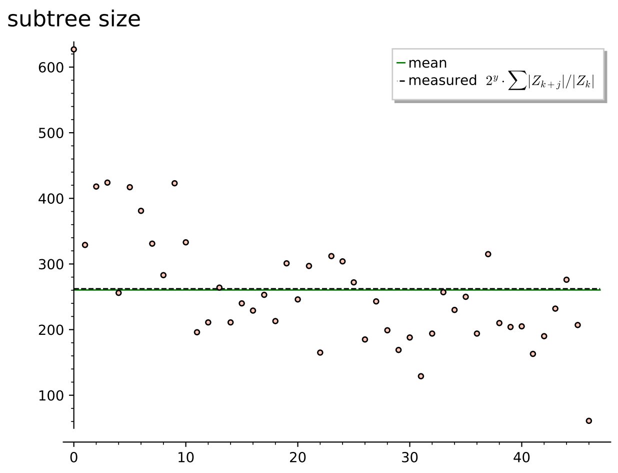

(f) $n = 40, k = 20, \text{tour} = 15$, BKZ block starting at b_{101}^*.

Figure 16: Size of sequential collections of 2^y subtrees routed at level k for various lattices encountered during BKZ reduction. The further along the x-axis, the later the subtrees in the collection were encountered.

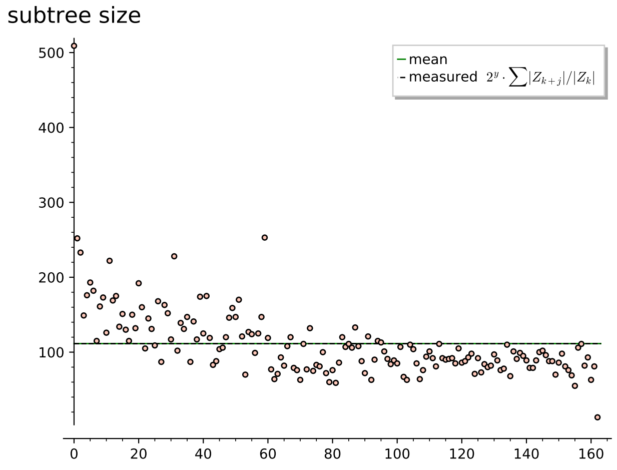

(a) $n = 50, k = 30, \text{tour} = 5$, BKZ block starting at b^*_{51}.

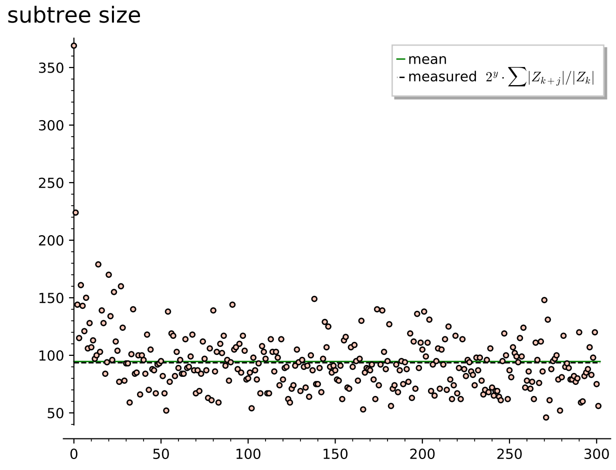

(b) $n = 50, k = 30, \text{tour} = 5$, BKZ block starting at b^*_{101}.

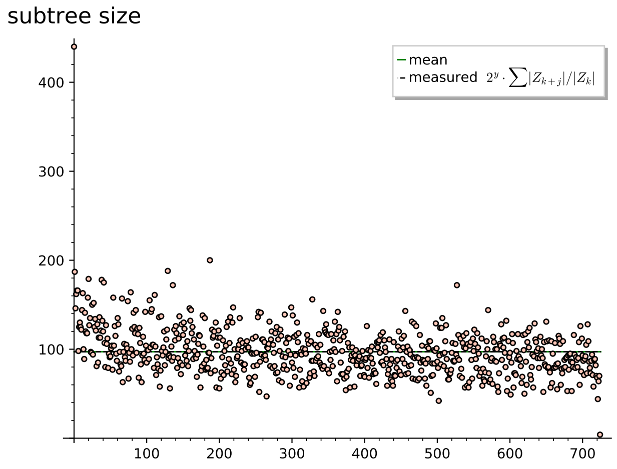

(c) $n = 50, k = 30, \text{tour} = 10$, BKZ block starting at b^*_{51}.

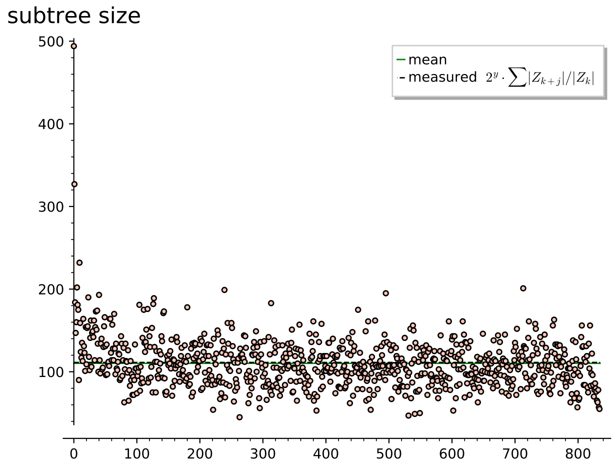

(d) $n = 50, k = 30, \text{tour} = 10$, BKZ block starting at b^*_{101}.

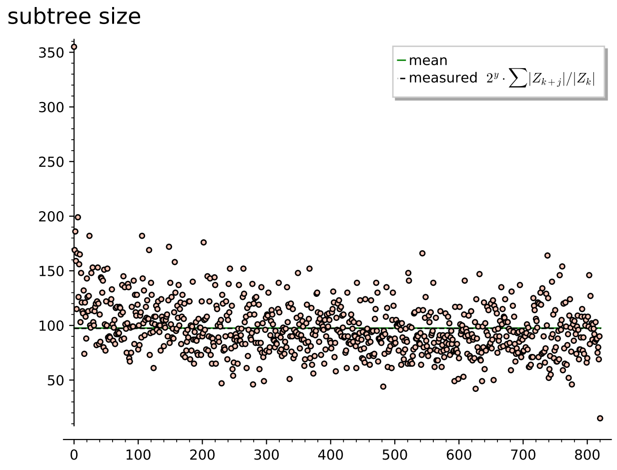

(e) $n = 50, k = 30, \text{tour} = 15$, BKZ block starting at b^*_{51}.

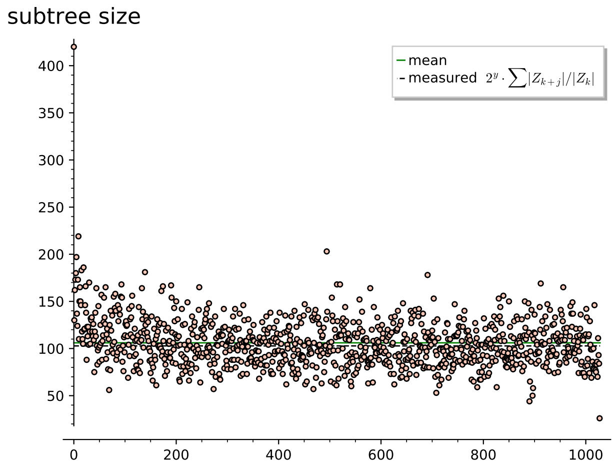

(f) $n = 50, k = 30, \text{tour} = 15$, BKZ block starting at b^*_{101}.

Figure 17: Size of sequential collections of 2^y subtrees routed at level k for various lattices encountered during BKZ reduction. The further along the x-axis, the later the subtrees in the collection were encountered.

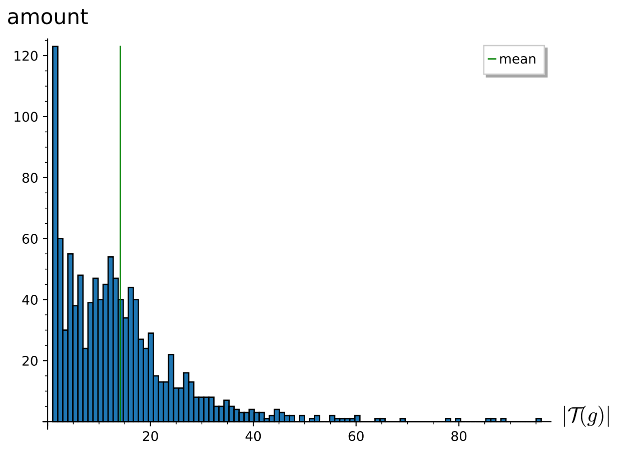

(a) $n = 40, k = 20, \text{tour} = 5$, BKZ block starting at b^*_{49}.

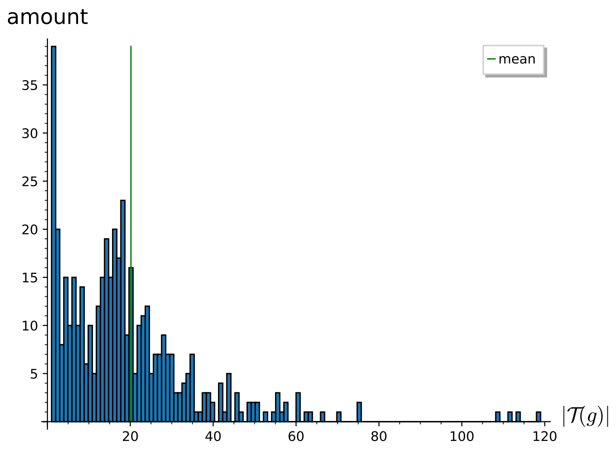

(b) $n = 40, k = 20, \text{tour} = 5$, BKZ block starting at b^*_{99}.

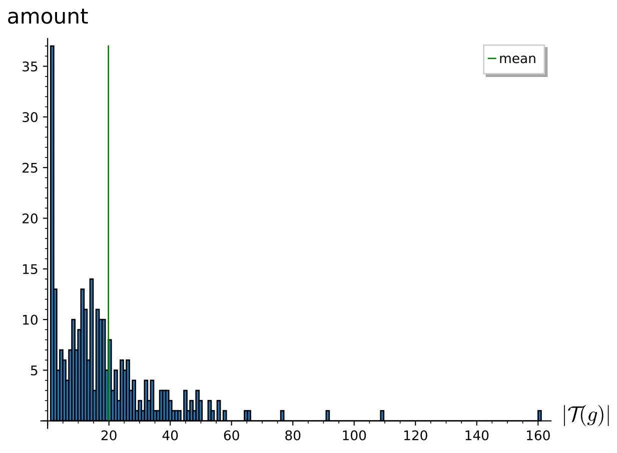

(c) $n = 40, k = 20, \text{tour} = 10$, BKZ block starting at b^*_{49}.

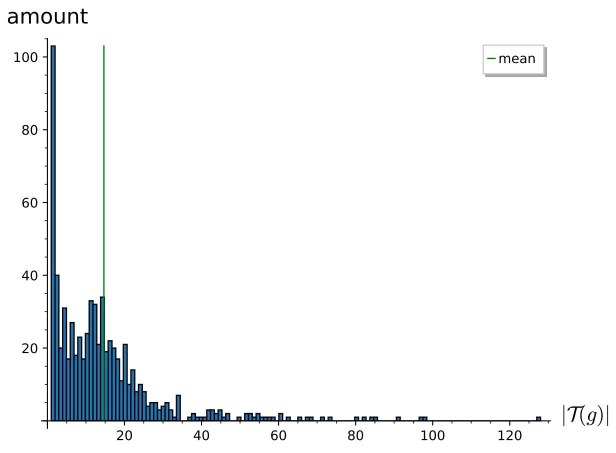

(d) $n = 40, k = 20, \text{tour} = 10$, BKZ block starting at b^*_{99}.

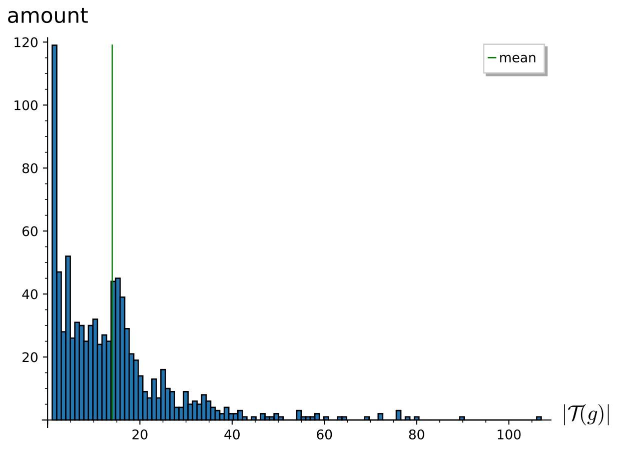

(e) $n = 40, k = 20, \text{tour} = 15$, BKZ block starting at b^*_{49}.

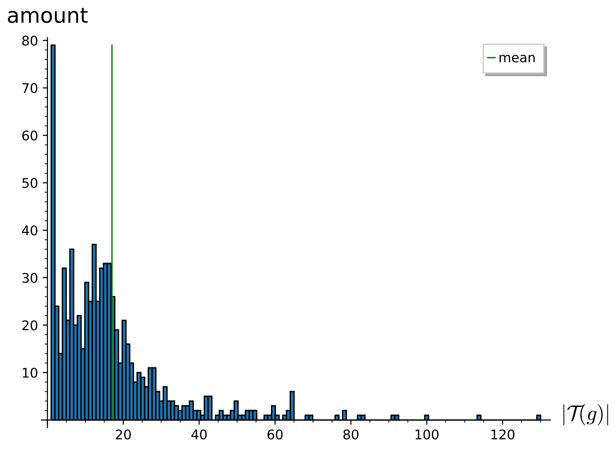

(f) $n = 40, k = 20, \text{tour} = 15$, BKZ block starting at b^*_{99}.

Figure 18: Histogram of the size of subtrees rooted at level k, excluding the first uniquely large subtree. The x-axis is tree size, the y-axis the number of times it is met.

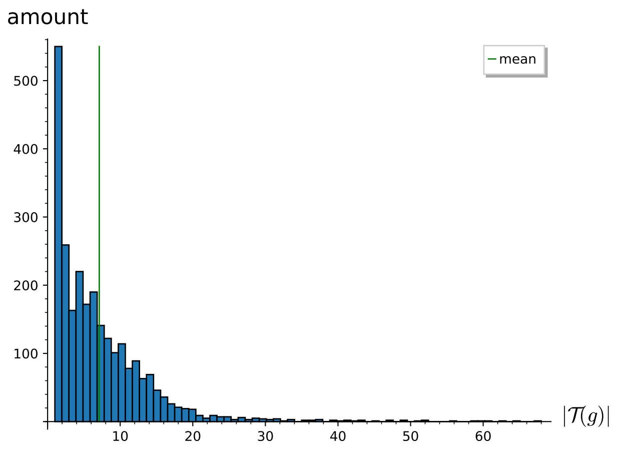

(a) $n = 50, k = 30, \text{tour} = 5$, BKZ block starting at b^*_{49}.

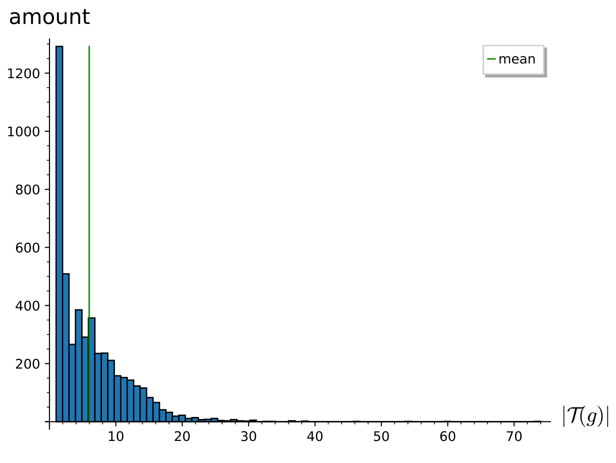

(b) $n = 50, k = 30, \text{tour} = 5$, BKZ block starting at b^*_{99}.

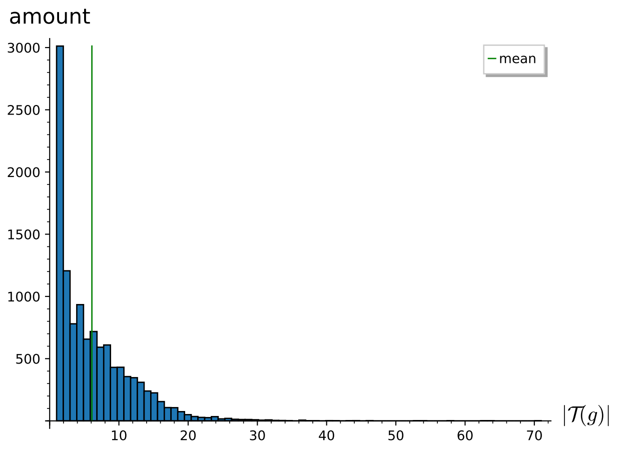

(c) $n = 50, k = 30, \text{tour} = 10$, BKZ block starting at b^*_{49}.

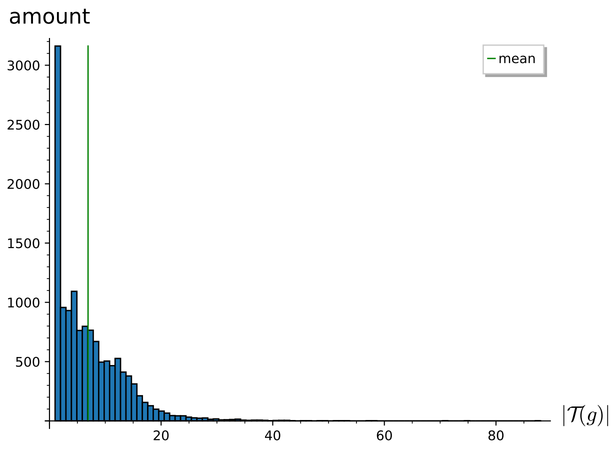

(d) $n = 50, k = 30, \text{tour} = 10$, BKZ block starting at b^*_{99}.

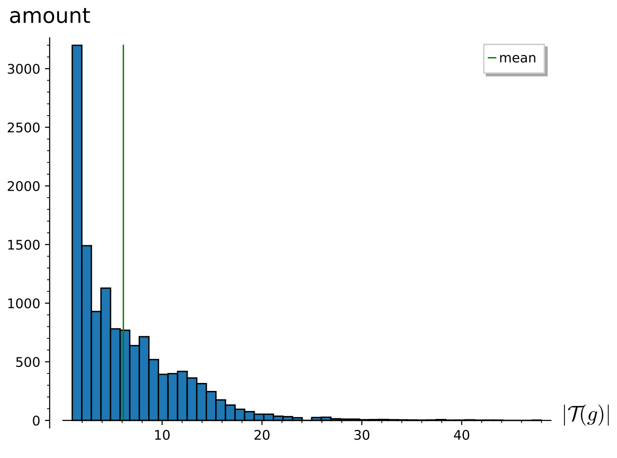

(e) $n = 50, k = 30, \text{tour} = 15$, BKZ block starting at b^*_{49}.

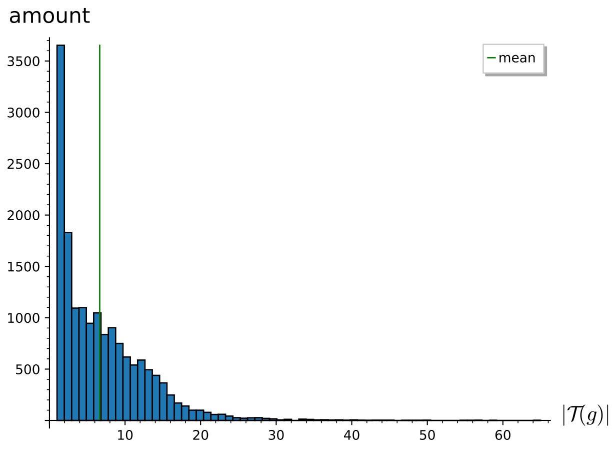

(f) $n = 50, k = 30, \text{tour} = 15$, BKZ block starting at b^*_{99}.

Figure 19: Histogram of the size of subtrees rooted at level k, excluding the first uniquely large subtree. The x-axis is tree size, the y-axis the number of times it is met.

F Instantiation of $\mathcal{W}$

In this appendix, we add a few more details to the analysis done in Section 4.

F.1 Components of $\mathcal{W}$

Given a tree $\mathcal{T}$ of height h, Montanaro [57] defines the operator $\mathcal{W}$ using two operators R_A and R_B, the first acting on all nodes with even distance from the root, and the second on all nodes with odd distance. The implementations of the two operators are nearly identical, and as such we will only capture the original description of R_A [57, Alg. 3] by decomposing it into the following operators:

$U_{\mathbf{Setup}}$**:** quantum operator that prepares the quantum state by advancing the variable assignment (*i.e.*, level k of the tree), and ensures that the operator acts on the *correct* set of nodes (*i.e.*, even or odd levels for $U_{\text{Setup}(R_A)}$ or $U_{\text{Setup}(R_A)}$, respectively).

$U_{\alpha,S}$**:** quantum operator that generates a superposition of children of a node, performing the map $|0\rangle \mapsto |\phi_{\alpha,S}\rangle$, where S is the set of all children of a node.

U_P**:** quantum operator that computes the norm of the projected lattice point being inspected, and compares the length of the projection with the pruning bound R_i. The predicate is executed to identify the children of a node.

U_0**:** reflection through $|0\rangle$. Together with the operator $U_{\alpha,S}$ it performs the diffusion operation $I - 2\,|\phi_{\alpha,S}\rangle\,\langle\phi_{\alpha,S}|$.

$U_{\mathbf{Uncompute}}$**:** quantum operator to uncompute the ancillary states and the inversion of the setup step U_{Setup}.

F.2 Quantum Arithmetic

Smallest known arithmetic circuits. The quantum arithmetic literature contains many design proposals for integer and floating point adders and multipliers. Generally, most algorithms are either "ports" of classical designs [28,37,38,61,59], or they rely on the quantum Fourier transform (QFT) to evaluate these operations [71,47]. As not all papers work using the same metrics or even quantum computing architectures, direct comparisons and trade-off evaluations can be difficult. For example, Pham and Svore [63] claim additions in constant depth and multiplications in logarithmic depth, however this seems to require a specifically designed quantum architecture. For a rule-of-thumb estimation of our attack costs, we opt to chose potentially more common asymptotics for adders and multipliers achieving the smallest T counts and depths in our literature review (other than [63]). We report these in Table 1, and ignore constants and lower order terms hidden by the $\mathcal{O}$. Whenever numbers of different bit lengths are multiplied, we conservatively assume both to have the smaller length, since we have not found sources describing quantum circuits for unbalanced multiplication. For the "$x \leq y$" comparison operator, we use a circuit with the same asymptotic size of an adder [28].

Floating point numbers. We also define a value ξ that equals the amount of floating point precision required to store the coefficient of the basis vectors b_i. The literature on this topic either proposes algorithms for estimating the required precision [67,27], appearing this to be about $\Theta(n)$, or uses double precision [40]. We notice that while the `fplll` library [78] includes support for arbitrary precision floating point numbers, often experiments use double- or quadruple-precision floating point numbers. As a conservative choice, we observe that any setting where quantum-enumeration would be advantageous would likely result in requiring more than double-precision, since otherwise cheap classical implementations are available, and therefore consider $\xi = 53$ to be a lower bound on the required precision.

F.3 Arithmetic Cost

Depth and cost estimation of $\mathcal{W}$. In our setting, quantum enumeration is being performed on a tree $\mathcal{T}(g \in Z_k)$ of height $h = n - k$, where n is the dimension of the full lattice Λ being enumerated. This process would require performing arithmetic using the projected lattice basis vectors $(\pi_{n-k+1}(b_{k+1}), \dots, \pi_{n-k+1}(b_n))$ of Λ. In an attempt to unburden notation, in this paragraph we temporarily relable these as $(b_1, \dots, b_h)$, and consider them to be h-dimensional by applying an appropriate rotation. Our estimate for the cost of each component of $W^{\min}$ is then:

$U_{\mathbf{Setup}}$**:** sets up the states, we assume $\text{GCost}(U_{\text{Setup}}) = \text{T-Depth}(U_{\text{Setup}}) = 0$.

$U^{\mathbf{min}}_{\alpha,S}$**:** generates a superposition of the children of a node. At a bare minimum, this requires a uniform superposition $\sum_{i=0}^{q-1} |i\rangle$ which is computed by a single (parallel) layer of Hadamard gates. Since we are only accounting for T, we assume $\text{T-Depth}(U^{\min}_{\alpha,S}) = \text{T-Depth}(U^{\min}_P)$ and $\text{GCost}(U^{\min}_{\alpha,S}) = \text{GCost}(U^{\min}_P)$, as Hadamard gates do not contribute T gates.

$U^{\mathbf{min}}_P$**:** evaluates the predicate P which identifies projected vectors $v \in \pi_{n-\ell+1}(\Lambda)$ such that $||v|| \le R_\ell$ and $\pi_{n-k+1}(v) = g$, for all levels $k < \ell \le n$. In order to lower-bound the cost of this operation, we only consider the case of evaluating this inequality at $\ell = n$, where the condition becomes checking whether

Table 8: Assumed cost of arithmetic operations in $U^{\min}_P$. Each operations has input numbers of bit length x_i and outputs numbers of size x_{i+1}

Operation	Input bit lengths	T-Depth	GCost
$(c_i, (\vec{b}_i)_j) \mapsto c_i(\vec{b}_i)_j$	$x_0 = \min(\lambda, \xi)$	$\log^2(x_0)$	$h^2 x_0 \log(x_0) \log(\log(x_0))$
$(c_i(\vec{b}_i)_j)_i \mapsto \sum_i c_i(\vec{b}_i)_j$	$x_1 = \lambda + \xi$	$\log h \log(x_1)$	$h^2 x_1$
$\sum_i c_i(\vec{b}_i)_j \mapsto (\sum_i c_i(\vec{b}_i)_j)^2$	$x_2 = \lambda + \xi + \log h$	$\log^2(x_2)$	$h x_2 \log(x_2) \log(\log(x_2))$
$((\sum_i c_i(\vec{b}_i)_j)^2)_j \mapsto \|\| \sum_i c_i \vec{b}_i \|\|^2$	$x_3 = 2(\lambda + \xi + \log h)$	$\log h \log(x_3)$	$h x_3$
$\|\| \sum_i c_i \vec{b}_i \|\|^2 \le R^2 - \|\|g\|\|^2$	$x_4 = 2(\lambda + \xi + \log h) + \log h$	$\log(x_4)$	x_4

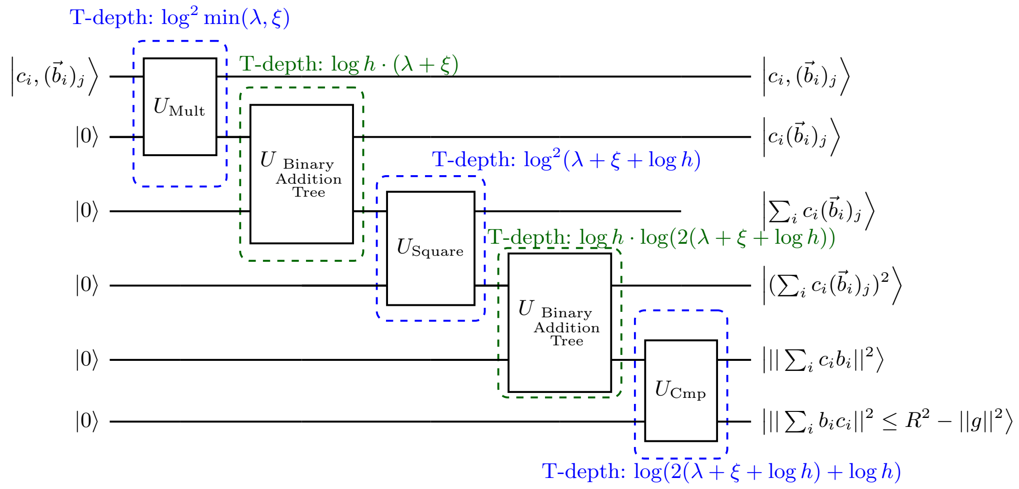
T-depth: $\log^2 \min(\lambda, \xi)$
$\left|c_i, (\vec{b}_i)_j\right\rangle$
U_{Mult}
T-depth: $\log h \cdot (\lambda + \xi)$
$|0\rangle$
U Binary Addition Tree
$|0\rangle$
T-depth: $\log^2(\lambda + \xi + \log h)$
U_{Square}
T-depth: $\log h \cdot \log(2(\lambda + \xi + \log h))$
$|0\rangle$
U Binary Addition Tree
$|0\rangle$
U_{Cmp}
$|0\rangle$
T-depth: $\log(2(\lambda + \xi + \log h) + \log h)$
$\left|c_i, (\vec{b}_i)_j\right\rangle$
$\left|c_i(\vec{b}_i)_j\right\rangle$
$\left|\sum_i c_i(\vec{b}_i)_j\right\rangle$
$\left|(\sum_i c_i(\vec{b}_i)_j)^2\right\rangle$
$\left|||\sum_i c_i b_i||^2\right\rangle$
$\left|||\sum_i b_i c_i||^2 \leq R^2 - ||g||^2\right\rangle$

Figure 20: Minimal quantum circuit of $U_P^{\min}$.

$||\sum_{i\leq h} c_i\vec{b}_i||^2 \leq R^2 - ||g||^2$.[14] The cost of the operation needs to account for at least the cost of the following operations (summarised in Table 8):

1. Parallel multiplication of h^2 pairs $(c_i, (\vec{b}_i)_j) \mapsto c_i(\vec{b}_i)_j$, of λ- and ξ-bit length, outputting numbers of bit length $\lambda + \xi$.
2. Addition of coefficients $(c_1(\vec{b}_1)_j, \dots, c_h(\vec{b}_h)_j) \mapsto \sum_i c_i(\vec{b}_i)_j$ for $j \in [h]$. These additions can be run in parallel over j. For a fixed j, the corresponding sum is run by adding terms in pairs, forming a binary tree of sums. Each $\sum_i c_i(\vec{b}_i)_j$ output is $\lambda + \xi + \log h$ bits long.
3. Squaring the $\sum_i c_i(\vec{b}_i)_j$ sums in parallel (output bit length $2(\lambda + \xi + \log h)$) and adding them in a binary-tree fashion to obtain $||\sum_{i\leq h} c_i\vec{b}_i||^2 = \sum_j(\sum_i c_i(\vec{b}_i)_j)^2$ of bit length $2(\lambda + \xi + \log h) + \log h$.
4. The last operation is the comparison with the (adjusted) pruning bound $R^2 - ||g||^2$.

We depict the implementation of the minimal $U_P^{\min}$ implementation in Fig. 20.

U_0: the quantum operator computing $2\,|0\rangle\langle 0| - \mathrm{Id}$ (with Id the identity operator) which requires mult-controlled-Z gates, we estimate requiring at least one T gate.

$U_{\text{Uncompute}}$: we conservatively assume that uncomputation does not require T gates, as in the case of measurement-based uncomputation of AND gates in [41], and assume T-DEPTH$(U_{\text{Uncompute}})$ = GCOST$(U_{\text{Uncompute}}) = 0$.

[14] In classical implementations, this computation benefits from extensive caching of Gram-Schmidt orthogonalisation operations and results [78]. Asymptotically, the number of individual arithmetic operations is the same as if computing directly from the basis $(b_1, \dots, b_h)$.

G Further results from Kyber Parameters

G.1 Tables for the Quasi-Sqrt and the Canonical Bit Security

As an alternative to the comparison with the cost of Grover on AES one can check whether the attack cost under depth constraints ever achieves a "quasi-quadratic" speedup over classical enumeration (meaning going from $\#\mathcal{T}$ gates to $\sqrt{\#\mathcal{T} \cdot h}$, where h is the height of $\mathcal{T}$), as it could be expected from Theorem 1. Alternatively, for a scheme like Kyber-512 (with analogous notions for -768 and -1024), one could consider an attack successful if its gate cost is lower than $2^{\text{canonical bit security}} = 2^{128}$, albeit this is explicitly not the cost metric chosen by NIST and hence plausibly not targeted by the Kyber team.

G.2 Figures for the Query-based Result

In this section we present the figures from our estimations of the cost of quantum enumeration that we have not reported in Section 5. For all cost estimations the quantum operator $\text{GC}\textsc{ost}(\mathcal{W})$ and $\text{T-Depth}(\mathcal{W})$ are estimated as in Section 4.1 and with $DF(\mathcal{W})$, $QD(\mathcal{W})$, $WQ(\mathcal{T}, W)$ as in Section 3,

- Fig. 23c shows the cost estimation for Kyber-512 with $\text{T-D}\textsc{epth}(\text{QPE}(\mathcal{W})) \leq 2^{64}$.
- Fig. 22 shows the cost estimation without any $\textsc{MaxDepth}$ constraint on $\text{T-D}\textsc{epth}(\text{QPE}(\mathcal{W}))$.
- Fig. 23 shows the cost estimation for Kyber-768 and Kyber-1024 assuming $\text{T-D}\textsc{epth}(\text{QPE}(\mathcal{W})) \leq \{2^{40}, 2^{64}, 2^{96}\}$.

Table 9: Summary of the values for the Jensen's gap 2^z at crossover points of our combined classical-quantum enumeration attacks against Kyber and the quasi-square root speed up $\sqrt{\#\mathcal{T} \cdot h}$. We remark that exact crossovers happen at fractional values of z. In this table we round down threshold values of z. MaxDepth is abbreviated to MD. Cost is as in Table 6

less likely to be feasible ▇▇▇▇▇▇ more likely to be feasible

Crossover points when comparing quasi-square-root against the total GCost (cf. Table 6) with …

		… $\mathcal{W}$ as in Section 4.1			… $\mathcal{W}$ as in Section 4.2		
MD	Kyber	LB/UB	UB/UB	LB/LB	LB/UB	UB/UB	LB/LB
2^{40}	-512	$z \geq 0, k \leq 25$ Cost $\geq 2^{63}$	$z \geq 29, k \leq 11$ Cost $\geq 2^{98}$	$z \geq 25, k \leq 59$ Cost $\geq 2^{89}$	$z \geq 2, k \leq 24$ Cost $\geq 2^{90}$	$z \geq 45, k \leq 12$ Cost $\geq 2^{98}$	$z \geq 41, k \leq 63$ Cost $\geq 2^{89}$
	-768	$z \geq 8, k \leq 75$ Cost $\geq 2^{166}$	$z > 64$	$z \geq 63, k \leq 77$ Cost $\geq 2^{165}$	$z \geq 25, k \leq 67$ Cost $\geq 2^{164}$	$z > 64$	$z > 64$
	-1024	$z \geq 41, k \leq 115$ Cost $\geq 2^{261}$	$z > 64$	$z > 64$	$z \geq 57, k \leq 105$ Cost $\geq 2^{262}$	$z > 64$	$z > 64$
2^{64}	-512	$z \geq 0, k \leq 26$ Cost $\geq 2^{63}$	$z \geq 17, k \leq 11$ Cost $\geq 2^{98}$	$z \geq 13, k \leq 59$ Cost $\geq 2^{89}$	$z \geq 0, k \leq 26$ Cost $\geq 2^{75}$	$z \geq 33, k \leq 5$ Cost $\geq 2^{98}$	$z \geq 29, k \leq 54$ Cost $\geq 2^{89}$
	-768	$z \geq 0, k \leq 64$ Cost $\geq 2^{157}$	$z \geq 54, k \leq 33$ Cost $\geq 2^{170}$	$z \geq 51, k \leq 77$ Cost $\geq 2^{165}$	$z \geq 13, k \leq 67$ Cost $\geq 2^{164}$	$z > 64$	$z > 64$
	-1024	$z \geq 28, k \leq 105$ Cost $\geq 2^{262}$	$z > 64$	$z > 64$	$z \geq 45, k \leq 100$ Cost $\geq 2^{262}$	$z > 64$	$z > 64$
2^{96}	-512	$z \geq 0, k \leq 26$ Cost $\geq 2^{63}$	$z \geq 1, k \leq 2$ Cost $\geq 2^{98}$	$z \geq 0, k \leq 40$ Cost $\geq 2^{89}$	$z \geq 0, k \leq 26$ Cost $\geq 2^{75}$	$z \geq 24, k \leq 1$ Cost $\geq 2^{98}$	$z \geq 24, k \leq 40$ Cost $\geq 2^{89}$
	-768	$z \geq 0, k \leq 53$ Cost $\geq 2^{126}$	$z \geq 38, k \leq 12$ Cost $\geq 2^{170}$	$z \geq 35, k \leq 77$ Cost $\geq 2^{165}$	$z \geq 0, k \leq 64$ Cost $\geq 2^{158}$	$z \geq 54, k \leq 12$ Cost $\geq 2^{171}$	$z \geq 52, k \leq 62$ Cost $\geq 2^{164}$
	-1024	$z \geq 12, k \leq 100$ Cost $\geq 2^{262}$	$z > 64$	$z > 64$	$z \geq 29, k \leq 100$ Cost $\geq 2^{262}$	$z > 64$	$z > 64$
∞	-512	$z \geq 0, k \leq 26$ Cost $\geq 2^{63}$	$z \geq 0, k \leq 1$ Cost $\geq 2^{97}$	$z \geq 0, k \leq 40$ Cost $\geq 2^{89}$	$z \geq 0, k \leq 26$ Cost $\geq 2^{75}$	$z \geq 24, k \leq 1$ Cost $\geq 2^{98}$	$z \geq 24, k \leq 40$ Cost $\geq 2^{89}$
	-768	$z \geq 0, k \leq 37$ Cost $\geq 2^{113}$	$z \geq 2, k \leq 3$ Cost $\geq 2^{171}$	$z \geq 0, k \leq 31$ Cost $\geq 2^{165}$	$z \geq 0, k \leq 37$ Cost $\geq 2^{138}$	$z \geq 28, k \leq 3$ Cost $\geq 2^{170}$	$z \geq 25, k \leq 31$ Cost $\geq 2^{165}$
	-1024	$z \geq 0, k \leq 33$ Cost $\geq 2^{206}$	$z \geq 2, k \leq 3$ Cost $\geq 2^{269}$	$z \geq 0, k \leq 1$ Cost $\geq 2^{262}$	$z \geq 0, k \leq 33$ Cost $\geq 2^{232}$	$z \geq 29, k \leq 3$ Cost $\geq 2^{268}$	$z \geq 26, k \leq 11$ Cost $\geq 2^{263}$
$\infty_{k=0}$	-512	$z \geq 0, k = 0$ Cost $\geq 2^{89}$	$z \geq 0, k = 0$ Cost $\geq 2^{97}$	$z \geq 0, k = 0$ Cost $\geq 2^{89}$	$z \geq 24, k = 0$ Cost $\geq 2^{90}$	$z \geq 24, k = 0$ Cost $\geq 2^{98}$	$z \geq 24, k = 0$ Cost $\geq 2^{90}$
	-768	$z \geq 0, k = 0$ Cost $\geq 2^{165}$	$z \geq 0, k = 0$ Cost $\geq 2^{170}$	$z \geq 0, k = 0$ Cost $\geq 2^{165}$	$z \geq 25, k = 0$ Cost $\geq 2^{165}$	$z \geq 25, k = 0$ Cost $\geq 2^{171}$	$z \geq 25, k = 0$ Cost $\geq 2^{165}$
	-1024	$z \geq 0, k = 0$ Cost $\geq 2^{262}$	$z \geq 0, k = 0$ Cost $\geq 2^{268}$	$z \geq 0, k = 0$ Cost $\geq 2^{262}$	$z \geq 26, k = 0$ Cost $\geq 2^{263}$	$z \geq 26, k = 0$ Cost $\geq 2^{269}$	$z \geq 26, k = 0$ Cost $\geq 2^{263}$

Table 10: Summary of the values for the Jensen's gap 2^z at crossover points of our combined classical-quantum enumeration attacks against Kyber and the canonical $128, 192, 256$ bit security respectively. We remark that exact crossovers happen at fractional values of z. In this table we round down threshold values of z. MaxDepth is abbreviated to MD. Cost is as in Table 6

less likely to be feasible ■ more likely to be feasible

Crossover points when comparing the canonical bit security against the total GCost (cf. Table 6) with …

		…$\mathcal{W}$ as in Section 4.1			…$\mathcal{W}$ as in Section 4.2		
MD	Kyber	LB/UB	UB/UB	LB/LB	LB/UB	UB/UB	LB/LB
2^{40}	-512	$z \geq 0, k \leq 25$ Cost $\geq 2^{63}$	$z \geq 15, k \leq 28$ Cost $\geq 2^{126}$	$z \geq 6, k \leq 92$ Cost $\geq 2^{127}$	$z \geq 0, k \leq 27$ Cost $\geq 2^{94}$	$z \geq 30, k \leq 24$ Cost $\geq 2^{127}$	$z \geq 22, k \leq 96$ Cost $\geq 2^{126}$
	-768	$z \geq 0, k \leq 87$ Cost $\geq 2^{184}$	$z \geq 56, k \leq 33$ Cost $\geq 2^{190}$	$z \geq 50, k \leq 114$ Cost $\geq 2^{191}$	$z \geq 12, k \leq 80$ Cost $\geq 2^{191}$	$z > 64$	$z > 64$
	-1024	$z \geq 44, k \leq 112$ Cost $\geq 2^{255}$	$z > 64$	$z > 64$	$z \geq 61, k \leq 105$ Cost $\geq 2^{254}$	$z > 64$	$z > 64$
2^{64}	-512	$z \geq 0, k \leq 26$ Cost $\geq 2^{63}$	$z \geq 3, k \leq 28$ Cost $\geq 2^{126}$	$z \geq 0, k \leq 83$ Cost $\geq 2^{115}$	$z \geq 0, k \leq 26$ Cost $\geq 2^{75}$	$z \geq 18, k \leq 24$ Cost $\geq 2^{127}$	$z \geq 10, k \leq 79$ Cost $\geq 2^{127}$
	-768	$z \geq 0, k \leq 64$ Cost $\geq 2^{157}$	$z \geq 44, k \leq 33$ Cost $\geq 2^{190}$	$z \geq 38, k \leq 114$ Cost $\geq 2^{191}$	$z \geq 0, k \leq 67$ Cost $\geq 2^{190}$	$z \geq 60, k \leq 37$ Cost $\geq 2^{191}$	$z \geq 54, k \leq 106$ Cost $\geq 2^{191}$
	-1024	$z \geq 32, k \leq 100$ Cost $\geq 2^{254}$	$z > 64$	$z > 64$	$z \geq 49, k \leq 100$ Cost $\geq 2^{254}$	$z > 64$	$z > 64$
2^{96}	-512	$z \geq 0, k \leq 26$ Cost $\geq 2^{63}$	$z \geq 0, k \leq 2$ Cost $\geq 2^{100}$	$z \geq 0, k \leq 40$ Cost $\geq 2^{89}$	$z \geq 0, k \leq 26$ Cost $\geq 2^{75}$	$z \geq 3, k \leq 5$ Cost $\geq 2^{126}$	$z \geq 0, k \leq 46$ Cost $\geq 2^{115}$
	-768	$z \geq 0, k \leq 53$ Cost $\geq 2^{126}$	$z \geq 28, k \leq 33$ Cost $\geq 2^{190}$	$z \geq 22, k \leq 77$ Cost $\geq 2^{191}$	$z \geq 0, k \leq 64$ Cost $\geq 2^{158}$	$z \geq 44, k \leq 26$ Cost $\geq 2^{191}$	$z \geq 39, k \leq 77$ Cost $\geq 2^{190}$
	-1024	$z \geq 16, k \leq 100$ Cost $\geq 2^{254}$	$z > 64$	$z > 64$	$z \geq 33, k \leq 100$ Cost $\geq 2^{254}$	$z > 64$	$z > 64$
∞	-512	$z \geq 0, k \leq 26$ Cost $\geq 2^{63}$	$z \geq 0, k \leq 1$ Cost $\geq 2^{97}$	$z \geq 0, k \leq 40$ Cost $\geq 2^{89}$	$z \geq 0, k \leq 26$ Cost $\geq 2^{75}$	$z \geq 0, k \leq 1$ Cost $\geq 2^{122}$	$z \geq 0, k \leq 40$ Cost $\geq 2^{113}$
	-768	$z \geq 0, k \leq 37$ Cost $\geq 2^{113}$	$z \geq 0, k \leq 3$ Cost $\geq 2^{173}$	$z \geq 0, k \leq 31$ Cost $\geq 2^{165}$	$z \geq 0, k \leq 37$ Cost $\geq 2^{138}$	$z \geq 7, k \leq 3$ Cost $\geq 2^{191}$	$z \geq 0, k \leq 31$ Cost $\geq 2^{190}$
	-1024	$z \geq 0, k \leq 33$ Cost $\geq 2^{206}$	$z \geq 16, k \leq 3$ Cost $\geq 2^{255}$	$z \geq 7, k \leq 1$ Cost $\geq 2^{255}$	$z \geq 0, k \leq 33$ Cost $\geq 2^{232}$	$z \geq 42, k \leq 3$ Cost $\geq 2^{255}$	$z \geq 34, k \leq 11$ Cost $\geq 2^{255}$
$\infty_{k=0}$	-512	$z \geq 0, k = 0$ Cost $\geq 2^{89}$	$z \geq 0, k = 0$ Cost $\geq 2^{97}$	$z \geq 0, k = 0$ Cost $\geq 2^{89}$	$z \geq 0, k = 0$ Cost $\geq 2^{114}$	$z \geq 0, k = 0$ Cost $\geq 2^{122}$	$z \geq 0, k = 0$ Cost $\geq 2^{114}$
	-768	$z \geq 0, k = 0$ Cost $\geq 2^{165}$	$z \geq 0, k = 0$ Cost $\geq 2^{170}$	$z \geq 0, k = 0$ Cost $\geq 2^{165}$	$z \geq 0, k = 0$ Cost $\geq 2^{190}$	$z \geq 5, k = 0$ Cost $\geq 2^{191}$	$z \geq 0, k = 0$ Cost $\geq 2^{190}$
	-1024	$z \geq 7, k = 0$ Cost $\geq 2^{255}$	$z \geq 13, k = 0$ Cost $\geq 2^{255}$	$z \geq 7, k = 0$ Cost $\geq 2^{255}$	$z \geq 34, k = 0$ Cost $\geq 2^{255}$	$z \geq 40, k = 0$ Cost $\geq 2^{255}$	$z \geq 34, k = 0$ Cost $\geq 2^{255}$

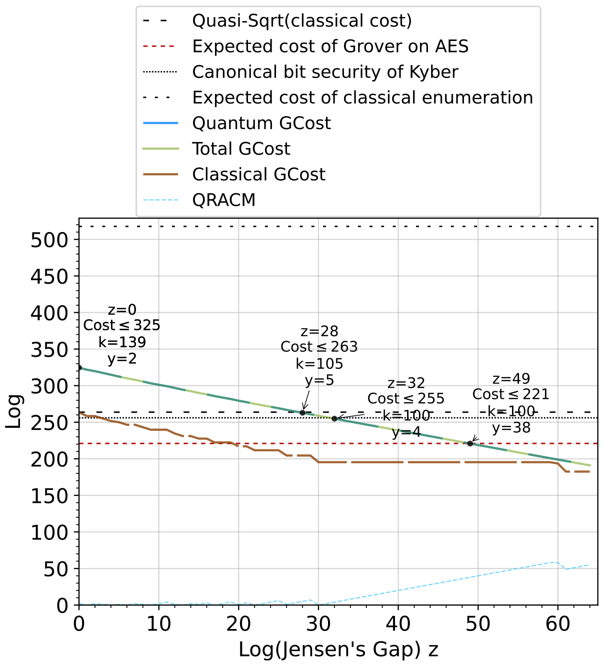

(a) Kyber-1024, MaxDepth $= 2^{64}$.

Figure 21: Cost estimation for Kyber-1024 under MaxDepth restriction 2^{64} with the instantiation for operator $\mathcal{W}$ as in Section 4.1, cf. Table 6 for an expanded legend, corresponding to the lower bound (LB/UB) for Conjecture 3.

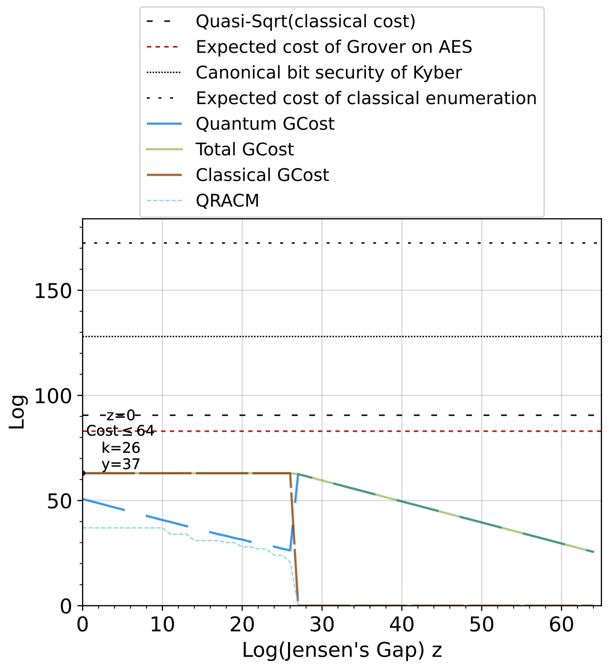

(a) Cost estimation for Kyber-512 without MaxDepth restrictions.

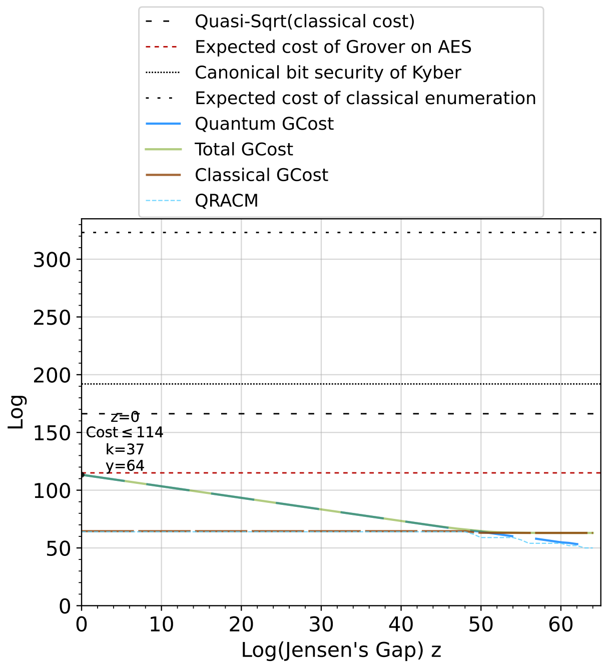

(b) Cost estimation for Kyber-768 without MaxDepth restrictions.

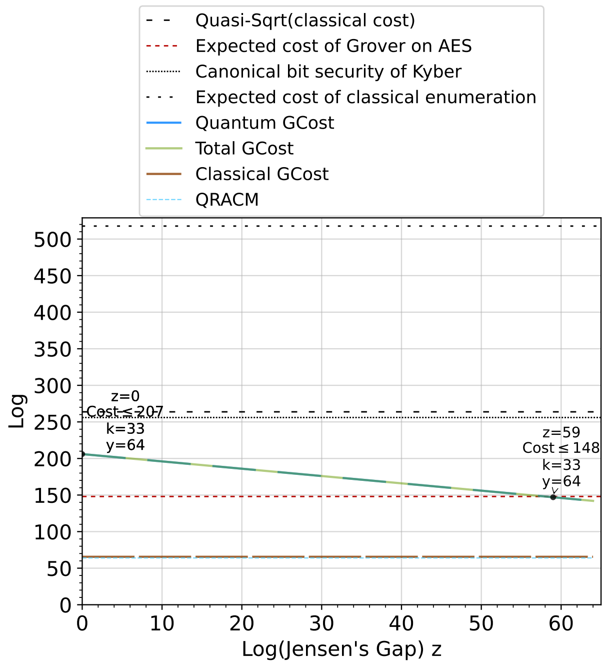

(c) Cost estimation for Kyber-1024 without MaxDepth restrictions.

Figure 22: Cost estimation for Kyber with the instantiation for operator $\mathcal{W}$ as in Section 4.1 and with DF = 1, QD = 1, $b = 1$ (see Section 3), corresponding to the lower bound (LB/UB) for the Conjecture 3.

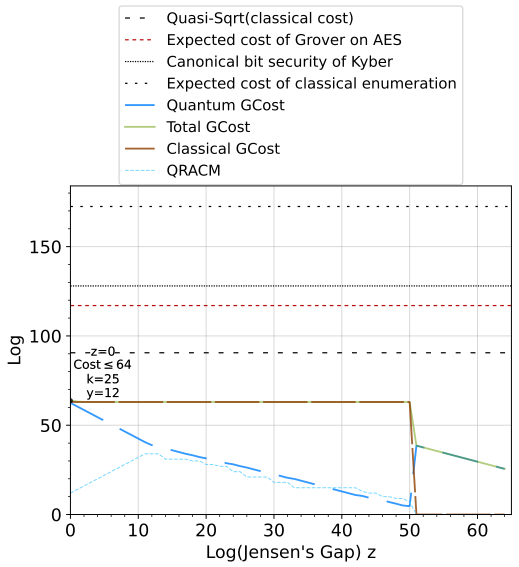

(a) Kyber-512, MaxDepth $= 2^{40}$

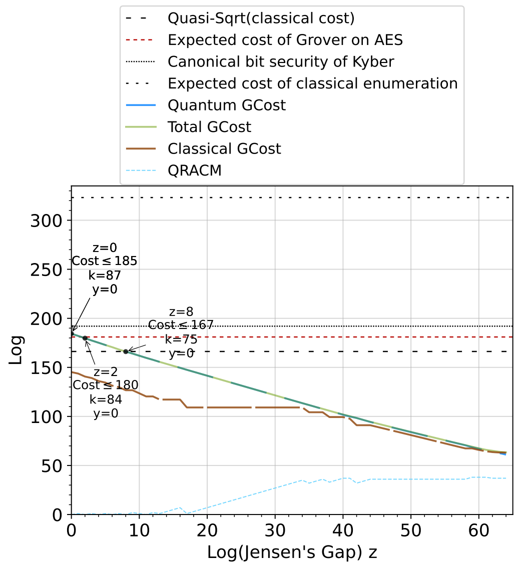

(b) Kyber-768, MaxDepth $= 2^{40}$.

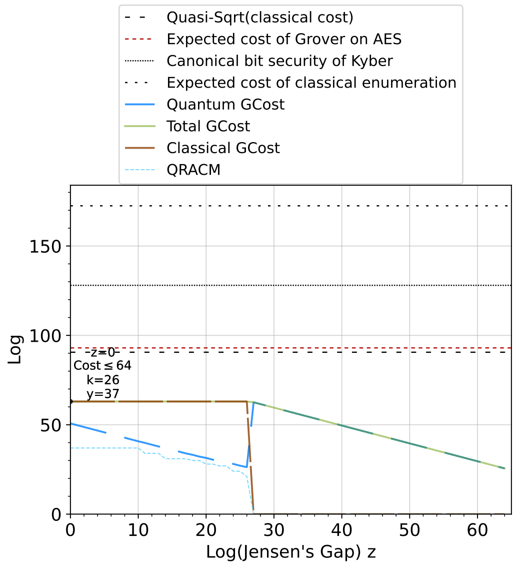

(c) Kyber-512, MaxDepth $= 2^{64}$

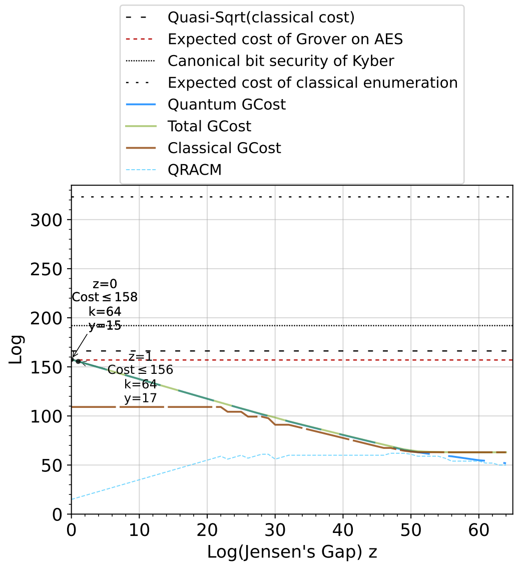

(d) Kyber-768, MaxDepth $= 2^{64}$.

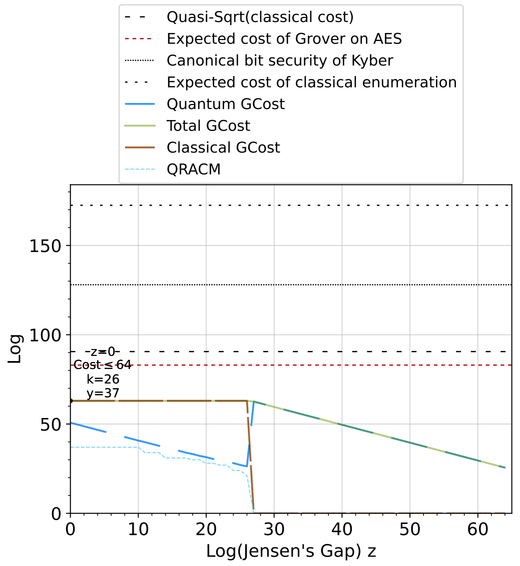

(e) Kyber-512, MaxDepth $= 2^{96}$

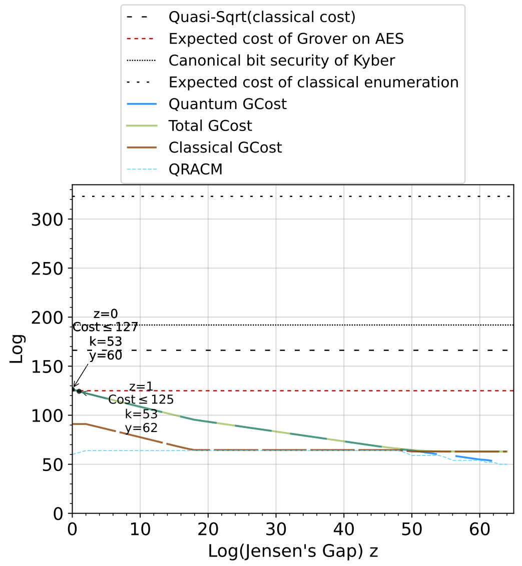

(f) Kyber-768, MaxDepth $= 2^{96}$.

Figure 23: Cost estimation for Kyber-512 and -768 under different MaxDepth restrictions with the instantiation for operator $\mathcal{W}$ as in Section 4.1 and with DF $= 1$, QD $= 1$, $b = 1$ (see Section 3), and corresponding to the lower bound (LB/UB) for Conjecture 3.

G.3 Figures for the Circuit-based Results

Next we present additional figures of quantum enumeration cost estimation to the ones in Section 5. As before, $\mathrm{GC\textsc{ost}}(\mathcal{W})$ and $\mathrm{TDepth}(\mathcal{W})$ are estimated as in Section 4.2 and $DF(\mathcal{W})$, $QD(\mathcal{W})$, $WQ(\mathcal{T}, W)$ as in Section 3,

– Fig. 24 shows the cost estimation without any $\textsc{MaxDepth}$ constraint on $\text{T-}\textsc{Depth}(\mathrm{QPE}(\mathcal{W}))$.
– Fig. 25 is the cost estimation for Kyber-512 with $\text{T-}\textsc{Depth}(\mathrm{QPE}(\mathcal{W})) \leq 2^{64}$.
– Fig. 26 shows the cost estimation for Kyber-768 and Kyber-1024 assuming $\text{T-}\textsc{Depth}(\mathrm{QPE}(\mathcal{W})) \leq \textsc{MaxDepth} \in \{2^{40}, 2^{64}, 2^{96}\}$.

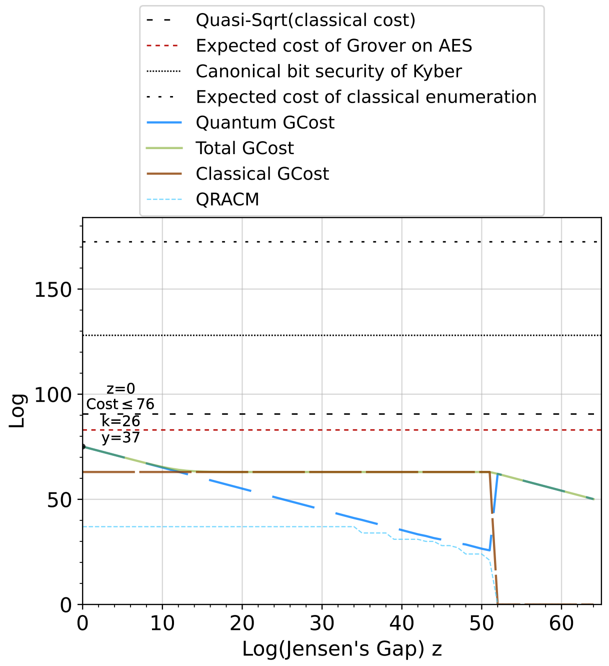

(a) Cost estimation for Kyber-512 w/ MaxDepth $= \infty$.

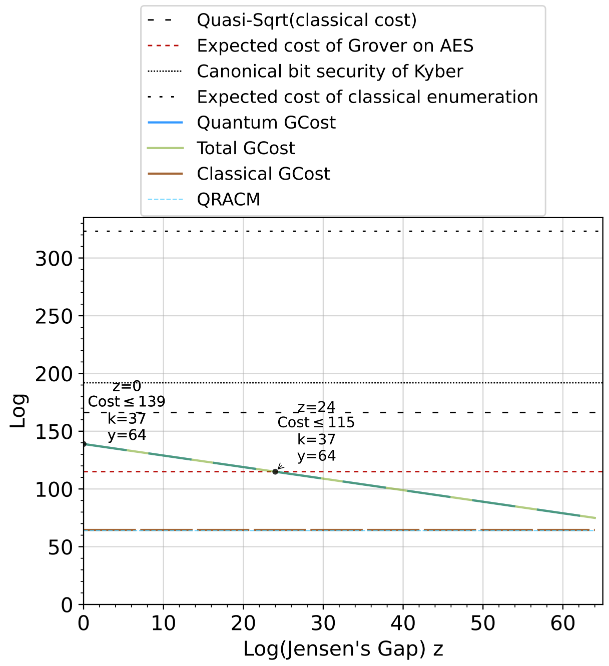

(b) Cost estimation for Kyber-768 w/ MaxDepth $= \infty$.

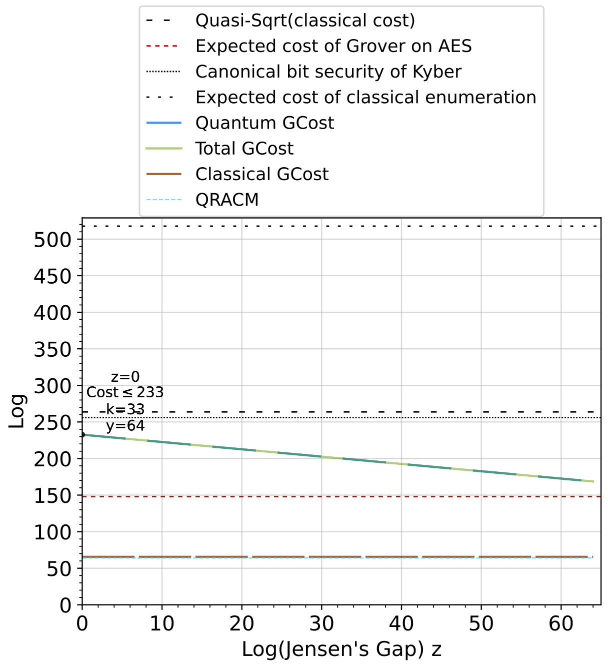

(c) Cost estimation for Kyber-1024 w/ MaxDepth $= \infty$.

Figure 24: Cost estimation for Kyber w/o MaxDepth restriction and for operator $\mathcal{W}$ as in Section 4.2 and with DF $= 1$, QD $= 1$, $b = 1$, and corresponding to the lower bound (LB/UB) for Conjecture 3.

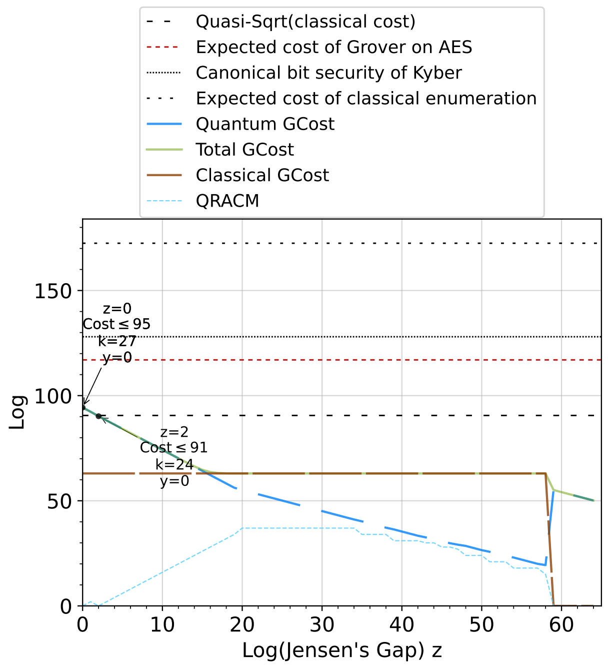

(a) Kyber-512, MaxDepth $= 2^{40}$

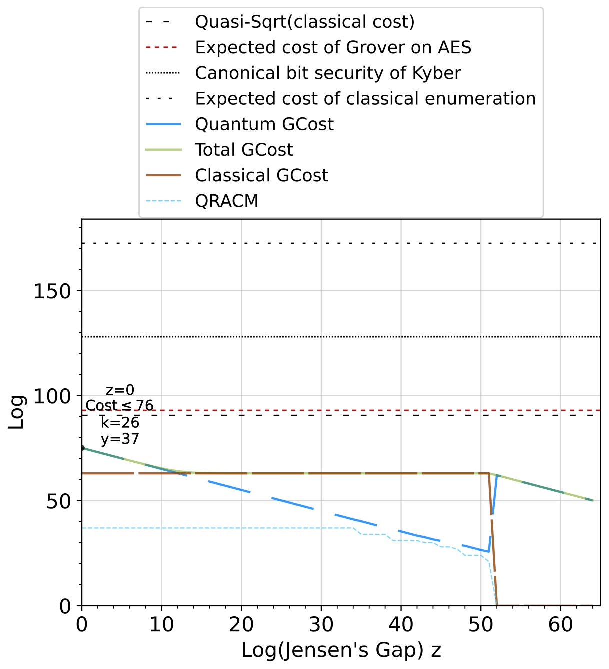

(b) Kyber-512, MaxDepth $= 2^{64}$

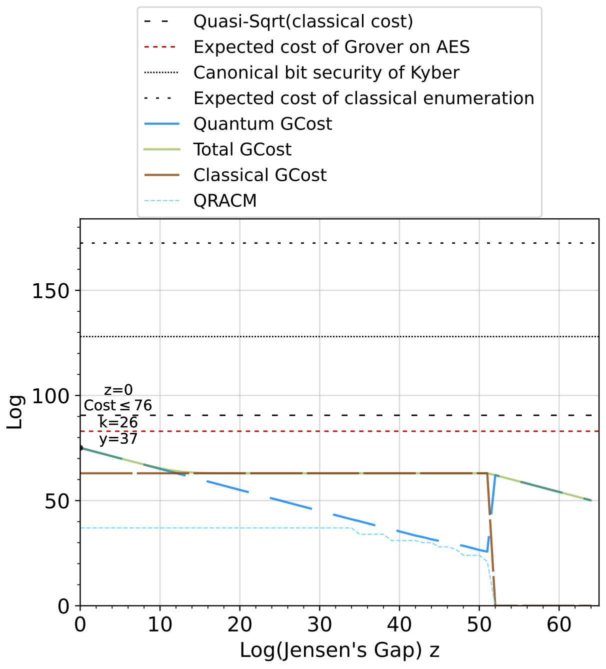

(c) Kyber-512, MaxDepth $= 2^{96}$

Figure 25: Cost estimation for Kyber-512 under different MaxDepth restrictions with operator $\mathcal{W}$ as in Section 4.2 and with DF $= 1$, QD $= 1$, $b = 1$, and corresponding to the lower bound (LB/UB) for Conjecture 3.

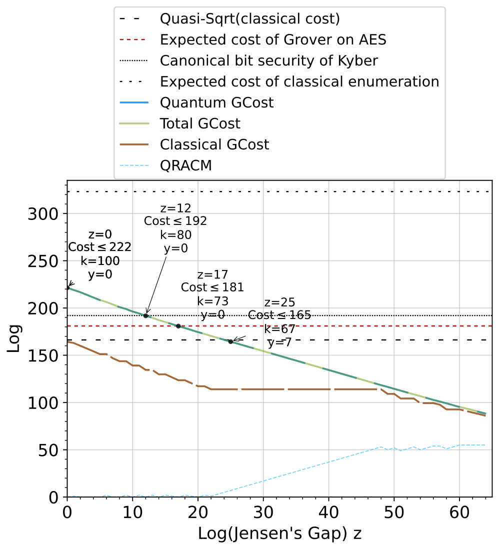

(a) Kyber-768, MaxDepth $= 2^{40}$

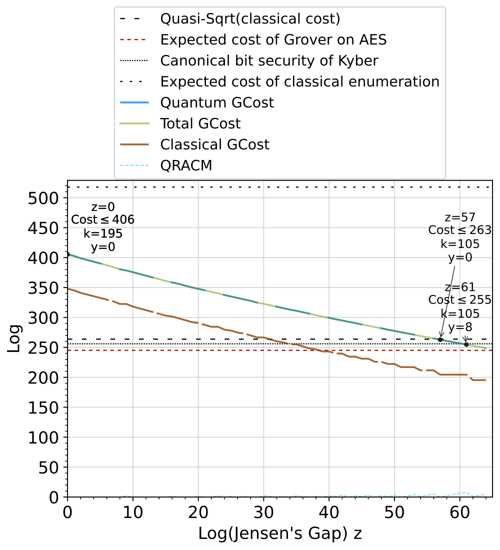

(b) Kyber-1024, MaxDepth $= 2^{40}$.

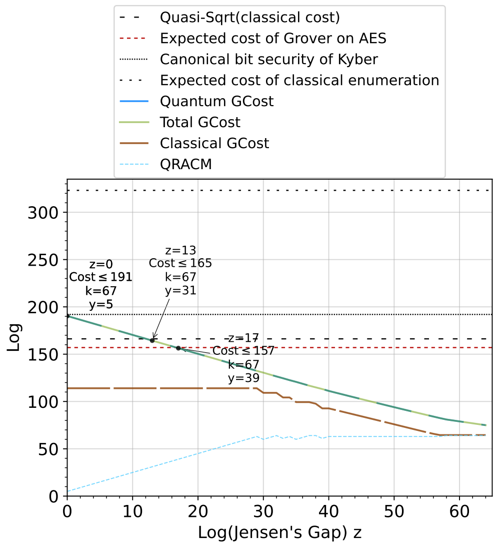

(c) Kyber-768, MaxDepth $= 2^{64}$

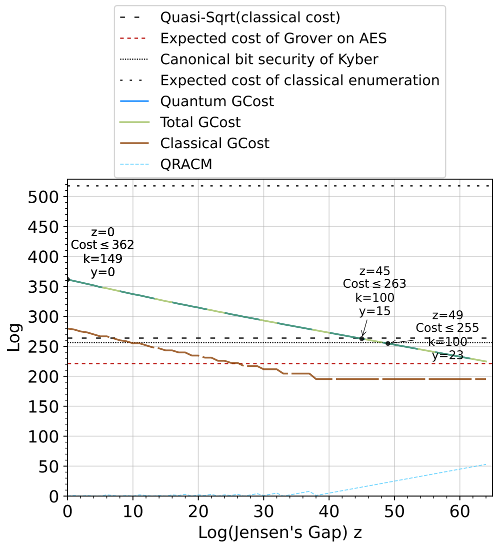

(d) Kyber-1024, MaxDepth $= 2^{64}$.

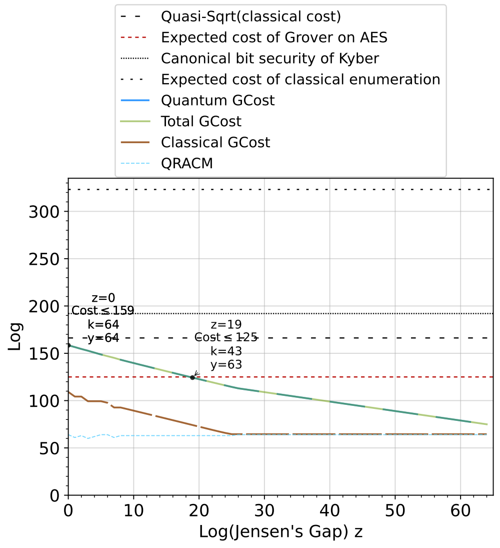

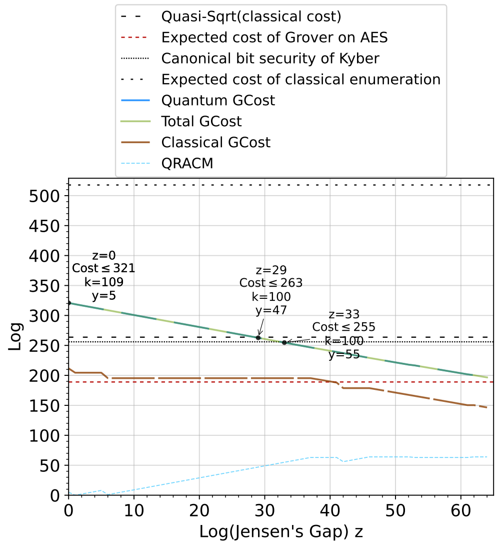

(e) Kyber-768, MaxDepth $= 2^{96}$

(f) Kyber-1024, MaxDepth $= 2^{96}$.

Figure 26: Cost estimation for Kyber-768 and Kyber-1024 under different MaxDepth restrictions with the instantiation for operator $\mathcal{W}$ as in Section 4.2 and with DF $= 1$, QD $= 1$, $b = 1$ (see Section 3), and corresponding to the lower bound (LB/UB) for Conjecture 3.

H Beyond Lower Bounds for DF, QD, WQ

In this section, we discuss alternative lower bounds for the quantities representing the number of calls of the FindMV and DetectMV (cf. Fig. 1), such that the depth and gate-cost of FindMV (of a tree $\mathcal{T}$ being searched be of depth h and the degree of each node be bound by $\mathcal{C}$) amount to

$$\begin{aligned}\text{T-Depth}(\text{FindMV}(\mathcal{T})) &= \text{DF}(\mathcal{T}) \cdot \text{QD}(\mathcal{T}) \cdot \text{WQ}(\mathcal{T}, \mathcal{W}) \cdot \text{T-Depth}(\mathcal{W}) \\ \text{GCost}(\text{FindMV}(\mathcal{T})) &= \text{DF}(\mathcal{T}) \cdot \text{QD}(\mathcal{T}) \cdot \text{WQ}(\mathcal{T}, \mathcal{W}) \cdot \text{GCost}(\mathcal{W}).\end{aligned}$$

In what follows, we first describe the alternative analysis and then provide respective experimental results.

H.1 Alternative Bound Estimation

DF($\mathcal{T}$). As mentioned in Section 3.1, the analysis in [13] assumes an implicit transformation of $\mathcal{T}$ into a binary tree of depth $h \log \mathcal{C}$. DetectMV is then called on the root level, in order to detect whether marked vertices are in the tree. If no marked vertices are found, no more calls are required, and $\text{DF}(\mathcal{T}) = 1$. If there are, further calls are made to identify the path from the root to the marked leaf, akin to a binary search. In total, in order to identify one marked leaf in $\mathcal{T}$ (or return error),

$$\text{DF}(\mathcal{T}) = \begin{cases} 1, & \text{if } \mathcal{T} \text{ contains no marked leaves,} \\ h \log \mathcal{C}, & \text{if } \mathcal{T} \text{ contains at least one marked leaf.} \end{cases}$$

In the setting of combined classical-quantum enumeration, most of the $H_k/2^y$ trees $\mathcal{T}(g)$ explored will not contain any marked leafs. Given that the quantum GCost is estimated (cf. Eq. (6)) as

$$\begin{aligned}\mathop{\mathbb{E}}_{\substack{\text{random} \\ \text{tree } \mathcal{T}}}[\text{Quantum GCost}] &\approx \frac{1}{2} \cdot \frac{H_k}{2^y} \cdot \mathbb{E}\left[\text{GCost}(\text{FindMV}(\mathcal{T}(g)))\right] \\ &= \frac{1}{2} \cdot \frac{H_k}{2^y} \cdot \mathbb{E}[\text{DF}(\mathcal{T}(g)) \cdot \text{QD}(\mathcal{T}(g)) \cdot \text{WQ}(\mathcal{T}(g), \mathcal{W}) \cdot \text{GCost}(\mathcal{W})],\end{aligned}$$

we could set $\text{DF}(\mathcal{T}(g)) = \left(\frac{H_k}{2^{y+1}} - 1 + h \log \mathcal{C}\right) \cdot \frac{2^{y+1}}{H_k}$ with $h = n - k + 1$ during cost estimation, to capture how when the enumeration radius is short enough, $h \log \mathcal{C}$ calls will likely be made on only one of the subtrees, and one call will be made to the remaining $\frac{H_k}{2^{y+1}} - 1$ many subtrees.

This discussion implicitly assumes the correctness of DetectMV, which however can return incorrect results, increasing the complexity of an estimation on DF. One option would be running DetectMV multiple times per level, with the amount of repetition depending on analysis of the specific DetectMV implementation, as well as the noise model of the quantum computer.

A simpler analysis would be to estimate the failure probability of FindMV when calling DetectMV once per level, assuming a tight failure probability upper bound for DetectMV($\mathcal{T}$) of δ_{DMV}. Then, the success probability of FindMV would be about $(1-\delta_{\mathrm{DMV}})^{\mathrm{DF}(\mathcal{T})}$, which is $\mathcal{O}(1)$ if $\delta_{\mathrm{DMV}} \approx 1/\mathrm{DF}(\mathcal{T})$.[15] Since *a priori* we do not know whether $\mathcal{T}$ contains a marked vertex, this would mean implementing DetectMV such that $\delta_{\mathrm{DMV}} \approx (h \log \mathcal{C})^{-1}$, to account for the in-principle $h \log \mathcal{C}$ successful calls required to detect the marked vertex in its subtree. We proceed to do this next.

$QD(\mathcal{T})$. The way DetectMV [57, Alg. 2] is computed is by performing multiple times, say K many, quantum phase estimation (QPE) on the $\mathcal{W}$ operator.

Let X_i be a random variable valued 1 when the i^{th} call to $QPE(\mathcal{W})$ returned an eigenvalue 1, and valued 0 otherwise, and let $Y_K = \sum_{i\in[K]} X_i$. The X_i are then *i.i.d.* Bernoulli random variables. Let MV denote the event that a marked vertex is contained in $\mathcal{T}$ and $\overline{MV}$ the opposite event. The core idea around DetectMV is that whenever a marked vertex exists, $QPE(\mathcal{W})$ will tend to return 1, and 0 otherwise. Indeed, from [57, Proof of Lemma 2.4] we have that $p_1 := \Pr[X_i = 1 \mid \overline{MV}] \leq 1/4$ and $p_2 := \Pr[X_i = 0 \mid MV] \leq 1/2$. In order to decide whether a tree contains a marked vertex, we run K instances of QPE on $\mathcal{W}$, and then check whether enough instances returned 1. Namely, for some fixed $\alpha \in (0,1]$ to be determined, we return "marked vertex exists" if and only if $Y_K \geq \alpha K$.

As seen in the previous paragraph on DF($\mathcal{T}$), we may want to fix a target failure probability δ_{DMV} for DetectMV, which can be achieved by picking K high enough. We start assuming we have found α, and use Chernoff bounds to estimate upper bounds on the "false positive/negative" probabilities $\Pr[Y \geq \alpha K \mid \overline{MV}]$ and $\Pr[Y \leq \alpha K \mid MV]$. By direct computation of the bound, recalling that the X_i are *i.i.d.*, we have

$$\begin{aligned}\Pr[Y_K \geq \alpha K \mid \overline{MV}] &\leq \exp(-t\alpha K)\mathbb{E}\left[\exp(tY_K)\right] = \exp(-t\alpha K)\mathbb{E}\left[\prod_{i=1}^{K}\exp(tX_i)\right] \\ &= \exp(-t\alpha K)\mathbb{E}\left[(\exp(tX_1))\right]^K = \left(\frac{1+p_1(\exp(t)-1)}{\exp(\alpha t)}\right)^K,\end{aligned}$$

for any $t > 0$. For $\Pr[Y_K \leq \alpha K]$ a similar computation on the left tail gives

$$\Pr[Y_K \leq \alpha K \mid MV] \leq \left(\frac{\exp(t)+p_2(1-\exp(t))}{\exp(\alpha t)}\right)^K, \text{ for any } t < 0.$$

We then identify values of α and ε such that $\inf_{y>0}\left(\frac{1+p_1(\exp(t)-1)}{\exp(\alpha t)}\right)^{\varepsilon} \leq 1/2$ and $\inf_{y<0}\left(\frac{\exp(t)+p_2(1-\exp(t))}{\exp(\alpha t)}\right)^{\varepsilon} \leq 1/2$. From a numerical search, and picking the smallest possible ε returned, we observe a valid pair at $\alpha = 0.369017$ and

[15] Specifically, it approaches e^{-1} as $\delta_{\mathrm{DMV}} \to 0$.

$\varepsilon = 20$.[16] Finally, we compute

$$\Pr[Y_K \geq \alpha K \mid \overline{MV}] \leq \inf_{y>0} \left(\frac{1 + p_1(\exp(t) - 1)}{\exp(\alpha t)} \right)^K \leq (1/2)^{K/\varepsilon},$$

and similarly for $\Pr[Y_K \leq \alpha K \mid MV]$, suggesting that to get an overall failure probability of at most δ_{DMV}, one should choose $K/\varepsilon \geq \log(1/\delta_{\mathrm{DMV}})$. Therefore, it should be sufficient to choose

$$\mathrm{QD}(\mathcal{T}) = K = \lceil 20 \log(h \log \mathcal{C}) \rceil \geq \varepsilon \log(1/\delta_{\mathrm{DMV}}).$$

H.2 Experimental Results Using Alternative Bounds

We replicate the analysis performed in Section 5.2, estimating the cost of a combined classical-quantum attack as described in Sections 3.2 and 3.3. In Tables 12 and 13 we summarize the values for the Jensen's gap 2^z at crossover points of our combined classical-quantum enumeration attacks against the quasi-square-root and the canonical $128, 192, 256$ bit security of Kyber.

The tables corresponds to attacks in the settings for $\mathcal{W}$ as in Section 4.1 and Section 4.2 with $DF(\mathcal{W})$ and $QD(\mathcal{W})$ as in Appendix H.1 (with $\mathcal{C} = 1$), and $b = 1/64$ in $WQ(\mathcal{T}, W)$. We note that we must set $\mathcal{C} = 1$ since we don't have a better lower bound available, again resulting in $DF(\mathcal{W}) = QD(\mathcal{W}) = 1$ lower bounds.

[16] In particular, our value of α is quite close to the $3/8 = 0.375$ proposed in [57]. This latter value would however imply $\varepsilon = 22$.

Table 11: Summary of the values for the Jensen's gap 2^z at crossover points of our combined classical-quantum enumeration attacks against Kyber and the cost of Grover's search against AES (cf. [41, Tables 10 and 12]). We remark that exact crossovers happen at fractional values of z. In this table we round down threshold values of z. MaxDepth is abbreviated to MD. Cost is as in Table 6. The results are estimated from the bounds $\mathcal{C} = 1, \mathrm{DF}(\mathcal{W}) = 1$, $\mathrm{QD}(\mathcal{W}) = 1$, $b = 1/64$.

less likely to be feasible ▨ more likely to be feasible

		Crossover points when comparing Grover on AES against the total GCost (cf. Table 6) with …					
		… $\mathcal{W}$ as in Section 4.1			… $\mathcal{W}$ as in Section 4.2		
MD	Kyber	LB/UB	UB/UB	LB/LB	LB/UB	UB/UB	LB/LB
2^{40}	-512	$z \geq 0, k \leq 25$ Cost $\geq 2^{74}$	$z \geq 26, k \leq 11$ Cost $\geq 2^{116}$	$z \geq 18, k \leq 83$ Cost $\geq 2^{115}$	$z \geq 0, k \leq 39$ Cost $\geq 2^{110}$	$z \geq 42, k \leq 22$ Cost $\geq 2^{115}$	$z \geq 34, k \leq 79$ Cost $\geq 2^{115}$
	-768	$z \geq 8, k \leq 84$ Cost $\geq 2^{179}$	$z > 64$	$z \geq 62, k \leq 106$ Cost $\geq 2^{179}$	$z \geq 23, k \leq 73$ Cost $\geq 2^{180}$	$z > 64$	$z > 64$
	-1024	$z \geq 56, k \leq 105$ Cost $\geq 2^{242}$	$z > 64$	$z > 64$	$z > 64$	$z > 64$	$z > 64$
2^{64}	-512	$z \geq 0, k \leq 26$ Cost $\geq 2^{63}$	$z \geq 26, k \leq 9$ Cost $\geq 2^{92}$	$z \geq 18, k \leq 64$ Cost $\geq 2^{91}$	$z \geq 0, k \leq 24$ Cost $\geq 2^{82}$	$z \geq 42, k \leq 5$ Cost $\geq 2^{92}$	$z \geq 34, k \leq 54$ Cost $\geq 2^{91}$
	-768	$z \geq 7, k \leq 64$ Cost $\geq 2^{155}$	$z > 64$	$z \geq 62, k \leq 77$ Cost $\geq 2^{155}$	$z \geq 23, k \leq 67$ Cost $\geq 2^{156}$	$z > 64$	$z > 64$
	-1024	$z \geq 55, k \leq 100$ Cost $\geq 2^{220}$	$z > 64$	$z > 64$	$z > 64$	$z > 64$	$z > 64$
2^{96}	-512	$z \geq 0, k \leq 26$ Cost $\geq 2^{63}$	$z \geq 21, k \leq 1$ Cost $\geq 2^{82}$	$z \geq 13, k \leq 40$ Cost $\geq 2^{82}$	$z \geq 0, k \leq 26$ Cost $\geq 2^{81}$	$z \geq 46, k \leq 1$ Cost $\geq 2^{82}$	$z \geq 37, k \leq 40$ Cost $\geq 2^{82}$
	-768	$z \geq 7, k \leq 53$ Cost $\geq 2^{124}$	$z > 64$	$z \geq 62, k \leq 44$ Cost $\geq 2^{123}$	$z \geq 25, k \leq 43$ Cost $\geq 2^{124}$	$z > 64$	$z > 64$
	-1024	$z \geq 57, k \leq 79$ Cost $\geq 2^{187}$	$z > 64$	$z > 64$	$z > 64$	$z > 64$	$z > 64$
∞	-512	$z \geq 0, k \leq 26$ Cost $\geq 2^{63}$	$z \geq 21, k \leq 1$ Cost $\geq 2^{82}$	$z \geq 13, k \leq 40$ Cost $\geq 2^{82}$	$z \geq 0, k \leq 26$ Cost $\geq 2^{81}$	$z \geq 46, k \leq 1$ Cost $\geq 2^{82}$	$z \geq 37, k \leq 40$ Cost $\geq 2^{82}$
	-768	$z \geq 5, k \leq 37$ Cost $\geq 2^{114}$	$z > 64$	$z \geq 57, k \leq 31$ Cost $\geq 2^{114}$	$z \geq 30, k \leq 37$ Cost $\geq 2^{114}$	$z > 64$	$z > 64$
	-1024	$z > 64$	$z > 64$	$z > 64$	$z > 64$	$z > 64$	$z > 64$
$\infty_{k=0}$	-512	$z \geq 13, k = 0$ Cost $\geq 2^{82}$	$z \geq 21, k = 0$ Cost $\geq 2^{82}$	$z \geq 13, k = 0$ Cost $\geq 2^{82}$	$z \geq 38, k = 0$ Cost $\geq 2^{82}$	$z \geq 46, k = 0$ Cost $\geq 2^{82}$	$z \geq 38, k = 0$ Cost $\geq 2^{82}$
	-768	$z \geq 57, k = 0$ Cost $\geq 2^{114}$	$z \geq 62, k = 0$ Cost $\geq 2^{114}$	$z \geq 57, k = 0$ Cost $\geq 2^{114}$	$z > 64$	$z > 64$	$z > 64$
	-1024	$z > 64$	$z > 64$	$z > 64$	$z > 64$	$z > 64$	$z > 64$

Table 12: Summary of the values for the Jensen's gap 2^z at crossover points of our combined classical-quantum enumeration attacks against Kyber and the quasi-square root speed up $\sqrt{\#\mathcal{T} \cdot h}$. We remark that exact crossovers happen at fractional values of z. In this table we round down threshold values of z. MaxDepth is abbreviated to MD. The results are estimated from the bounds $\mathcal{C} = 1, \mathrm{DF}(\mathcal{W}) = 1$, $\mathrm{QD}(\mathcal{W}) = 1$, $b = 1/64$.

less likely to be feasible ■ more likely to be feasible

		Crossover points when comparing quasi-square-root against the total GCost (cf. Table 6) with …					
		… $\mathcal{W}$ as in Section 4.1			… $\mathcal{W}$ as in Section 4.2		
MD	Kyber	LB/UB	UB/UB	LB/LB	LB/UB	UB/UB	LB/LB
2^{40}	-512	$z \geq 0, k \leq 25$ Cost $\geq 2^{74}$	$z \geq 35, k \leq 11$ Cost $\geq 2^{98}$	$z \geq 31, k \leq 59$ Cost $\geq 2^{89}$	$z \geq 8, k \leq 24$ Cost $\geq 2^{90}$	$z \geq 51, k \leq 12$ Cost $\geq 2^{98}$	$z \geq 47, k \leq 63$ Cost $\geq 2^{89}$
	-768	$z \geq 14, k \leq 75$ Cost $\geq 2^{166}$	$z > 64$	$z > 64$	$z \geq 31, k \leq 67$ Cost $\geq 2^{164}$	$z > 64$	$z > 64$
	-1024	$z \geq 47, k \leq 115$ Cost $\geq 2^{261}$	$z > 64$	$z > 64$	$z \geq 63, k \leq 105$ Cost $\geq 2^{262}$	$z > 64$	$z > 64$
2^{64}	-512	$z \geq 0, k \leq 26$ Cost $\geq 2^{63}$	$z \geq 23, k \leq 11$ Cost $\geq 2^{98}$	$z \geq 19, k \leq 59$ Cost $\geq 2^{89}$	$z \geq 0, k \leq 24$ Cost $\geq 2^{82}$	$z \geq 39, k \leq 5$ Cost $\geq 2^{98}$	$z \geq 35, k \leq 54$ Cost $\geq 2^{89}$
	-768	$z \geq 2, k \leq 64$ Cost $\geq 2^{165}$	$z \geq 60, k \leq 33$ Cost $\geq 2^{170}$	$z \geq 57, k \leq 77$ Cost $\geq 2^{165}$	$z \geq 19, k \leq 67$ Cost $\geq 2^{164}$	$z > 64$	$z > 64$
	-1024	$z \geq 34, k \leq 105$ Cost $\geq 2^{262}$	$z > 64$	$z > 64$	$z \geq 51, k \leq 100$ Cost $\geq 2^{262}$	$z > 64$	$z > 64$
2^{96}	-512	$z \geq 0, k \leq 26$ Cost $\geq 2^{63}$	$z \geq 7, k \leq 2$ Cost $\geq 2^{98}$	$z \geq 5, k \leq 40$ Cost $\geq 2^{90}$	$z \geq 0, k \leq 26$ Cost $\geq 2^{81}$	$z \geq 30, k \leq 1$ Cost $\geq 2^{98}$	$z \geq 30, k \leq 40$ Cost $\geq 2^{89}$
	-768	$z \geq 0, k \leq 61$ Cost $\geq 2^{137}$	$z \geq 44, k \leq 12$ Cost $\geq 2^{170}$	$z \geq 41, k \leq 77$ Cost $\geq 2^{165}$	$z \geq 3, k \leq 67$ Cost $\geq 2^{164}$	$z \geq 60, k \leq 12$ Cost $\geq 2^{171}$	$z \geq 58, k \leq 62$ Cost $\geq 2^{164}$
	-1024	$z \geq 18, k \leq 100$ Cost $\geq 2^{262}$	$z > 64$	$z > 64$	$z \geq 35, k \leq 100$ Cost $\geq 2^{262}$	$z > 64$	$z > 64$
∞	-512	$z \geq 0, k \leq 26$ Cost $\geq 2^{63}$	$z \geq 6, k \leq 1$ Cost $\geq 2^{97}$	$z \geq 5, k \leq 40$ Cost $\geq 2^{90}$	$z \geq 0, k \leq 26$ Cost $\geq 2^{81}$	$z \geq 30, k \leq 1$ Cost $\geq 2^{98}$	$z \geq 30, k \leq 40$ Cost $\geq 2^{89}$
	-768	$z \geq 0, k \leq 37$ Cost $\geq 2^{119}$	$z \geq 8, k \leq 3$ Cost $\geq 2^{171}$	$z \geq 5, k \leq 31$ Cost $\geq 2^{166}$	$z \geq 0, k \leq 37$ Cost $\geq 2^{144}$	$z \geq 34, k \leq 3$ Cost $\geq 2^{170}$	$z \geq 31, k \leq 31$ Cost $\geq 2^{165}$
	-1024	$z \geq 0, k \leq 33$ Cost $\geq 2^{212}$	$z \geq 8, k \leq 3$ Cost $\geq 2^{269}$	$z \geq 5, k \leq 1$ Cost $\geq 2^{263}$	$z \geq 0, k \leq 33$ Cost $\geq 2^{238}$	$z \geq 35, k \leq 3$ Cost $\geq 2^{268}$	$z \geq 32, k \leq 11$ Cost $\geq 2^{263}$
$\infty_{k=0}$	-512	$z \geq 6, k = 0$ Cost $\geq 2^{89}$	$z \geq 6, k = 0$ Cost $\geq 2^{97}$	$z \geq 6, k = 0$ Cost $\geq 2^{89}$	$z \geq 30, k = 0$ Cost $\geq 2^{90}$	$z \geq 30, k = 0$ Cost $\geq 2^{98}$	$z \geq 30, k = 0$ Cost $\geq 2^{90}$
	-768	$z \geq 6, k = 0$ Cost $\geq 2^{165}$	$z \geq 6, k = 0$ Cost $\geq 2^{170}$	$z \geq 6, k = 0$ Cost $\geq 2^{165}$	$z \geq 31, k = 0$ Cost $\geq 2^{165}$	$z \geq 31, k = 0$ Cost $\geq 2^{171}$	$z \geq 31, k = 0$ Cost $\geq 2^{165}$
	-1024	$z \geq 6, k = 0$ Cost $\geq 2^{262}$	$z \geq 6, k = 0$ Cost $\geq 2^{268}$	$z \geq 6, k = 0$ Cost $\geq 2^{262}$	$z \geq 32, k = 0$ Cost $\geq 2^{263}$	$z \geq 32, k = 0$ Cost $\geq 2^{269}$	$z \geq 32, k = 0$ Cost $\geq 2^{263}$

Table 13: Summary of the values for the Jensen's gap 2^z at crossover points of our combined classical-quantum enumeration attacks against Kyber and the canonical $128, 192, 256$ bit security respectively. We remark that exact crossovers happen at fractional values of z. In this table we round down threshold values of z. MaxDepth is abbreviated to MD. Cost is as in Table 6. The results are estimated from the bounds $\mathcal{C} = 1, \mathrm{DF}(\mathcal{W}) = 1$, $\mathrm{QD}(\mathcal{W}) = 1$, $b = 1/64$.

less likely to be feasible — more likely to be feasible

Crossover points when comparing the canonical bit security against the total GCost (cf. Table 6) with …

		… $\mathcal{W}$ as in Section 4.1			… $\mathcal{W}$ as in Section 4.2		
MD	Kyber	LB/UB	UB/UB	LB/LB	LB/UB	UB/UB	LB/LB
2^{40}	-512	$z \geq 0, k \leq 25$ Cost $\geq 2^{74}$	$z \geq 21, k \leq 28$ Cost $\geq 2^{126}$	$z \geq 12, k \leq 92$ Cost $\geq 2^{127}$	$z \geq 0, k \leq 39$ Cost $\geq 2^{110}$	$z \geq 36, k \leq 24$ Cost $\geq 2^{127}$	$z \geq 28, k \leq 96$ Cost $\geq 2^{126}$
	-768	$z \geq 3, k \leq 92$ Cost $\geq 2^{191}$	$z \geq 62, k \leq 33$ Cost $\geq 2^{190}$	$z \geq 56, k \leq 114$ Cost $\geq 2^{191}$	$z \geq 18, k \leq 80$ Cost $\geq 2^{191}$	$z > 64$	$z > 64$
	-1024	$z \geq 50, k \leq 112$ Cost $\geq 2^{255}$	$z > 64$	$z > 64$	$z > 64$	$z > 64$	$z > 64$
2^{64}	-512	$z \geq 0, k \leq 26$ Cost $\geq 2^{63}$	$z \geq 9, k \leq 28$ Cost $\geq 2^{126}$	$z \geq 0, k \leq 92$ Cost $\geq 2^{127}$	$z \geq 0, k \leq 24$ Cost $\geq 2^{82}$	$z \geq 24, k \leq 24$ Cost $\geq 2^{127}$	$z \geq 16, k \leq 79$ Cost $\geq 2^{127}$
	-768	$z \geq 0, k \leq 64$ Cost $\geq 2^{169}$	$z \geq 50, k \leq 33$ Cost $\geq 2^{190}$	$z \geq 44, k \leq 114$ Cost $\geq 2^{191}$	$z \geq 6, k \leq 67$ Cost $\geq 2^{190}$	$z > 64$	$z \geq 60, k \leq 106$ Cost $\geq 2^{191}$
	-1024	$z \geq 38, k \leq 100$ Cost $\geq 2^{254}$	$z > 64$	$z > 64$	$z \geq 55, k \leq 100$ Cost $\geq 2^{254}$	$z > 64$	$z > 64$
2^{96}	-512	$z \geq 0, k \leq 26$ Cost $\geq 2^{63}$	$z \geq 0, k \leq 4$ Cost $\geq 2^{112}$	$z \geq 0, k \leq 40$ Cost $\geq 2^{96}$	$z \geq 0, k \leq 26$ Cost $\geq 2^{81}$	$z \geq 9, k \leq 5$ Cost $\geq 2^{126}$	$z \geq 0, k \leq 58$ Cost $\geq 2^{127}$
	-768	$z \geq 0, k \leq 61$ Cost $\geq 2^{137}$	$z \geq 34, k \leq 33$ Cost $\geq 2^{190}$	$z \geq 28, k \leq 77$ Cost $\geq 2^{191}$	$z \geq 0, k \leq 67$ Cost $\geq 2^{170}$	$z \geq 50, k \leq 26$ Cost $\geq 2^{191}$	$z \geq 45, k \leq 77$ Cost $\geq 2^{190}$
	-1024	$z \geq 22, k \leq 100$ Cost $\geq 2^{254}$	$z > 64$	$z > 64$	$z \geq 39, k \leq 100$ Cost $\geq 2^{254}$	$z > 64$	$z > 64$
∞	-512	$z \geq 0, k \leq 26$ Cost $\geq 2^{63}$	$z \geq 0, k \leq 1$ Cost $\geq 2^{103}$	$z \geq 0, k \leq 40$ Cost $\geq 2^{95}$	$z \geq 0, k \leq 26$ Cost $\geq 2^{81}$	$z \geq 1, k \leq 1$ Cost $\geq 2^{127}$	$z \geq 0, k \leq 40$ Cost $\geq 2^{119}$
	-768	$z \geq 0, k \leq 37$ Cost $\geq 2^{119}$	$z \geq 0, k \leq 3$ Cost $\geq 2^{179}$	$z \geq 0, k \leq 31$ Cost $\geq 2^{171}$	$z \geq 0, k \leq 37$ Cost $\geq 2^{144}$	$z \geq 13, k \leq 3$ Cost $\geq 2^{191}$	$z \geq 5, k \leq 31$ Cost $\geq 2^{191}$
	-1024	$z \geq 0, k \leq 33$ Cost $\geq 2^{212}$	$z \geq 22, k \leq 3$ Cost $\geq 2^{255}$	$z \geq 13, k \leq 1$ Cost $\geq 2^{255}$	$z \geq 0, k \leq 33$ Cost $\geq 2^{238}$	$z \geq 48, k \leq 3$ Cost $\geq 2^{255}$	$z \geq 40, k \leq 11$ Cost $\geq 2^{255}$
$\infty_{k=0}$	-512	$z \geq 0, k = 0$ Cost $\geq 2^{95}$	$z \geq 0, k = 0$ Cost $\geq 2^{103}$	$z \geq 0, k = 0$ Cost $\geq 2^{95}$	$z \geq 0, k = 0$ Cost $\geq 2^{120}$	$z \geq 1, k = 0$ Cost $\geq 2^{127}$	$z \geq 0, k = 0$ Cost $\geq 2^{120}$
	-768	$z \geq 0, k = 0$ Cost $\geq 2^{171}$	$z \geq 0, k = 0$ Cost $\geq 2^{176}$	$z \geq 0, k = 0$ Cost $\geq 2^{171}$	$z \geq 5, k = 0$ Cost $\geq 2^{191}$	$z \geq 11, k = 0$ Cost $\geq 2^{191}$	$z \geq 5, k = 0$ Cost $\geq 2^{191}$
	-1024	$z \geq 13, k = 0$ Cost $\geq 2^{255}$	$z \geq 19, k = 0$ Cost $\geq 2^{255}$	$z \geq 13, k = 0$ Cost $\geq 2^{255}$	$z \geq 40, k = 0$ Cost $\geq 2^{255}$	$z \geq 46, k = 0$ Cost $\geq 2^{255}$	$z \geq 40, k = 0$ Cost $\geq 2^{255}$

I Lower-Bounding Additive and Multiplicative Jensen's Gaps

Let X be the random variable for $\#\mathcal{T}$ with support $\mathrm{supp}(X) \subset [1, +\infty)$, $\mu = \mathbb{E}[X] < \infty$, $\sigma^2 = \mathbb{V}[X] < \infty$. In this section, we explore two different derivations for lower bounds of the additive ($\sqrt{\mathbb{E}[X]} - \mathbb{E}[\sqrt{X}]$) and multiplicative ($\sqrt{\mathbb{E}[X]}/\mathbb{E}[\sqrt{X}]$) Jensen's gaps of X. As part of our derivations, we will use the notion of Hölder continuity, which we recall next.

Definition 2 (Hölder continuity). *A real function $f\colon \mathbb{R} \to \mathbb{R}$ is α-Hölder continuous over an interval $(a, b) \subset \mathbb{R}$ if for any $x, y \in (a, b)$, there exists $M > 0$ such that $|f(x) - f(y)| \leq M \cdot |x - y|^{\alpha}$.*

I.1 Bounding the Additive Jensen's Gap

To lower bound the additive gap, we start by proving that the square root function $\sqrt{x}$ is $\frac{1}{2}$-Hölder continuous.

Lemma 2. *$\sqrt{x}$ is $\frac{1}{2}$-Hölder continuous over $(0, \infty)$ with $M \geq 1$.*

Proof. Let $x, y \geq 0$. First we write

$$|\sqrt{x} - \sqrt{y}| = \frac{|\sqrt{x} - \sqrt{y}| \cdot |\sqrt{x} + \sqrt{y}|}{|\sqrt{x} + \sqrt{y}|} = \frac{|x - y|}{\sqrt{x} + \sqrt{y}} = \sqrt{|x - y|} \cdot \frac{\sqrt{|x - y|}}{\sqrt{x} + \sqrt{y}}.$$

Now, we note that $|x - y| \leq |x| + |y| = x + y \leq x + y + 2\sqrt{xy} = (\sqrt{x} + \sqrt{y})^2$. Since $\sqrt{x}$ is strictly increasing over $(0, \infty)$, it holds that

$$|x - y| \leq (\sqrt{x} + \sqrt{y})^2 \iff \sqrt{|x - y|} \leq \sqrt{x} + \sqrt{y}. \iff \frac{\sqrt{|x - y|}}{\sqrt{x} + \sqrt{y}} \leq 1.$$

Hence, $|\sqrt{x} - \sqrt{y}| = \sqrt{|x - y|} \cdot \frac{\sqrt{|x-y|}}{\sqrt{x}+\sqrt{y}} \leq \sqrt{|x - y|}$, which concludes the proof. □

Lemma 3. *The additive Jensen's gap of X is in absolute value $|\mathbb{E}[\sqrt{X}] - \sqrt{\mu}| \leq \sqrt{\sigma}$.*

Proof. Following [35, Eq 1.1], it holds that

$$\begin{aligned}
|\mathbb{E}[\sqrt{X}] - \sqrt{\mu}| &= \left| \sum_{x \in \mathrm{supp}(X)} \left[\sqrt{x} \Pr[X = x]\right] - \sqrt{\mu} \right| \\
&= \left| \sum_{x \in \mathrm{supp}(X)} (\sqrt{x} - \sqrt{\mu}) \Pr[X = x] \right| \quad (\text{by } \sum_{x \in \mathrm{supp}(X)} \Pr[X = x] = 1) \\
&\leq \sum_{x \in \mathrm{supp}(X)} \left|\sqrt{x} - \sqrt{\mu}\right| \Pr[X = x]
\end{aligned}$$

$$
\begin{aligned}
&\le \sum_{x \in \mathrm{supp}(X)} \sqrt{|x-\mu|}\,\Pr[X=x] && \text{(by Lemma 2)}\\
&= \mathbb{E}\left[\sqrt{|x-\mu|}\right] && \text{(by definition of } \mathbb{E}\text{)}\\
&\le \sqrt{\mathbb{E}\left[|x-\mu|\right]} && \text{(by Jensen's inequality)}\\
&\le \mathbb{E}\left[(x-\mu)^2\right]^{1/4} && \text{(by Jensen's inequality)}\\
&= \sqrt{\sigma}. && \text{(by definition of } \sigma\text{)}
\end{aligned}
$$

This concludes the proof. □

From this the following bound on $\mathbb{E}[\mathrm{GC{\small OST}}(\mathrm{QPE}(\mathcal{W}))]$ can be derived.

Lemma 4. *$\mathbb{E}[\mathrm{GC{\small OST}}(QPE(\mathcal{W}))] \ge \sqrt{h}\left(\sqrt{\mu}-\sqrt{\sigma}\right)\cdot \mathrm{GC{\small OST}}(\mathcal{W})$, where h is the height of $\mathcal{T}$.*

Proof. From Lemma 3, it holds that

$$
\begin{aligned}
|\mathbb{E}[\sqrt{X}] - \sqrt{\mu}| \le \sqrt{\sigma} &\iff -\sqrt{\sigma} \le \mathbb{E}[\sqrt{X}] - \sqrt{\mu} \le \sqrt{\sigma}\\
&\implies \mathbb{E}[\sqrt{X}] \ge \sqrt{\mu} - \sqrt{\sigma}.
\end{aligned}
$$

Since it holds that

$$
\mathrm{GC{\small OST}}(\mathrm{QPE}(\mathcal{W})) = \mathrm{WQ}(\mathcal{T},\mathcal{W}) \cdot \mathrm{GC{\small OST}}(\mathcal{W}),
$$

and under Conjecture 1, letting $X = \#\mathcal{T}$, the statement follows. □

I.2 Bounding the Multiplicative Jensen's Gap

We start by proving that the natural logarithm function $\ln(x)$ is $\frac{1}{2}$-Hölder continuous and that $\ln\sqrt{x}$ is $\frac{1}{2}$-Hölder continuous.

Lemma 5. *$\ln(x)$ is $\frac{1}{2}$-Hölder continuous over $[1,\infty)$ with $M \ge 1$.*

Proof. Let $p = 2$. We note that $\frac{d}{dx}\ln x = \frac{1}{x}$, and that $x, y \ge 1$. Then

$$
\begin{aligned}
|\ln x - \ln y| &= \left|\int_x^y \frac{dt}{t}\right| \le \int_{\min(x,y)}^{\max(x,y)} \left|\frac{1}{t}\right| dt\\
&\le \left(\int_{\min(x,y)}^{\max(x,y)} 1^2 dt\right)^{1/2} \left(\int_{\min(x,y)}^{\max(x,y)} \left|\frac{1}{t}\right|^2 dt\right)^{1/2} \quad \text{(by Hölder's inequality)}\\
&= |y-x|^{1/2} \left(\int_{\min(x,y)}^{\max(x,y)} \frac{1}{t^2} dt\right)^{1/2}\\
&\le |y-x|^{1/2} \left(\int_1^{\infty} \frac{1}{t^2} dt\right)^{1/2} \le |y-x|^{1/2} \cdot \left[-\frac{1}{x}\right]_1^{\infty} = |y-x|^{1/2}.
\end{aligned}
$$

□

Lemma 6. $\ln\sqrt{x}$ *is* $\frac{1}{2}$*-Hölder continuous over* $[1,\infty)$ *with* $M \geq 1/2$*.*

Proof. The statement follows immediately as

$$|\ln\sqrt{x} - \ln\sqrt{y}| = \frac{1}{2}|\ln x - \ln y| \leq \frac{1}{2}|x-y|^{1/2},$$

where the second inequality follows from Lemma 5. $\square$

Lemma 7. *Given a multiplicative Jensen's gap* 2^z *such that* $\mathbb{E}[\sqrt{x}] = 2^{-z}\sqrt{\mathbb{E}[x]}$*, then* $z \leq \frac{1}{2\ln 2}\sqrt{\sigma}$*.*

Proof. First, we take logarithms, *i.e.*,

$$\mathbb{E}[\sqrt{x}] = 2^{-z}\sqrt{\mathbb{E}[x]} \iff \ln\mathbb{E}[\sqrt{x}] = -z\ln 2 + \ln\sqrt{\mu}.$$

Then we upper bound z as

$$\begin{aligned}
z &= \frac{1}{\ln 2}(\ln\sqrt{\mu} - \ln\mathbb{E}[\sqrt{x}]) \\
&\leq \frac{1}{\ln 2}(\ln\sqrt{\mu} - \mathbb{E}[\ln\sqrt{x}]) && \text{(by Jensen's inequality, } \mathbb{E}\ln \leq \ln\mathbb{E}) \\
&= \frac{1}{\ln 2}\sum_{\mathrm{supp}(X)}\left(\ln\sqrt{\mu} - \ln\sqrt{x}\right)\Pr[X=x] \\
&\leq \frac{1}{\ln 2}\sum_{\mathrm{supp}(X)}\left|\ln\sqrt{\mu} - \ln\sqrt{x}\right|\Pr[X=x] \\
&\leq \frac{1}{\ln 2}\sum_{\mathrm{supp}(X)}\frac{1}{2}\left|\mu - x\right|^{1/2}\Pr[X=x] && \text{(by Lemma 6)} \\
&= \frac{1}{2\ln 2}\mathbb{E}[|\mu - x|^{1/2}] && \text{(by definition of } \mathbb{E}) \\
&\leq \frac{1}{2\ln 2}\mathbb{E}\left[(x-\mu)^2\right]^{1/4} = \frac{1}{2\ln 2}\sqrt{\sigma} && \text{(by applying Jensen's inequality twice)}
\end{aligned}$$

$\square$

We can conclude with the following bound on $\mathbb{E}[\text{GCost}(\text{QPE}(\mathcal{W}))]$.

Lemma 8. $\mathbb{E}[\text{GCost}(\mathit{QPE}(\mathcal{W}))] \geq 2^{-\frac{1}{2\ln 2}\sigma}\sqrt{\mu\cdot h}\cdot\text{GCost}(\mathcal{W})$*, where* h *is the height of* $\mathcal{T}$*.*

Proof. Using Lemma 7, it holds that

$$\mathbb{E}[\sqrt{X}] = 2^{-z}\sqrt{\mu} \geq 2^{-\frac{1}{2\ln 2}\sqrt{\sigma}}\sqrt{\mu}.$$

Combined with

$$\text{GCost}(\text{QPE}(\mathcal{W})) = \text{WQ}(\mathcal{T},\mathcal{W})\cdot\text{GCost}(\mathcal{W}),$$

and under Conjecture 1, letting $X = \#\mathcal{T}$ concludes the proof. $\square$

I.3 Experimentally Estimating $\sqrt{\sigma}$

Unfortunately, we are not aware of any techniques to estimate the variance of $\#\mathcal{T}(g)$ for an element $g \in Z_k$ of a pruned enumeration tree. Therefore, we have implemented an extension to the experiments from Appendix D originally used to experimentally measure some multiplicative Jensen's gaps. This extension lets us measure the unbiased sample variance s^2 of the number of nodes $\#\mathcal{T}(g)$. Using s^2 as an estimate for the variance σ^2 of the distribution, we then plot $\sqrt[4]{s^2}$ as an estimate for $\sqrt{\sigma}$ in Figs. 27 and 28.

Our results seem to indicate that $\sqrt{\sigma}$ increases with the dimension of the tree β and with the height of the subtree $\beta - k$, suggesting that deeper subtrees are more exposed to variations in their size compared to shallower trees. The value of the measured estimates $\sqrt[4]{s^2}$ seems also to stay relatively low (in absolute value) in our experiments, peaking at around 20. In any case, these experiments are no more or less conclusive than those in Appendix D, and hence this analysis does not seem to significantly improve on the methodology used in Section 5.2 for estimating the cost of the attack, that is testing multiple values of possible Jensen's gaps.

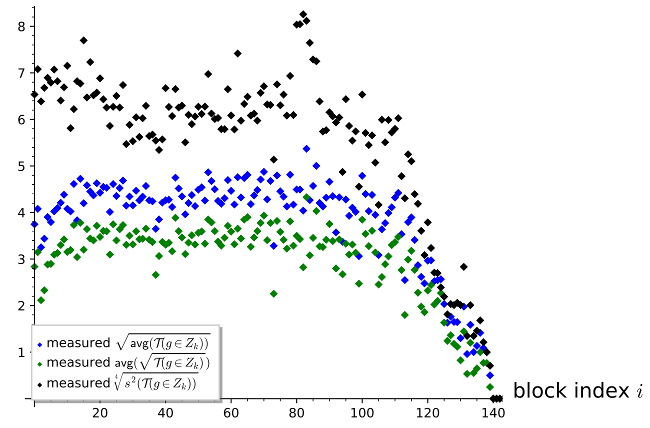

(a) $n = 72$ (cf. Table 7), block size $\beta = 50$, 10^{th} tour, $k = 20$.

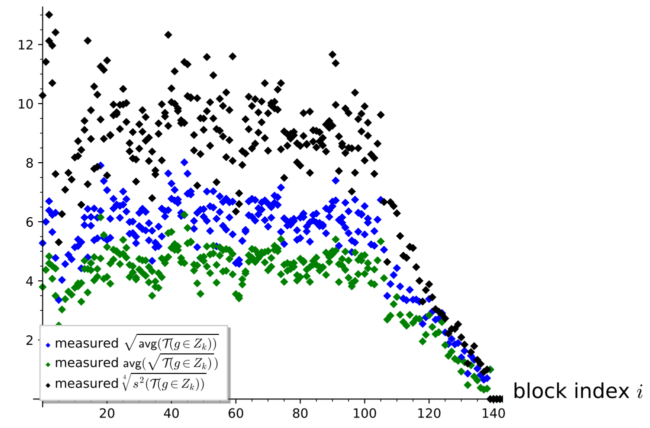

(b) $n = 72$ (cf. Table 7), block size $\beta = 60$, 10^{th} tour, $k = 20$.

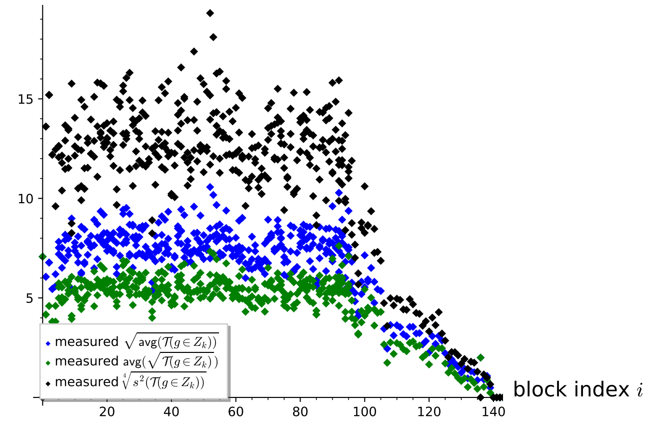

(c) $n = 72$ (cf. Table 7), block size $\beta = 70$, 10^{th} tour, $k = 20$.

Figure 27: Measurement on the Jensen's gap of subtrees of height $h = \beta - k$ rooted on level k in pruned enumeration experiments. The height h is reduced in the last few blocks of the basis of dimension smaller than β. As the block index i increases, we plot the measurements done during enumeration of the projective sublattice $\pi_i(\text{span}_{\mathbb{Z}}(b_i, \dots, b_{i+\beta}))$. Blue dots are the squared root of the average, green dots are the average of the squared root, black dots are the fourth root of the unbiased sample variance.

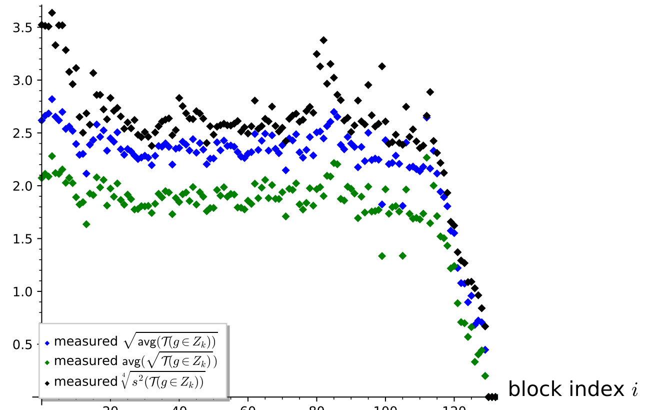

(a) $n = 72$ (cf. Table 7), block size $\beta = 50$, 10th tour, $k = 30$.

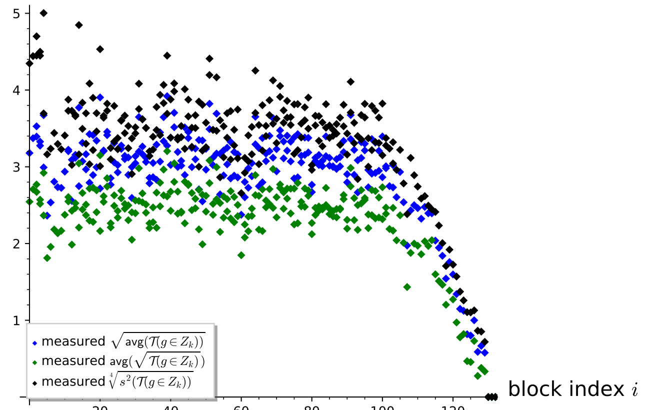

(b) $n = 72$ (cf. Table 7), block size $\beta = 60$, 10th tour, $k = 30$.

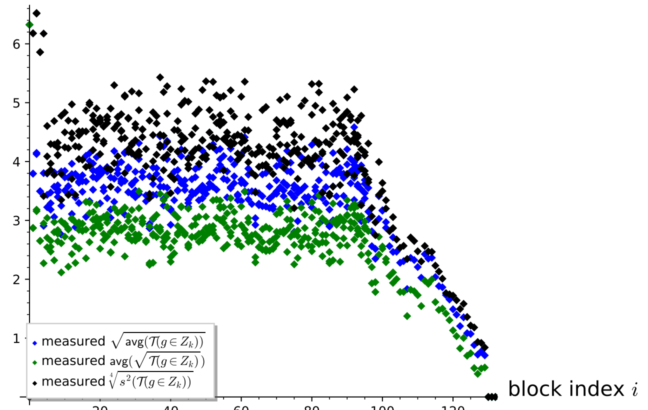

(c) $n = 72$ (cf. Table 7), block size $\beta = 70$, 10th tour, $k = 30$.

Figure 28: Continuation of Fig. 27.